URBAN FACADES

Photocatalytic building envelope for passive remediation of air pollution

Yamuna Sakthivel

Delft University of Technology

Urban Facades

Photocatalytic Building Envelope for Passive Remediation of Air Pollution

by

Yamuna Sakthivel

4738578

In partial fulfillment of the requirements for the degree of
Master of Science in Building Technology
at Delft University of Technology, Netherlands

Date: 25 June 2019

Thesis Committee

Dr. Alejandro Prieto Hoces | Mentor 1 | TU Delft
Dr. Truus Hordijk | Mentor 2 | TU Delft
Prof. Dr. ir. Ruud van Ommen | Consultant | TU Delft

TU Delft

ABSTRACT

Air pollution is a worldwide prevailing issue affecting the health of human beings in urban areas requiring urgent measures to adopted. This graduation project targets on adoption of passive air remediation techniques that can be widely applied into urban areas. Within the passive technical measures available, integrating greeneries on the infrastructure and photocatalytic materials prove promising to be incorporated in a broader perspective. Photocatalytic materials one-time installation, easy to maintain and self-cleaning properties has led to the selection of this material to quantify its air purifying capability.

TiO_2 coating has been used in building materials for its self-cleaning property. However, its capability to break down NOx compounds has broadened its scope for pollution abatement. Though it can be applied as a coating, the performance of the photocatalyst in urban scenarios is affected by contact wind speeds and incident UV irradiation. Also, increased surface area provides more area of photo catalytically active sites. These factors are governed by the geometrical form of the panel. Hence, the main objective of this research is to design a façade panel with enlarged surface area and surface roughness to manipulate the environmental factors to favor photocatalysis. Also, its air purification effect is quantified to understand the effectiveness of this passive strategy and the design.

The façade concept has been designed following a series of strategies to respond to wind and irradiation. The concept with optimum surface enlargement and irradiation is developed into modular panels which are materialized by choosing the material with least environmental impact.

The final part of this graduation project is about applying these panels in the street canyons, a controlled urban environment and evaluating the pollution abatement. The results indicate a pollution abatement of 3.5% - 8.9% in winter and 18% - 37.5% in percentage in summer for London.

Keywords: Urban facades, Urban air purification, photocatalytic building materials, TiO_2

ACKNOWLEDGEMENT

I would like to express my gratitude to Dr. Alejandro Prieto Hoces and Dr. Truus Hordijk, my thesis mentors for their immaculate guidance, encouragement and useful critiques throughout the framework of this thesis. Dr. Alejandro has helped me streamline this thesis with his insights as to how I could further develop my graduation project.

My special thanks to Dr. Ir. Ruud van Ommen for his guidance in applied chemistry of the photocatalytic building materials. He has provided me with the necessary chemistry knowledge which formed the base to take the research forward.

I am extremely thankful to Sampath Raghunathan Srikumar and Alberto Martínez González for teaching and helping me understand to set up the work flow for CFD and COMSOL simulations. I am grateful to Gowtham Pandiarajan for helping me with the installation of the required software.

My immense thanks to my amazing parents Sakthivel Ramasamy & Pushpavathi Sakthivel and my brother Gokul for being supportive and motivating in all my decisions towards my academics. My heartfelt thanks to all my friends in Delft for providing me with beautiful memories and for standing by my side throughout my journey in this institution.

CONTENTS

1. INTRODUCTION 1
   1.1. Context 2
   1.2. Problem Statement 2
   1.3. Environment and Urban regulations 3
   1.4. Research Question 5
   1.5. Sub-Research Question 5
   1.6. Research Overview 6

2. LITERATURE REVIEW 8

   2.1. Photocatalysis 9
      2.1.1. Photocatalysts 9
      2.1.2. Mechanism of Photocatalysis 10
      2.1.3. Operating and affecting Parameters 12
      2.1.4. Conclusion 19

   2.2. State of the art in Building industry 20
      2.2.1. Photocatalytic Concrete 21
      2.2.2. NOx abatement by cementitious materials 23
      2.2.3. Field experiments by PICADA Project 25
      2.2.4. NOx abatement performance in Umbreto Tunnel – Rome 28
      2.2.5. Case study– Leopold Tunnel 31
      2.2.6. Summary of the performance of photocatalytic concrete 32
      2.2.7. NOx abatement of non-Cementitious Materials 33
      2.2.8. Case study - Torre de Especialidades Hospital Manuel Gea Gonzales 34
      2.2.9. Case study – TiO_2 Panel 37

   2.3. Pollution in Urban Areas 38
      2.3.1. Air Pollutants 38
      2.3.2. Built forms and Pollution dispersion 40
      2.3.3. Variation of Pollutants with heights 45
      2.3.4. NOx Pollution in Urban Areas 45
      2.3.5. Calculation of NOx emission in reference street 47

   2.4. Theory for Evaluation of photocatalytic façade 48

2.4.1. Kinetic equations for photocatalysis 49
2.4.2. Extension of Irradiance into kinetic equations 49
2.5. Conclusion 51

3. DESIGN SITUATIONS & PARAMETERS 52
3.0. Climatic Context: London 53
3.1. Translation of parameters to urban scenario 55
3.1.1. Extracting UV Irradiance from solar spectrum 55
3.1.2. Surface Wind velocity fields 56
3.1.3. Tools for analyzing the parameters 57
3.2. Design Situations 59
3.2.1. Case 1: Stand-alone building 59
3.2.2. Case 2: Street canyon 60

4. DESIGN STRATEGIES 63
4.0. Strategies for surface enlargement 64
4.0.1. Effect of surface enlargement on UV irradiance 66
4.1. Strategies for reduction of contact wind speeds 67
4.1.1. Roughness Strategy 1 67
4.1.2. Roughness Strategy 2 68
4.2. Conclusion 68

5. DESIGN METHODOLOGY 69
5.0. Conceptual Design 70
5.0.1. Wind velocity field on finalized concept 74
5.1. Conceptual Development 75
5.1.1. Optimization of results & comparison 76
5.2. Application in Street canyon 78
5.3. Conclusion 78

6. DESIGN DEVELOPMENT 79
6.0. Façade Modules 80
6.0.1. Façade Module 1 81
6.0.2. Façade Module 2 82
6.0.3. Façade Module 3 83
6.0.4. Façade Module 4 84
6.1. Materialization 85
6.1.1. Criteria for selection of materials 85
6.1.2. Comparison of the substrates 86
6.1.3. Fabrication of the panel 88
6.2. Fixing system of the panel 92

6.3. Application in urban scenario 94

7. Air Purification effect 95
7.0. Evaluation of photocatalytic façade for air purification 96
7.1. Simulation methodology 97
7.2. Fluid dynamics 98
7.3. Validation of parameters in the reactor model 100
7.3.1. Geometrical setup and boundary Conditions 100
7.3.2. Model Parameters 100
7.3.3. Visualization of Results 102
7.3.4. Comparison and validation 102
7.4. Translation of reaction Kinetics into urban environment 105
7.4.1. Geometrical Setup and boundary conditions 105
7.4.2. Model parameters 106
7.4.3. Visualization of results 109
7.4.4. Pollution abatement performance 111
7.5. Conclusion on the impact 112

8. CONCLUSION 113

9. RECOMMENDATIONS 115

10. REFERENCES 116

11. APPENDIX 121

LIST OF TABLES

Table 1 Reactions with target pollutants 12
Table 2 Effect of relative humidity on photocatalytic degradations 14
Table 3 Effect of light intensity on photocatalytic degradation 15
Table 4 Analysis of substrates and influence of coating technique 19
Table 5 Photocatalytic material properties and their corresponding applications in built forms 21
Table 6 NOx abatement with for varying weight of TiO2 in cement mortar (Cárdenas, Tobón, García, & Vila, 2012) 22
Table 7 Comparison of Pollutant degradation by photocatalytic pavements 24
Table 8 Pollutant degradation at the surface of the right-side walls 27
Table 9 Pollutant degradation at the surface of the left side walls 27
Table 10 Umbreto Tunnel environmental Conditions 29
Table 11 Summary of photocatalytic NOx abatement activities of TiO2-based concretes in bulk and spray coating for an irradiation of 10 W/m^2 33
Table 12 Literature summary of the photocatalytic NOx abatement activity of TiO2-based paints 34
Table 13 Target pollutants and their regulatory limits in urban policies 40
Table 14 Emissions in Putney high Street (G.J.M.Velder, 2013) (Savage & Turpin, 2011) 48
Table 15 Maximal daily total global irradiance for sunlight and UV-A (lumthaler et al, 1997) 56
Table 16 Summary of the design situations in urban environment 62
Table 17 Comparison of materials for facade panels 88
Table 18 Material properties used in Karamba for structural analysis of UHPC and ABS polymer panels 89
Table 19 Calculation of weight of UHPC Panels and analysis of stress developed in the panels 89
Table 20 Calculation of weight of ABS Panels and analysis of stress developed in the panels 90
Table 21 Determination of type of in reactor and street models 99
Table 22 Description of variables in equations for turbulent flow 100
Table 23 Boundary conditions applied in Navier Stokes and Mass balance equation 101
Table 24 Input parameters applied for validation of the setup (Hunger et al., 2010) 102
Table 25 Concentration of NO in the inflow air for the reactor model setup 102
Table 26 Comparison of the outlet NO concentration of the simulation model and the Laboratory experiment results from Hunger et al, 2010. 104
Table 27 Analysis scenarios for reference and TiO_2 treated street 105
Table 28 Boundary Condition of the Street reactor model 107
Table 29 Emission from vehicles passing over the street per second 108
Table 30 Input data used in in kinetic equations 108

LIST OF FIGURES

Figure 1 Air pollution in megacities across the globe 1
Figure 2 a) Via Verde Project, Mexico b) Smog-eating façade of the Hospital Manuel Gea González in Mexico 4
Figure 3 Simplified Research plan 6
Figure 4 Detailed Research Plan 7
Figure 5 Schematic representation of the charge transfer across semiconductor interface. 11
Figure 6 Heterogeneous photocatalytic degradation of Nitric Oxide 11
Figure 7 Effect of inlet NO_x concentration on NO_x degradation rate (Hüsken et al. (2009) 13
Figure 8 ΔE values reported on cementitious materials for different types of coatings (a: North, b: South) . 14
Figure 9 Pollutant degradation dependence on the UV irradiance 15
Figure 10 Influence of flow rate in pollutant degradation in laboratory (Angelo, Andrade, Madeira, & Mendes, 2013) 17
Figure 11 Characteristics of substrate and coating 17
Figure 12 Potential field of applications of TiO_2 coatings 20
Figure 13 Experimental set-up of the photocatalytic pavement (Chen, Li, & Yuan, 2007) 23
Figure 14 Percentage of pollutant degradation for 3 different concentrations over residence time (Chen, Li, & Yuan, 2007). 24
Figure 15 Section of the model street in PICADA Project 25
Figure 16 Field set up of the street canyon by PICADA with and without (reference) active surfaces 26
Figure 17 Diagrammatic representation of the pollutant degradation in the street canyon influenced by wind movement 28
Figure 18 Representation of the positions of the NOx measurement devices 29
Figure 19 A comparison of the NOx level at the center of the tunnel before (up) and after the renovation (down) 30
Figure 20 Experimental set-up scheme for Leopold Tunnel II test site in Brussels for NOx abatement 31
Figure 21 Photocatalytic paint on the busy lanes of Manila, Philippines 33
Figure 22 Photocatalytic facade of Torre de Especialidades Hospital Manuel Gea Gonzales, Mexico 34
Figure 23 Modelled X-shape Prosolve370e module (Red highlighted portion is analyzed for irradiance) 35
Figure 24 Average Irradiance analysis for three different sun altitude angles in a year on a module of Prosolve370e 36
Figure 25 Fixing detail of Prosolve370e 36
Figure 26 Design Parameter and panel generation (Red spots: Zones of maximum annual irradiation) 38
Figure 27 Perspective and elevation of the panels by elimination of low irradiation zones form the panel .. 38
Figure 28 Primary air pollutants and their sources (IEA, 2015) 39
Figure 29 Types of Pollutants and their transformation to secondary pollutants 39
Figure 30 Quick dispersion of pollutants with wind in urban sprawls like highways (left) & Circulation of Pollutants inside a Tunnel (right) 40
Figure 31 Wind flow pattern within the canyon for winds greater than 1. 5m/s perpendicular or almost perpendicular to the built forms 41
Figure 32 Pollutant recirculation on the leeward side of the street canyon (T.-B. Ottosen, 2015) 42
Figure 33 Pollutant dispersion fields for perpendicular and parallel wind flow in a street canyon measured at 0.5H of the street canyon for different lengths of the street (Wind speed = 4 m/s & aspect ratio 5) 42
Figure 34 Pollutant dispersion fields in the street canyon at 0.5H for wind flow at an angle between 0 to 90° to the street (Wind speed = 2.0 m/s & aspect ratio 3); (Barmpas, Moussiopoulos, & Vlahocostas, 2006) . 43
Figure 35 Pollutant dispersion field for wind velocity of 2.0 m/s at an angle of 45° (aspect ratio 1) 43
Figure 36 Pollutant dispersion along the section of the street with an aspect ratio of 1 ((Muilwijk, Schrijvers, Wuerz, & Kenjeres, 2016) 44
Figure 37 Variation of pollutant concentration over the height of a building in London while concentration at ground floor level is considered as 100% 45

Figure 38 Most polluted cities with vehicular traffic (Annual mean NO_x level = 40 $\mu g/m^3$); Source: EEA, Aerosol and Air quality Research; Central Pollution board 46
Figure 39 NOx Pollution in London and exceedance of annual limits 46
Figure 40 Dependence of reaction rate constant of NO as a function of irradiation 50
Figure 41 Yearly average humidity levels (left); Yearly average wind speed (right) (Climate Consultant 6.0) 53
Figure 42 Number of precipitation days for various months in a year (Source: Meteoblue) 54
Figure 43 Incident solar radiation on the vertical built surfaces 55
Figure 44 Solar spectrum and its energy composition (Source: WE forum) 55
Figure 45 Influence of surface roughness on the velocity field on the facade; from left case a, case b and case c 57
Figure 46 Computational domain for Wind velocity field analysis for perpendicular flow (left) and parallel flow (right) 58
Figure 47 UV-irradiation (7-hour average) on the South facade of a stand-alone building (10 m height) .. 59
Figure 48 Wind velocity-field over the surface of the facade for perpendicular flow with velocity 5 m/s 60
Figure 49 UV irradiation (8-hour average) over the south facade in a street canyon of aspect ratio 1. 61
Figure 50 Wind velocity field between the street canyon for wind flow parallel to the street 61
Figure 51 Surface enlargement design principle for south façade 64
Figure 52 Conceptual surface enlargement strategies of 1 x 1 m facade panel 66
Figure 53 UV irradiation level on a sinusoidal test panel (not optimized for irradiation) 66
Figure 54 Wind velocity field measured for surface with projection elements at a height of 5m for a 10 m tall building (Computational domain 2 (right) is used from Figure 46) 67
Figure 55 Wind velocity field measured for surface with voids at a height of 5m for a 10 m tall building (Computational domain 2 (right) is used from Figure 52) 68
Figure 56 Methodology of design and tools used to achieve the objective 69
Figure 57 Chart depicting the considerations accounted for the conceptual phase 70
Figure 58 Grid patterns chosen to apply design strategies 70
Figure 59 Variables to modify the surface enlargement and roughness factors 71
Figure 60 Comparison of output on surface enlargement for various shapes and selection of ones with similar enlargement values 72
Figure 61 Comparison of UV irradiance for the analysis period for the outputs 73
Figure 62 Wind flow path and velocity field over the facade surface of the concept with flow parallel to the façade 74
Figure 63 Growth of the hexagonal tessellation using rotation as the principle 75
Figure 64 Hexagons indicated using same colors have same variables for the optimization process 75
Figure 65 Graph from Octopus plugin plotted with the optimized results 76
Figure 66 Comparison of Optimized geometries for year-round irradiation for South facade 77
Figure 67 Variations in level of Irradiance on the designed panels in a street canyon of a south façade of aspect ratio 1 78
Figure 68 Basic module that repeats to create the facade pattern (left); side view of the tile module (right) 80
Figure 69 Step 1: Triangulating the facade pattern; Step 2: Magnifying the scale of the panels into hexagonal patterns 80
Figure 70 Hexagonal facade modules 81
Figure 71 Modularizing along the profile of the panel as an extension of the hexagonal packing 82
Figure 72 Simplified rectangular paneling 83
Figure 73 Final module of the facade 84
Figure 74 Spacing between the pattern is introduced to accommodate the support. 89
Figure 75 Fabrication techniques considered for casting UHPC Panels 90
Figure 76 Process of Injection casting of UHPC using a male and a female mold for the façade panel. 91
Figure 77 Supporting structural grid for the facade panels on a loadbearing wall 92
Figure 78 Fixing detail of the facade panels 92
Figure 79 Layout of the Facade system mounted over a wall 93
Figure 80 Front view of the facade panels installed on facade 94
Figure 81 Application of facade panels as acoustic barriers and cladding for elevated roadways 94
Figure 82 Process of Evaluation of the designed facade panel 97

Figure 83 Steps involved in setting up the model in COMSOL Multiphysics 98
Figure 84 Pavement model in COMSOL for NO abatement evaluation 101
Figure 85 Velocity field in the reactor indicating the laminar flow 102
Figure 86 Concentration of NO flowing over the photocatalytic surface 103
Figure 87 Points at which NO measurement is taken at the outlet 103
Figure 88 Comparison of the Concentration NO at the outlet of the simulated reactor and laboratory experiments. 104
Figure 89 Representation of street scenarios indicating the treated surfaces 105
Figure 90 Section of the modelled street with the designed facade indicating the boundaries, flux and the measurement section (left); The surface highlighted in red are modeled as the flux (right)..... 106
Figure 91 Faces of the facade panels included and excluded in the evaluation model are highlighted 107
Figure 92 Wind Velocity field for the street with flat facade (Scenario 1: left); Designed facade (Scenario 2: right) at velocity = 2 m/s 109
Figure 93 Flat panel: Pollutant (NO) concentration profile without (left) and with photoactive surface (right) for flat façade panels with inflow velocity of 2 m/s 110
Figure 94 Designed Panel: Pollutant (NO) Concentration profile without(left) and with (right) photoactive surface (inflow velocity: 2 m/s)..... 110
Figure 95 Pollution abatement by the flat facade with and without the photocatalytic active surface for summer and winter for inlet velocity of 2 m/s..... 111
Figure 96 Pollution abatement by the designed facade with and without the photocatalytic active surface for summer and winter for inlet velocity of 2 m/s 111
Figure 97 Pollution abatement by the designed facade with and without active surface for summer and winter for inlet velocity 3 m/s..... 112

Graduation Calender

	November				December				January				February				March				April				May				June				July
	W-1	W-2	W-3	W-4	W-1	W-2	W-3	W-4	W-1	W-2	W-3	W-4	W-1	W-2	W-3	W-4	W-1	W-2	W-3	W-4	W-1	W-2	W-3	W-4	W-1	W-2	W-3	W-4	W-1	W-2	W-3	W-4	W-1
Problem Statement - Urban Air Quality																																	
Technological Possibilities (Air quality)																																	
Presentation		P1																															
Selection of technology																																	
Photocatalytic Building Materials																																	
Principle of Pollutant degradation																																	
Urban Air pollution - Norms & Regulations																																	
State of Art																																	
Photocatalytic Products & Applications																																	
Operating conditions																																	
Lab and Field Application & Tests																																	
Quantitative performance & Comparison																																	
Case study in Building applications																																	
Types of coatings and possible substrates																																	
Formulating Research Questions																																	
Application in Urban Context																																	
Emission from Vehicles																																	
Dispersion of Pollutants in Urban areas																																	
Urban envelopes - A review																																	
Presentation										P2																							
Design Principles and Objectives																																	
Possibilities and restraints for design																																	
Research on Individual design objectives																																	
Geometrical Influence in Design (Wind)																																	
Surface Enlargement																																	
Achieving Maximum Irradiation																																	
Tools to achieve the objectives																																	
First design phase (Photocatalytic Surface)																																	
Presentation																			P3														
Façade Concepts																																	
Combining the design objectives																																	
Adaptating design- various built typologies																																	
Façade Taxonomy, Assembly & Details																											P4						
Evaluation of the performance of material																																	
Final Design Products																																	
Report & Presentation																																	
Conclusion & Recommendations																																	
Report & Presentation																																	P5

1. INTRODUCTION

Figure 1 Air pollution in megacities across the globe

Air is vital for the survival of any creature. Clean air is a basic requirement of human health and well-being. However, the air that we breathe today is composed of dangerous pollutant particles that harm our health over long-term exposure. Today 55% of the world's population live in urban areas, a proportion that is expected to increase to 68% by 2050 (UN DESA, 2018). Air pollution continues to pose a significant threat to health worldwide. According to World Health Organization, more than 80% of the population residing in urban environments are exposed to air quality levels that breach the limits set by the organization.

While many parts of the world are affected by such adverse situations, urban air quality is a global concern especially in megacities (cities with population more than 10 million people). 98 % of the cities in low-income and middle-income countries and 56% of cities in high-income countries do not meet WHO air quality guidelines (World Health Organization, 2016).

Poor air quality is attributed to rapid urbanization, change in land-use pattern, industrialization, population growth, transportation sector and intensive energy use patterns. The complex interaction between the emissions from these anthropogenic activities and surrounding environmental factors results in poor air quality. This has a major effect on the human health, animals, plants and the urban climate (formation of smog, urban heat island effect etc..).

Hence, air pollution is inescapable with dirty air blanketing our cities, and the microscopic pollutants penetrate deep into the respiratory and circulatory system resulting in high risk of stroke, heart diseases, lung cancer, chronic and acute respiratory diseases like asthma. The major consequence of the poor air quality is 7 million early deaths every year (World Health Organization, 2016).

Every industry is resource consuming and is responsible for the current situation in their own way by adding to adverse emissions. Though, the most appropriate solution would be curbing the pollution at its sources, additional active and passive measures need to be undertaken at various scales to reverse the situation.

Building industries have evolved to adapt net-zero energy strategies to reduce the pressure on energy grids and become self-sustained. It is necessary to go a step further to also understand and adopt strategies to respond to the immediate urban scenario by offering environmental benefits.

This thesis focusses on adopting passive pollution abatement strategies that can be widely integrated into dense urban areas and understand the beneficial impact on pollution abatement.

1.1. Context

Large areas of urban environment are comprised of built surfaces that are boundaries between indoors and the outdoors. Building envelopes are designed to achieve maximum comfort for the interior occupants sealing it from the outdoor environment ignoring its potential to contribute to the urban scenario. However, little is done to design the envelopes to benefit the public sphere. In many contexts, there is a strong interface of people between the urban environment and built forms.

Hence, it is required to re-imagine the large surfaces of the built-form as potential infrastructure that could improve the urban climate by alleviating problems like urban heat island effect and pollution. Facades should be designed to contribute to the public health by filtering air, regulating temperature, generating breeze etc. In this consideration, the building surface could be treated as an urban infrastructure under public works or private development (Sung, 2016).

1.2. Problem Statement

Current approaches for urban responsive façades are green surfaces that dissipate the solar radiation and improve the surrounding air quality. Though they offer a wide range of benefits, high initial cost of installation and intensive regime of maintenance, irrigation and care system has restricted its adoption in a broader context. Henceforth, it is appropriate to think of building materials that can passively reduce air pollutants in the environment.

One such advancement in the material science is the application of photocatalysts such as TiO_2 in the form of nanoparticles in the construction materials which reduce the concentration of surrounding pollutants. These innovative materials can be easily applied on facades, with both de-soiling and de-polluting properties would be a significant step towards beautification of cities and improvement of air quality (Maggos, et al., 2007). The objective of this thesis is to focus on facades systems contributing to air quality especially using photocatalytic building materials that require a one-time installation and less maintenance regime.

As a designer, it is important to apply TiO_2 coatings on façade panels such that they achieve optimal conditions for good performance. Therefore, understanding the working principles and operating conditions of photocatalysts is necessary to derive the design principles. Further research about its applications on various materials is required to integrate them onto façade systems. The geometrical form of the façade governs the amount of incident irradiation and contact wind speed which supports the efficiency of the material. Integration of design with suitable material in pollution hotspots would give the best result for the surroundings. Hence, identifying urban situations as variables is also necessary and would be a governing principle in the application of design.

1.3. Environment and Urban regulations

Most cities around the world are affected by sub-standard air quality especially in the past few decades. And, urban policies have a crucial role in mitigation of pollution and widespread adoption of pollution abatement strategies.

The current environmental regulations imposed by the governments of various countries have stimulated the development of new strategies to assess the lessening of polluting agents like the nitrogen oxides (NOx), sulfur oxides (SO_2), carbon monoxide, volatile organic compounds (VOCs) and particulates.

Countries like Mexico that stood at No:1 as the most polluted city in 1992 has been taking measures at urban scale in the form of vertical gardens in pollution hot spots of the city (Via Verde Project). Via Verde is a community-initiated project with the goal of interconnecting the 1000 pillars of the elevated motorways into a vertical garden over a span of 27 Km. They function as air filters, noise barriers and heat regulators of the immediate surroundings. Research suggests that it will filter 27,000 tons of gas and provide clean oxygen for 25,000 citizens.

Apart from green walls, they have also been adopting photocatalytic building materials to enhance the air quality.

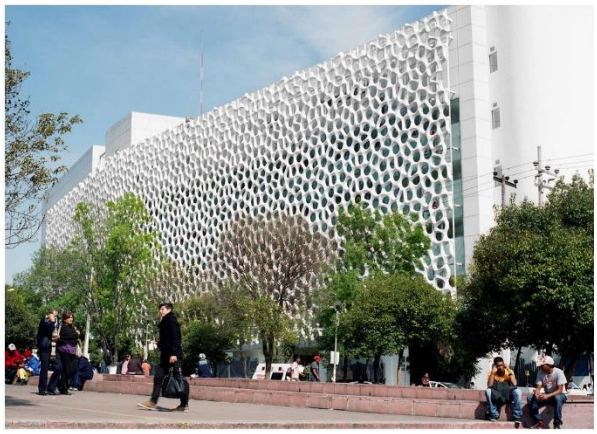

Figure 2 a) Via Verde Project, Mexico b) Smog-eating façade of the Hospital Manuel Gea González in Mexico

In, UK, the Environmental Industries Commission (EIC) recently published a report on the technological options for tackling air pollution (EIC, 2015). Five options had been investigated in detail for policy-framing to mitigate air pollution. They were: (i) Replacing 300,000 diesel cars with electric vehicles (ii) Replacing 90,000 diesel cars with new Euro 6c diesel cars, (iii) Retrofitting 10,000 old buses with diesel particulate filter (DPF) and selective catalytic reduction (SCR) systems, (iv) Switching 3,000 electricity generators on urban construction sites from red diesel to renewable diesel and **(v) Applying titanium dioxide-based coatings** (that can degrade NOx in air under the action of UV light) along highly polluted roadways. The study had also concluded that TiO2 based coatings were the second low cost strategy to reduce NOx pollution from vehicles. Hence, there is a potential in adapting photocatalytic material from the perspective of policy framework.

1.4. Research Question

The question is framed as a result of understanding the dependence of efficiency of the photocatalyst onto which it is coated and performance inhibiting factors:

How can façade cladding panels with photocatalytic coating be designed to increase the active surface area for pollutant degradation in response to performance inhibiting factors in urban environments and what would be their effect in improving the air quality?

1.5. Sub-research Questions

The potential effect in pollution abatement obtained for this material is based on its functional chemistry. Understanding the material science and the chemistry involved is necessary.

- **What is photocatalysis mechanism, necessary operating conditions and their scope in pollutant degradation?**

Photocatalytic building materials have been developed by various construction industries for urban applications and have been tested to prove their capabilities in air purification.

- **What is the state of art of these materials for air purification in urban scenarios for air purification?**

Surface design of the façade module is dependent on the irradiance levels and flow rate of pollutants. Identifying suitable design variables and tools to achieve optimal solar irradiation is critical.

- **What are the parameters and constraints driving the design and application of the photocatalytic façade panels?**

It is necessary to accommodate the design into a conventional system for widespread application and easy fabrication and installation.

- **How could this technology be integrated into façade systems for widespread applications?**

The goal is integrating these technologies into everyday scenario to realize the air quality improvement. Therefore, it is necessary to quantify the air purification effect of the TiO_2 coating on façade panels. A stepped strategy would be followed to answer this sub-research question.

What is the extent to which these materials can reduce the air pollutants in an urban scenario?

- To what extent is the designed panel's performance better than a flat façade panel coated with TiO_2?
- What would be the range of pollution abatement percentage that can be obtained in street canyons?

1.6. Research Overview

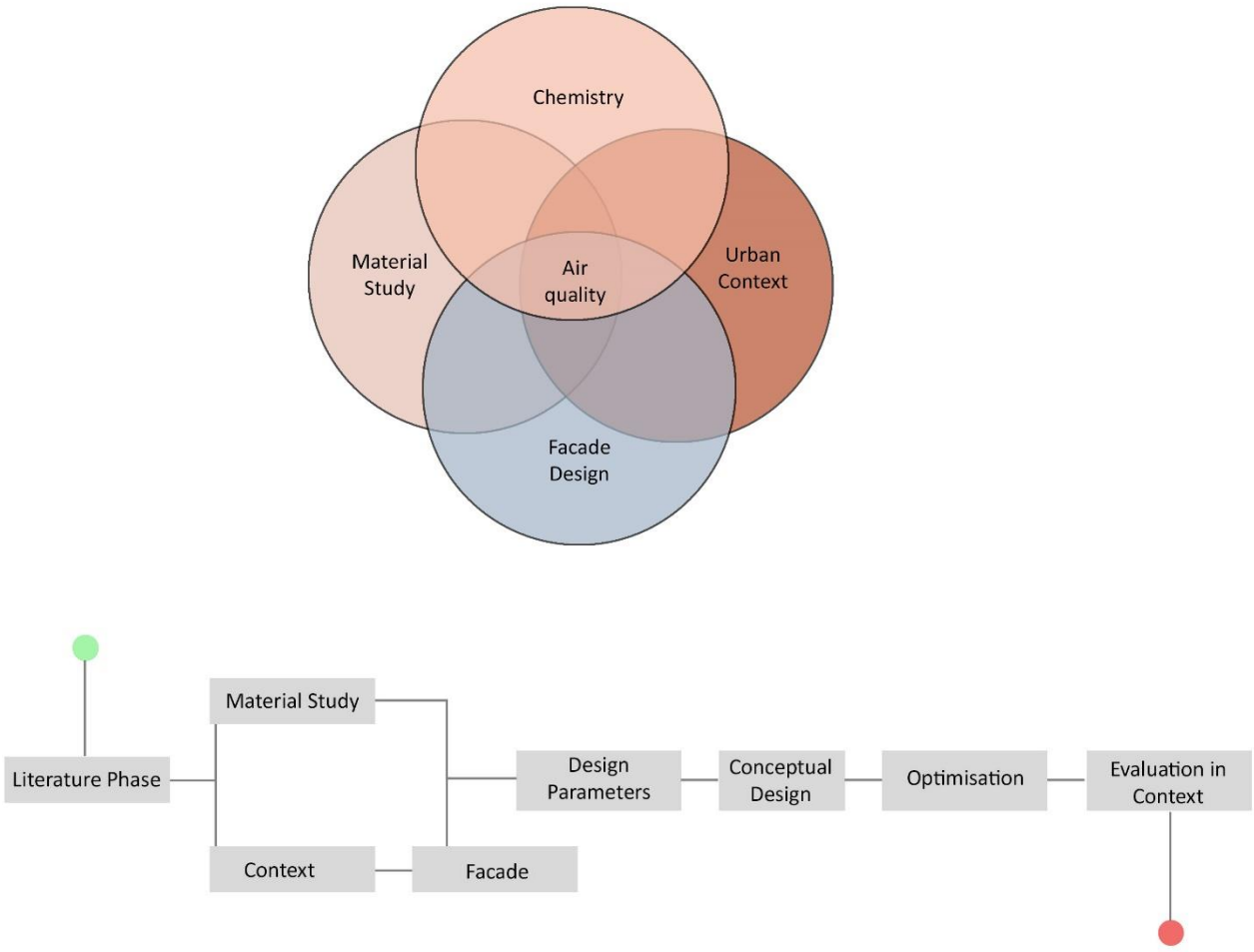

Figure 3 Simplified Research plan

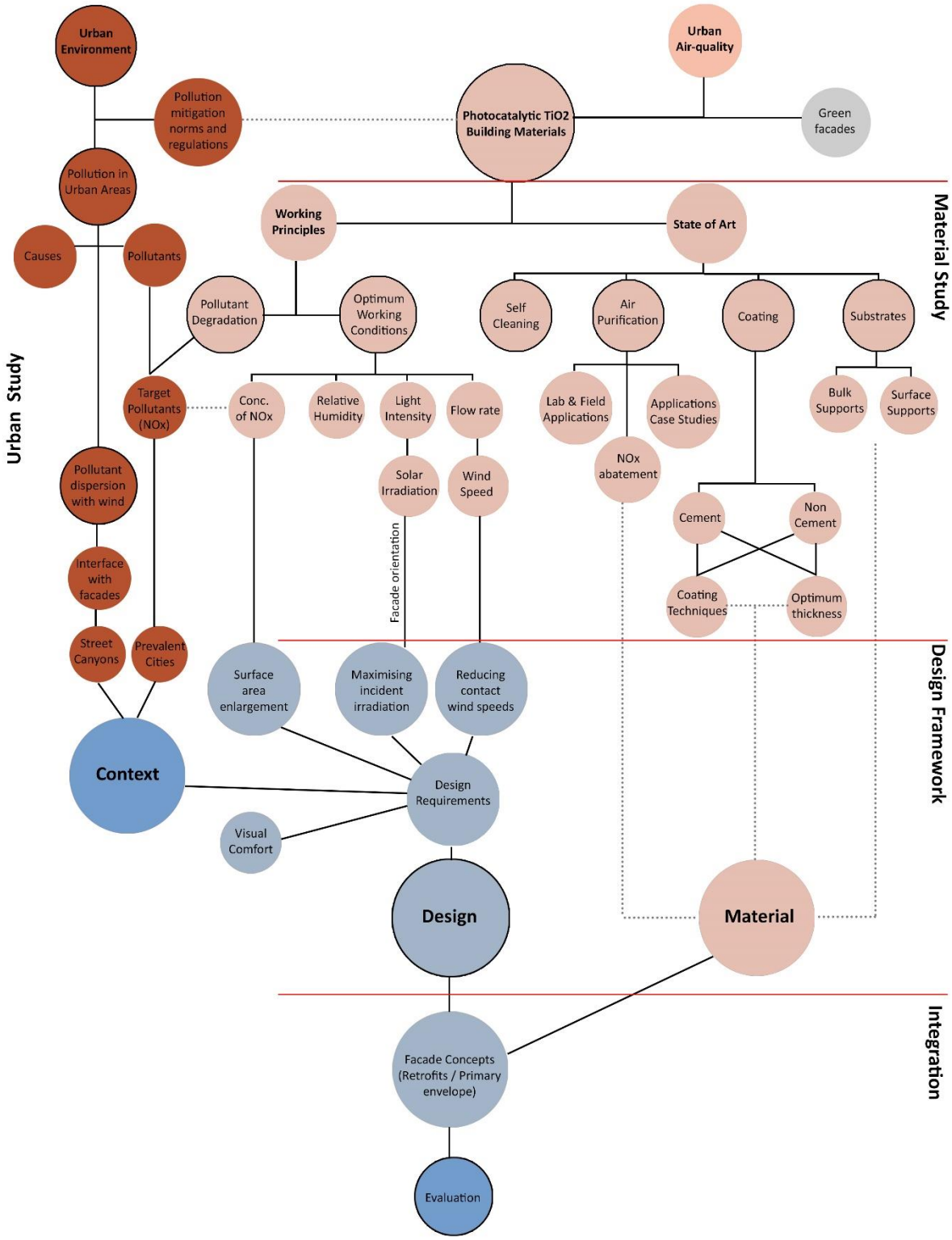

Figure 4 Detailed Research Plan

02 LITERATURE REVIEW

Chapter Overview

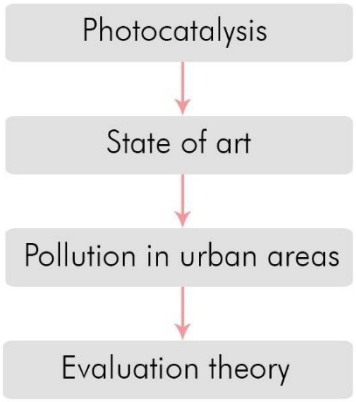

The chapter has been divided into four parts. The first part is an overview of the chemistry of photocatalysis, photocatalyst application and their favorable operating conditions for pollutant degradation.

The second part of this chapter explains their current application in urban environments like tunnel systems, pavements and façade surfaces along with applied case studies. First few case studies justify the pollution abatement capacity of such materials in urban scenarios while the rest talks about the design methods ad strategies.

Third part gives a brief of the air pollution and pollutants in cities, their causes of emissions and their dispersion pattern amidst the built forms and justifies the potential of façade surfaces as photocatalytic substrates.

The last part of this chapter is a theoretical description of the Langmuir-Hinshelwood model adopted to evaluate the air purification effect of photocatalytic façade which will be used in the final part of this thesis.

2.1. Photocatalysis

Photocatalysis can be defined as the acceleration of photoreaction in the presence of a catalyst using light energy and water. The word is derived from Greek language where:

- The prefix photo means light and
- Catalysis is the process where a substance involves in altering the rate of a chemical transformation of the reactants without the catalyst itself being altered in the end.

Hence, photocatalysis is a process where light and catalysts are concurrently used to support or speed up a chemical reaction (Saravanan, Gracia, & Stephen, 2017).

Interest in photocatalysis and progress can be traced back to 1972 when Fujishima and Honda discovered the photochemical splitting of water into hydrogen and oxygen in the presence of TiO_2 under ultraviolet (UV) light in solar spectrum (Ibhadon & Fitzpatrick, 2013). This was the pioneering project using photocatalyst under natural light. From then on, extensive research had been carried out to produce hydrogen from splitting water molecules as an alternative for fuel using the semiconductor catalyst materials. Over the years, this use of this catalyst has been shifted towards removal of organic and inorganic pollutants from water and gaseous phase focusing towards environmental clean-up applications.

Titanium dioxide (TiO_2) based photocatalysts are widely considered as an attractive approach for their rapid destruction capabilities of organic compounds from polluted air and wastewater. (Hashimoto, Irie, & Fujishima, 2005).

2.1.1. Photocatalysts

Various photocatalysts have been widely used and studied like ZnO (Zinc Oxide), WO_3 (Tungsten trioxide), TiO_2 (Titanium dioxide), CdS (Cadmium Sulphide) and PbS (Lead Sulphide). An ideal photocatalyst must have good photoactivity (especially in visible or UV range of sunlight), biological and chemical inertness, stability towards photo-corrosion, low toxicity and low cost (Ibhadon et al., 2013). Among the previously mentioned metallic oxides TiO_2 has excellent pigmentary characteristics, high UV absorption and stability for catalysis which makes it the most suitable for applications in large scale purification.

Titanium dioxide (TiO_2) occurs in three crystalline forms – rutile, anatase and brookite. Since brookite is unstable, it is not discussed in terms of photocatalysis. Anatase is the most stable form of TiO_2 which can be converted to rutile phase at temperature above 700 °C. High stability and ease of preparation of anatase makes it the most efficient in terms of photocatalysis compared to rutile. Hence, the TiO_2 discussed throughout the literature review and further is only in anatase phase.

Property	Anatase	Rutile	Brookite
Stability	Highly stable	Stable	Unstable
Band gap (eV)	3.26	3.00	3.13

Degussa P-25 is the most commonly used commercially available form of TiO_2 which is composed of 75% of anatase and 25% of rutile. However, current developments are focused at doping these catalysts with metals and non-metals that could enable them to function under visible light and shorten the time needed for degradation (Ibhadon et al., 2013). Application of doped catalysts lead to increased degradation of pollutants over a very short range of time compared to their functionality in UV range of light. However, in the literature review, doped catalysts are neglected.

2.1.2. Mechanism of photocatalysis

The photocatalytic reactions are initiated by the absorption of UV radiation with energy equal to or greater than the band gap of the semiconductor (Ibhadon et al., 2013). A photocatalyst like TiO_2 when it absorbs UV-A irradiation (320 – 400 nm), it generates electron-hole pairs as shown in the equation below:

$TiO_2 + hv = e^{-cb} (TiO_2) + h^{+vb} (TiO_2)$

where cb is the conduction band and
vb is the valence band
hv is the incident UV radiation
e^- is the electron donor while h+ is the hole.

Conduction band is the electron orbitals that an electron can jump into a valence band. The electrons in these orbitals have enough energy to move freely in the material and participate in redox reactions.

At times the electron and hole can recombine resulting in no chemical reaction by releasing the absorbed light energy as heat. Or on the other hand, they can participate in redox reactions with adsorbed species as the valence band hole is strongly oxidizing while the conduction band electron is strongly reducing.

On the semiconductor surface, the excited electron and the hole can participate in redox reactions with water, hydroxide ion (OH^-), organic compounds or oxygen leading to mineralization of the pollutant (Ibhadon et al, 2013).

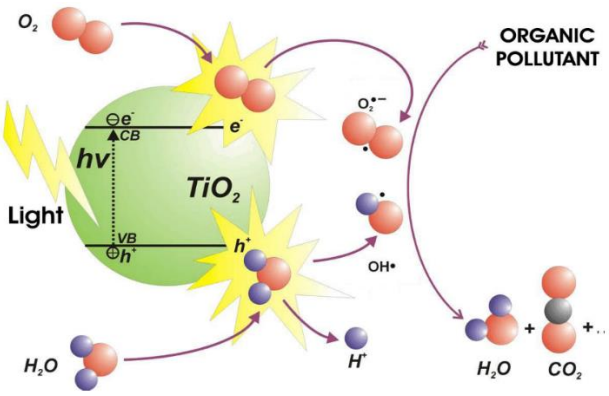

Figure 5 Schematic representation of the charge transfer across semiconductor interface.

Thus, the mechanism of photocatalytic degradation can be divided into three stages:

i. Diffusion of reactants (Pollutants) to the surface of semiconductor
ii. Adsorption of gaseous reactants (Pollutants) on the photocatalytic surface (Equations 1-3)
iii. Generation of electron-hole pairs (Equations 4&5)
iv. Oxidation of NO and reduction of water (Redox reactions: Equations 6-10)
v. Desorption of products from the surface of the semiconductor in the form of nitrates for Nitrogen dioxides (NO_x) and sulphates for Sulphur dioxides (Ibhadon & Fitzpatrick, 2013).

$$TiO_2 + H_2O \overset{K_{H_2O}}{\rightleftarrows} H_2O_{ads} \quad \text{.....} \quad 1$$

$$TiO_2 + O_2 \overset{K_{O_2}}{\rightleftarrows} O_{2ads} \quad \text{.....} \quad 2$$

$$TiO_2 + NO \overset{K_{NO}}{\rightleftarrows} NO_{ads} \quad \text{.....} \quad 3$$

$$TiO_2 \overset{h\nu}{\rightarrow} e^-_{CB} + h^+_{VB} \quad \text{.....} \quad 4$$

$$TiO_2\left(e^-_{CB} + h^+_{VB}\right) \rightarrow TiO_2 \quad \text{.....} \quad 5$$

$$h^+_{VB} + H_2O_{ads} \rightarrow HO^{\bullet} + H^+ \quad \text{.....} \quad 6$$

$$e^-_{CB} + O_{2,ads} \rightarrow O_2^{\bullet -} \quad \text{.....} \quad 7$$

$$NO_{ads} + OH^{\bullet} \overset{k_{NO}}{\rightarrow} HNO_{2,ads} \quad \text{.....} \quad 8$$

$$HNO_{2,ads} + OH^{\bullet} \overset{k_{HNO_2}}{\rightarrow} NO_{2,ads} + H_2O \quad \text{.....} \quad 9$$

$$NO_{2,ads} + OH^{\bullet} \overset{k_{NO_2}}{\rightarrow} NO_3^- + H^+ \quad \text{.....} \quad 10$$

Figure 6 Heterogeneous photocatalytic degradation of Nitric Oxide

Other target pollutants of the photocatalytic materials and their reactions are mentioned in the table below:

Pollutant	Photocatalytic Reaction	References
Sulphur dioxide (SO_2)	OH + SO2 → HOSO2, HOSO2 + O* → OH + SO3	(Zhao, Han, Shao, & Feng, 2009)
Volatile Organic Compounds (VOC's)	Multiple reactions possible	(R & Brown, 1995)
Carbon monoxide (CO)	CO + O* → CO2	(Hwang, Lee, & Choi, 2003)

Table 1 Reactions with target pollutants

In simple terms, the hydroxyl and oxide radicals created from the humid air reacts with the pollutants like SO_2, CO and NO_x to give harmless byproducts like sulphates, CO2 and nitrates respectively.

$$OH^- + \text{Pollutants} + O_2 \rightarrow \text{Products } (CO_2 + H_2O \text{ etc})$$

Though TiO_2 photocatalyst can degrade various pollutants, NO is the only pollutant considered for the evaluation of the façade panel in section 7.0.

2.1.3. Operating Conditions for Photocatalysis

Various operating conditions influence the performance of the photocatalyst towards pollutant degradation in an urban environment. The concentration of the pollutants in the immediate surroundings, mass transfer of the pollutants towards the photocatalytic sites, relative humidity of the air, light intensity, flow rate / residence time, amount of photocatalyst per unit area and types of substrates (materials supporting the photocatalyst) are the most prominent factors that will be discussed below.

Concentration of the pollutants:

As mentioned in section 2.1.2, the target pollutants are NO_x, SO_2, VOC's and CO. But TiO_2's high selectivity for NO_x and their dreadful effects of photochemical smog has led to focus on NO_x as the major target pollutants. Further discussion about pollutants refer to Nitrogen dioxides (NO_x) in the environment emitted from vehicular sources by combustion. Higher the concentration of pollutants, lesser is the degradation as most of the photocatalytic surface sites are used up and they attain passivation.

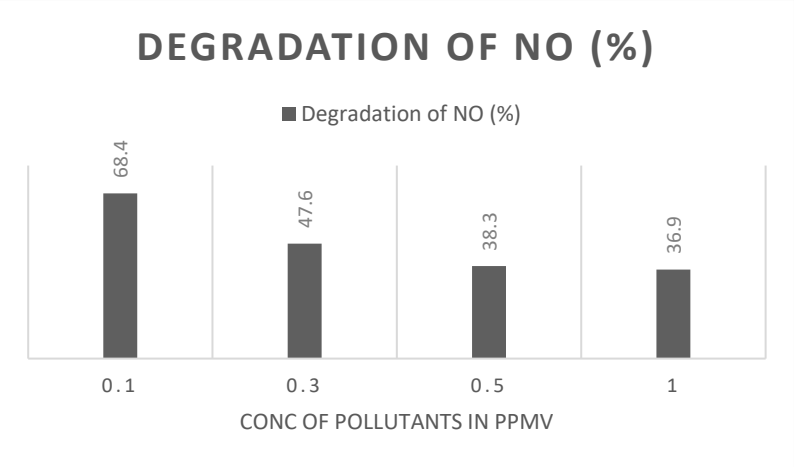

Figure 7 Effect of inlet NO_x concentration on NO_x degradation rate (Hüsken et al. (2009).

Hence, it is important to design photocatalytic surfaces with higher surface area to increase the active sites.

Relative humidity:

From equation 6 in Figure 6, it is seen that water plays an important role in photooxidation process since it contributes to the formation of active species OH^- and O_2^- radicals. Henceforth, it is expected that increase in RH increases the rate of the reaction. On the other hand, under the influence of UV irradiation, the surface of TiO_2 coating becomes hydrophilic and the water molecules tend to adsorb on the surface of TiO_2, thereby competing with the pollutants for the active sites. As can be seen, humidity could have both positive and negative effects on the photooxidation rate of a pollutant. The photocatalytic conversion of NO increases with the decrease of relative humidity from 50% to 20% (Maggos, Bartzis, Leva, & Kotzias, 2007).

The effect of humidity on the conversion of a pollutant also depends on its concentration. At ppb level the competition for adsorption sites between NO and water vapor is a thousand times more than applying ppm level pollutants. Thus, the photocatalytic activity decreases (Maggos et al, 2007). In urban scenarios when the pollution concentration is in the range of 100 – 200 ppb, high humidity range is an inhibiting factor.

Pollutant Tested	RH Range (%)	Effect on degradation	Reference
Nitrogen oxides	20 – 50%	Increase in RH, decrease in removal	(Maggos, Bartzis, Leva, & Kotzias, 2007)
Nitric oxide (NO)	0 to 75%	0 to 50%: Increased removal of NO 50 - 75%: remained constant	(Devahasdin, Fan, Li, & Chen, 2003)

Nitric oxide (NO)	80 to 100%	8 – 60%: Rate of NO removal increases quickly as RH increases 60 – 100 %: Rate of NO removal is reduced	(Wang & Hsieh, 2007)
Nitrogen oxides	30%, 50% and 70%	Increase in RH, decrease in removal	(Melo, Trichês, Gleize, & Villena, 2012)

Table 2 Effect of relative humidity on photocatalytic degradations

Effect of light intensity:

The band gap of TiO_2 is 3.2 eV which is effective only under UV radiation. The photocatalytic rate varies with light intensity which has been quantified by researchers. The degradation rate is proportional to light intensity to a certain threshold intensity beyond which it is proportional to the square root of the intensity. This has been showed by Herrmann et al. (2007) that the **threshold intensity is equal to 250 W/m² of irradiation**.

The intensity of light varies on different orientation of the façade. In fact, on a Northern elevation, less sunlight reaches the material surface compared to other orientations. Under this condition, the titanium dioxide needs more time to complete its photo activation (Maggos et al. 2007), which makes the presence of the coating less efficient as compared to the same application on a Southern façade.

Presence of direct solar radiation enhances the photocatalytic degradation. Andaloroa et al. 2016 has proved with an experiment where the northern and southern facades were covered with photocatalytic cement and the variation in the color of the material was analyzed for both the facades. Variation in color was measured as ΔE. Lower the ΔE, higher is the photocatalytic activity. In figure below, the values indicate the variation in color for different types of coatings.

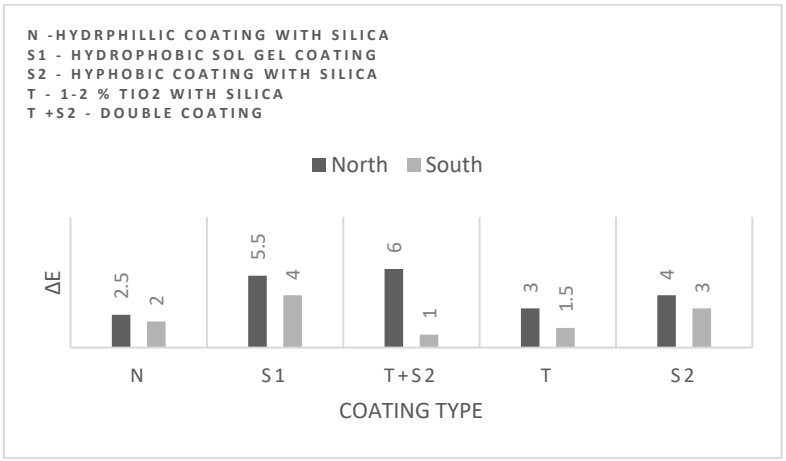

Figure 8 ΔE values reported on cementitious materials for different types of coatings (a: North, b: South)

Pollutant Tested	Light Intensity (W/m2)	Effect on degradation	Reference
Nitric oxide (NO)	0 – 12 W/m2	Reaction constant k increased from 0.06 mg/m3s at 1 W/m2 to 0.26 mg/m3s at 11 W/m2	(Hüsken, Hunger, & Brouwers, 2009)
Nitrogen oxides (NO & NO_2)	10 – 40 W/m2	With light intensity from 10 to 25 W/m2, significant increase in pollutant degradation rate. With intensity in 25 – 40 W/m2, pollutant degradation not as significant.	(Melo, Trichês, Gleize, & Villena, 2012)

Table 3 Effect of light intensity on photocatalytic degradation

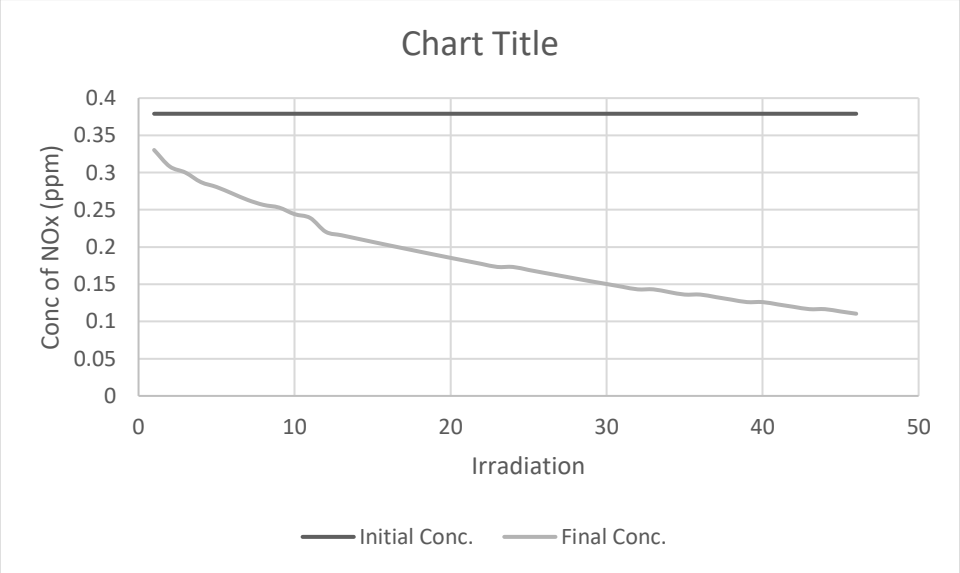

Figure 9 Pollutant degradation dependence on the UV irradiance

From the table, it can be concluded that **incident light intensity should be higher than 10 W/m²** for achieving more than 30% pollutant degradation at the surface of the photocatalytic material. UV irradiance below 10 W/m² is classified under low irradiance in many studies. Hence, 10 W/m² is set as the average threshold intensity over 7-hour average for an analysis day for comparing the modules of the façade.

Effect of particle size and amount of photocatalyst:

The particle size of TiO_2 has a strong influence on the photocatalytic activity. The size of the particles can range from a few nanometers to micrometers. The smaller the particle, larger is the surface area per unit volume (specific area) (Folli, Jakobsen, Guerrini, & Macphee, 2009). Micro-sized TiO_2 has shown to be moderately active while nanoparticle have higher activity due to increase in specific area (Folli et al. 2009).

The reactivity of TiO_2 is measured in terms of the reactive oxygen species (ROS) generated by different sizes of TiO_2 nanoparticles. According to Jiang et al (2008), the ROS activity per unit area measured was highest for 30 nm particles and the values were constant for sizes beyond 30 nm. For smaller particle sizes, the activity per area was found to decrease between 30 nm to 10 nm and becomes constant for particles smaller than 10 nm (Jiang, 2008).

For all catalysts, high active surface area is required. Therefore, typical photocatalysts should have a particle size in the range of 10-20 nm. This not only provides surface sites for adsorption, a necessary step in the photocatalytic process, but also reduces recombination processes, where photogenerated charge carriers recombine, preventing their participation in the important surface reactions. Hence, **the optimum size of the particles to be used in Nano deposition of TiO2 is 10-20 nm anatase particles**. Apart from the particle size, the distribution of particles is also important. According to Toma et al (2004), **4 mg/cm^2 distribution of TiO_2 powder is necessary to obtain a good photocatalytic conversion of pollutants**.

Effect of flow rate:

Flow rate is the volume of fluid which passes per unit time over a surface. The flow rate of pollutants on to the photoreactor strongly influences the absorption and degradation of the pollutants. **Higher the flow rate, lesser is the residence time of pollutants on the photoreactive surface.** An increase in the photocatalytic rate was observed for residence time (Ibhadon et al. 2013).

While flow rate can be controlled in a laboratory condition, it is harder to control the flow rate in an outdoor environment. This leads to lower performance of the photocatalytic materials in roads, tunnels and on built forms. This is one aspect that needs careful design of façade panels to channelize polluted air, reduce the wind speed and provide longer contact time (increasing the turbulence).

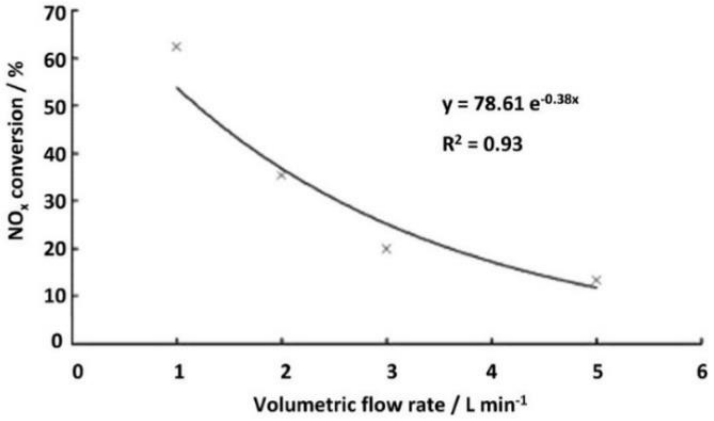

Figure 10 Influence of flow rate in pollutant degradation in laboratory (Angelo, Andrade, Madeira, & Mendes, 2013)

Effect of substrate and coating:

TiO_2 takes the form of the substrate on which it is coated. It is necessary to immobilize the coating on a substrate that supports it with durability. TiO_2 could be applied as a thin coating in a silicate binder or mixed in a bulk of material like cementitious mortar. The combination of the right type of substrate and right coating process gives maximum photocatalytic activity on the surface.

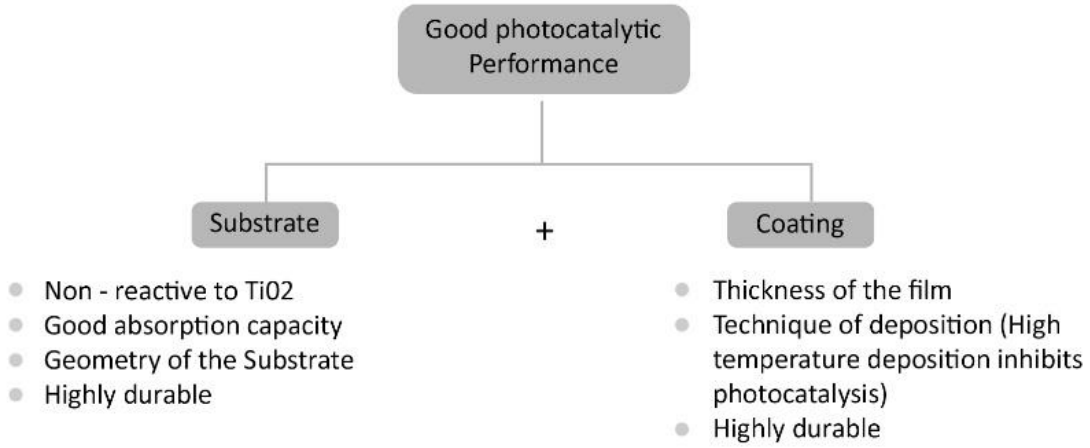

Figure 11 Characteristics of substrate and coating

The specific requirements for the substrate and method of immobilization are:

- It is highly important that the photocatalytic activity is not inhibited during the immobilization process.
- Good adhesion of the coating with the substrate.
- The substrate must be chemically inert to the catalyst.
- The substrate must be compatible with the environmental use.

Most commonly used substrates are glasses, quartz, concrete, thermoset plastics, porcelain, terracotta etc. Several studies have been conducted on NO degradation on glass substrates, building mortar and activated carbon filter. It was observed that over time pollutant degradation capacity of glass decreased due to its non-absorptive surface while NO_x oxidation on a mortar and activated carbon substrate remained constant due to their high absorption capacity (Martinez et al., 2011).

Apart from the substrate's nature, technique of deposition has a major influence on photocatalytic activity. Photocatalysis being a surface phenomenon, direct interaction of TiO_2 with UV is essential. Hence, mixing of TiO_2 in the bulk of mortar can only have a limited degradation of pollutant at the air/surface interface. In this case, the amount of TiO_2 used is high, and most of the photocatalyst is wasted in the internal structure where light is not available.

In this regard, coating technique is more beneficial as the thin film of nanoparticles is highly exposed to the polluted atmosphere. This results in less consumption of photocatalyst, better abatement of pollutants and cost reduction. Also, photocatalytic capacities can be replenished periodically by washing the top surface. However, it may not be the most durable coating.

The coating method must also render TiO_2 solidly fixed on the support. This can be achieved via a thermal treatment, addition of an anchoring substance to TiO_2, or by both methods. Several coating techniques like dip coating and spin coating can be used to spread the coating mixture over the support. Also post annealing at high temperature after coating provide strong immobilization. However, they require a large industrial set-up for implementing them. Hence, both these processes are neglected as high temperatures sinter the photocatalyst.

An intermediate approach would be to use a binder such as silica that achieves a balance between photocatalytic activity and immobilization (Angelo et al., 2013). Hence spray coating with silicate paints or cementitious suspensions with TiO_2 would be the most suitable option for surface treatment.

Substrate	Type of TiO2 coating	Process of Coating	Advantages of the Substrate	Disadvantages of the Substrate
Concrete	Mortar	5 % dry weight TiO2 is mixed in the bulk material	- Good absorption capacity of pollutant gases - Permanent Immobilization of the photocatalyst	- Relatively less photocatalytic activity than spray coated surfaces. - Large surface areas are required for air-purification

	Spray Coating	Cold Spray Technique	- Good absorption capacity of pollutant gases	- Requires periodic application of the coating
Quartz	Mortar / Spray coating		- Good absorption capacity of pollutant gases	-Good photocatalytic activity
Glass	Embedding	Thermal Spraying at high temperature	-Strong immobilization of TiO_2	-Poor absorption capacity -Less degradation of pollutants
Porcelain / Ceramic Tiles	Embedding	Thermal Spraying at high temperature	-Strong immobilization of TiO_2 -Absorption capacity can be controlled by porosity of the material	Anatase form of TiO_2 converts into rutile and loses its photoactivity
	Spray Coating	Cold Spray Technique	-Absorption capacity can be controlled by porosity of the material	- Requires periodic application of the coating
Polymer	Paint	-	-Good photocatalytic activity	An intermediate barrier between the polymer and photocatalytic coating is required

Table 4 Analysis of substrates and influence of coating technique

Effect of thickness of the photocatalytic films:

A material could be made photocatalytic either by applying a thin film of TiO_2 on a substrate or by mixing it with a bulk of material. The maximum thickness of crack free coatings that can be achieved is 0.5 microns. Sol-gel TiO_2 films vary in thickness from 0.2 microns to 0.8 microns.

In a material test conducted by Hanson et al (2013), the specimens with a thin topcoat of TiO_2 had a photocatalytic efficiency of 74% which is more than 3.5 times more effective as the specimens which had TiO_2 throughout the bulk.

2.1.4. Conclusion:

The operating conditions show the strong dependence of photocatalysis on climatic aspects like RH and light intensity. Careful choice of substrate and type of photocatalyst coating for the façade panel are critical for a good and long-term functionality of the material. Hence, the factors discussed above will be used as driving parameters for materialization of the façade concept in section 6.2.

2.2. State of the art in Building Industry

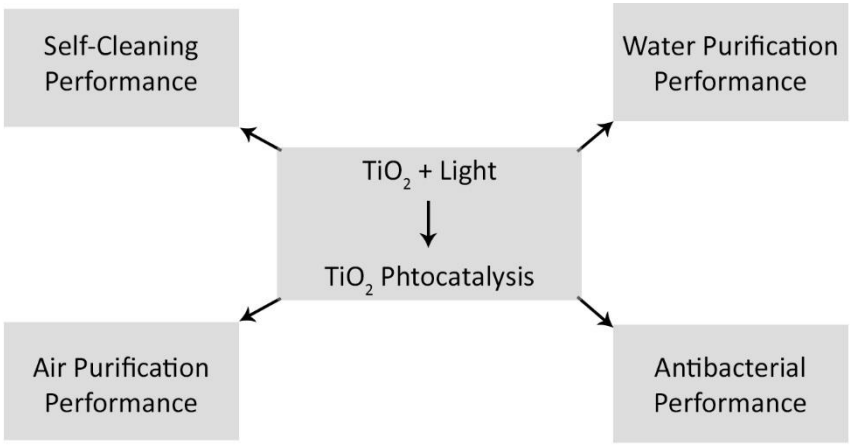

Figure 12 Potential field of applications of TiO_2 coatings

Two important properties of photocatalytic coatings of TiO2 had been discovered i.e. Self-cleaning effect (Hoffmann, Martin, Choi, & Bahnemann, 1995) and a photo-induced hydrophilicity ((Wang & Hsieh, 2007). Glass was the first of the construction materials to be tested with these coatings for providing self-cleaning and anti-fogging properties. The success achieved with application on this material broadened its scope to concrete.

From the mid-1990s, Mitsubishi Corp. (Japan), Italcementi SpA (Italy) and Toto (Japan), patented a range of photocatalytic concrete applications and cementitious products, including the famous brand NOxer and Italcementi launched TX-Aria (Self-cleaning concrte) and TX-Arca (Depolluting concrete) (Murata, Kamitami, & Takeuchi, 2018).

Sources	Material property	Category	Application
(Ibhadon et al. 2013)	Self - Cleaning	Buildings	Aluminum panels, tiles, building stone, crystallized glass and glass film
		Roads	Tunnel lighting, tunnel walls, traffic signs and soundproof walls
		Houses	Tiles on kitchen walls and bathrooms, exterior tiles, roofs and windows
		Paint	General-purpose paints and coatings
		Vehicles	Paint work, coatings for exterior surfaces of windows and headlights
(Beeldens, Cassar, Guerrini, &	Air cleaning	Indoor air cleaners	Room air cleaner, photocatalyst-equipped air conditioners and interior air cleaner for factories

Pimpinelli, 2007)		Outdoor air purifiers	**Horizontal Applications:** Concrete pavements, Paving blocks and paving plates, Other coating systems for pavements and roads (white topping, self-levelling mortars, ...), Roofing tiles, Roofing panels, Cement-based tiles **Vertical applications:** Indoor and outdoor paints - Finishing coatings, plasters and other final rendering cement-based materials, covering precast panels, Permanent formworks, Masonry blocks, Sound-absorbent elements for buildings and roads applications, Traffic divider elements, Street furniture, Retaining fair-faced elements **Tunnels:** Paints and renderings, Concrete panels, Concrete pavements, Ultra-thin white topping

Table 5 Photocatalytic material properties and their corresponding applications in built forms

Since 2000's, a large number of structures have been built using Italicementi's TX products in the southern part of Europe. The goal of these projects was to maintain the aesthetic appeal with pollution abatement. Some well-known examples include Church "Dives in Misericordia", Rome, ITALY; Air France Building, Roissy – Charles de Gaulle Airport, FRANCE; and Ciments Maroc Headquarter, MOROCCO. Palazzo pavillion, Milan is one recent example built in 2015 with a photocatalytic second skin that helps in NOx abatement.

Apart from these, 40 sites in Europe have been laid with photocatalytic pavements. However, amongst the best known are a parking lane in Antwerp, BELGIUM; the Castorweg road (1000 m^2) in The Netherlands.

2.2.1. Photocatalytic Concrete

Conventionally, photocatalysts are mixed directly with the concrete mix and are thus distributed throughout the bulk of the concrete. Cardena et al. 2012, had conducted an experiment to understand the optimum amount of TiO_2 that should be added to the cement mixture. De-pollution activity of cement paste samples, added with 0.5%, 1.0%, 3.0% and 5.0% (based on the dry weight of the cement used) of titanium dioxide nanoparticles was evaluated through the degradation of nitrogen oxides pollutants (Cárdenas, Tobón, García, & Vila, 2012).

Efficiency of the photocatalyst's abatement of pollutants was tested by the standardised procedure of ISO 22197-1 (Test methodology to predict the removal of Nitric oxide).

TiO2 (%) in Mortar	Anatase : Rutile	$X_{NOx, 65h}$ (%)	$X_{NOx, 28d}$ (%)
0.5	85:15	2.67	1.66
1	85:15	3.78	2.51
3	85:15	14.5	3.14
5	85:15	17.33	8.85
1	100:0	1.84	3.32
3	100:0	8.26	4.83
5	100:0	9.04	9.40

Table 6 NOx abatement with for varying weight of TiO2 in cement mortar (Cárdenas, Tobón, García, & Vila, 2012)

All cement pastes containing TiO_2 were proven to show photocatalytic properties, regardless of the ratio of anatase: rutile used or the percentage of TiO_2 added (Cárdenas et al. 2012). With increase in the percentage of photocatalyst, there was an increase in the NOx abatement. From the table above, for 5% of TiO_2 by dry weight in the mortar, the performance towards NO_x abatement was higher at both early and later stages. TiO_2 with 100:0 anatase: rutile shows a uniform performance over the 28 days of testing phase (Cárdenas et al. 2012).

According to Hanson et al, the quantity of TiO_2 used per square foot of surface area is an important factor due to the additional cost associated with adding TiO_2 to the mixture design. The mixture with 3% TiO_2 had a photocatalytic efficiency of 9% whereas the specimen containing 15% TiO_2 had an efficiency of 19%. The increase in photocatalytic efficiency was not linear, and specimens with 5% and greater TiO_2 percentages had similar results. This plateau effect is likely caused by the layering of particles which reduces the total number of TiO_2 particles available to participate in the photo-catalytic reactions. Hence, in all photocatalytic mortar 5% of TiO_2 by dry weight of cement is used.

Apart from academic studies on photocatalysis in construction materials, various projects have been initiated to test the depolluting capabilities of these photocatalytic materials. For example, EU projects, of which PICADA (Photocatalytic Innovative Coverings Applications for Depollution Assessment program) is one of the best known and has provided relatable comparisons of TiO_2 performances between laboratory and field studies. Other projects, e.g. NANOCRETE, HELIOCLEAN and LIGHT2CAT have contributed to the construction and NO_x abatement analysis of photocatalytic structures, e.g. street paving, vertical walls in street canyons, motorway barriers, etc. as realistic tests of concrete-supported photocatalysis under ambient and service conditions. The case studies from PICADA project and LIGHT2CAT are discussed in section 2.2.3 & 2.2.5.

2.2.2. NOx abatement of cementitious materials

NOx abatement performance of various urban applications is summarized in the forthcoming sections in a hierarchy from lab experiments to street canyon setup.
Lab experiments that are similar to the urban environment in pollutant concentration and irradiation level were studied to understand the extent to which photocatalytic materials could abate the NO_x content in air. The studies indicated below show the extent of pollutant removal for every meter square of the material.
The study discussed below is NOx abatement for a photocatalytic pavement setup in a laboratory:

Experimental set-up:

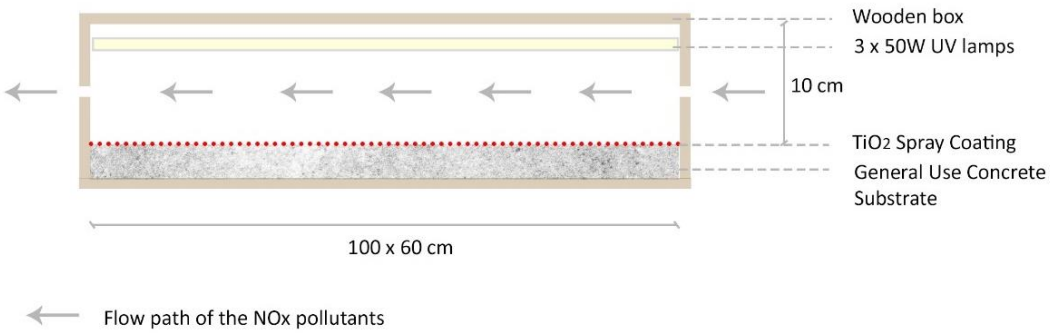

Figure 13 Experimental set-up of the photocatalytic pavement (Chen, Li, & Yuan, 2007)

Material:

The pavement slab (1 x 0.6 x 0.03 m^3) is made from 1:2:3 mix of cement: fine aggregate: coarse aggregate. The ingredients are mixed in the concrete mixing machine and cast in a wooden mold whose upper portion is covered with a reflective sheet and fixed with UV lamps as indicated in Figure 13. Once casted, TiO_2 Degussa P-25 is spray coated on the concrete surface with a loading of 33.33 mg/cm^2. The sample is cured periodically for seven days.

Light source:

The upper part of the wooden mold is fixed with three 50 W high output fluorescent lamps. Each lamp is individually controllable to alter the irradiation required. The total UV irradiance on the surface is 250 W/m^2 which is similar to that of the sunlight exposure for 11 hours. The reactors upper surface was covered with aluminum foil to reflect most of the light produced by the light source.

Residence time:

Residence time is reactor volume divided by flow rate. The experiment was performed at two different residence time of 5 min and 20 min.
Reactor volume: 1 x 0.1 x 0.6 m^3

Experimental Results:

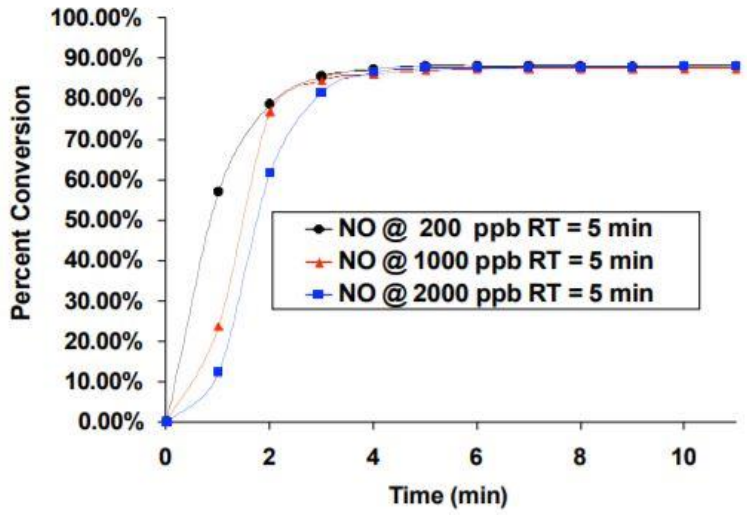

Figure 14 Percentage of pollutant degradation for 3 different concentrations over residence time (Chen, Li, & Yuan, 2007).

For a residence time 0-4 minutes in the reactor, the NOx abatement keeps increasing and becomes constant after 4 minutes up to 10 minutes.

Type of Coating	Light irradiation	Flow rate	RH (%)	Initial Conc. of pollutant	Final Conc. of pollutant	NOx abatement %	NOx abatement rate	Source
P-25 Spray coating	250 W/m^2	12 L/min	50 %	200 ppb	20 ppb	90%	0.01 $g/m^2/day$	(Chen et al. 2007)
10 mm thick TiO_2 mortar (NOXER)	-	9 L/min	50 %	400 ppb	288 ppb	26.9%	-	(Marwa M. Hassan, 2010)
5mm thick TiO_2 mortar (NOXER)	12 W/m^2	3 L / min	50 %	50-150 ppb	6-18 ppb	88%	0.013 $g/m^2/day$	(Murata, Kamitami, & Takeuchi, 2018)
3-10mm Mortar with 10% TiO_2	10 W/m^2	-		200ppb	-	-	0.21 $g/m^2/day$	(Melo et al. 2012)

Table 7 Comparison of Pollutant degradation by photocatalytic pavements

In Table 7, various experiments on photocatalytic pavements are summarized. Spray coated concrete block and mortar coated concrete block have similar NO_x abatement capacity in outdoor conditions. However, the experiment conducted by Melo et al. 2012 shows NO_x abatement that is 20 times higher than the NOXER and spray coated blocks. Further studies have been done to conclude on the extent of performance.

2.2.3. Case Study: Field Experiments by PICADA Project

Photocatalytic Innovative Coverings Application for Depollution Assessment (PICADA) is a project carried out under various organizations to assess the extent of NO_x abatement by cementitious photocatalytic materials under real environmental setup with controlled pollution and street geometry conditions. This project is an intermediate step between a real scale testing and laboratory testing to eliminate the unrealistic parameters.

Among various experiments conducted by PICADA, a pilot site of a street canyon was established in CTG cement plant in Guerille, France which will be discussed below. The pilot site comprises of three artificial street canyons with a pollution source at the center of the street continuously emitting NO_x, measurements of pollutants and meteorological measurements.

During real life tests, a significant number of unknown parameters (i.e. meteorological, human activities, types of air pollutants, street configuration etc.) arise difficulties on the establishment of quality and assurance of the measuring procedures and results. This study can be relied upon for urban applications as it considers the real world climatic and wind conditions of the site.

Context: Street measurements as set up at the site in 1:5 scale:

- Height of the building = 4 m;
- Width of the street= 2 m;
- Length of the street= 5 m

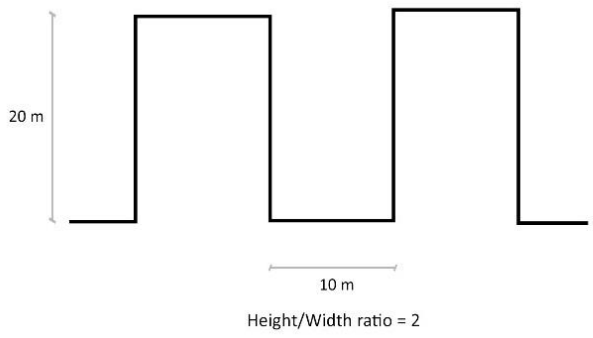

Figure 15 Section of the model street in PICADA Project

A series of four street canyons using shipping containers were constructed in 1:5 scale as indicated in figure above. Two street canyon's facades were covered with ordinary cement mortars with one canyon fed with pollution source. The other two street canyons were covered with Photocatalytic mortars with one canyon fed with pollutants from line source. The orientation of the axis of the street was 52.24° towards west from north.

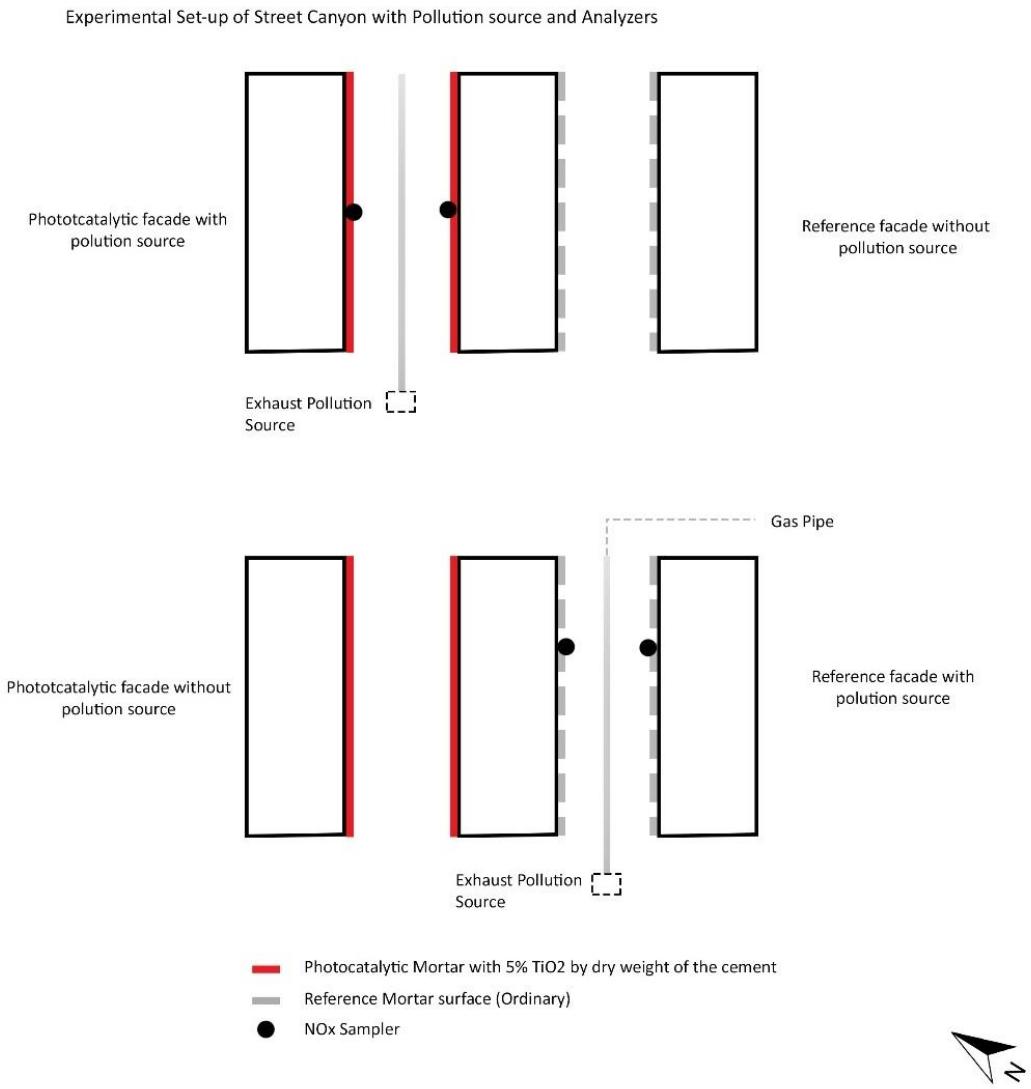

Figure 16 Field set up of the street canyon by PICADA with and without (reference) active surfaces

Material:

The material was a mortar mix for external covering produced by Italcementi Group, based on mineral binder treated with 3% TiO_2 (based on dry weight of the cement) and sand. The walls of the two canyons were covered with non-TiO_2 treated mortar panels (Reference Street) and the rest of the walls were covered with TiO_2 mortars. Street's floors were treated with a 2-layer protection coating with tar emulsion and gravels.

The campaign took place from 9th July 2004 to 3rd September 2004 between 9:00 and 16:00 hours. To ensure that the reference canyons and TiO2 mortar canyons were tested under similar conditions, both canyons were set up at the same location in two different times during the testing phase. Also, NO_x concentrations were evaluated per wind sector so that differences in wind directions could not affect the comparison between the two periods.

The difference in the pollutant levels between the reference canyon and TiO2 treated canyon would be a clear indicator of the performance of the material in pollution abatement. The

difference in NO_x levels in the street canyons depended a lot on the wind direction. This could be concluded from the considerable differences of NO_x levels near the left and the right walls of TiO_2 coated canyons. Right walls showed higher NOx abatement than the left walls.

Depending on the wind sector, the NOx concentration in TiO_2 canyon (right wall) presented 41.2 up to 82% variation than the one observed in the reference canyon for the same conditions. The corresponding percentages for the left wall varied between 36.7 and 75.1%. overall. Comparing with the reference canyons from Figure 17, it can be inferred that NO_x recorded in TiO_2 canyon were 36.7–82.0% lower than the ones observed in the reference one. The difference in the variation of pollutants closer to the walls are due to wind direction and the orientation of the wall. While the solar irradiation remained the same over the test periods, variation in wind speed and direction significantly affected the results.

	Wind Direction	Initial Conc of Pollutants	Final Concentration of Pollutants	Percentage of NOx abatement
Right Wall	North	45 ppb	20 ppb	44%
	North-east	43 ppb	25 ppb	41 %
	East	40 ppb	15 ppb	62.5 %
	South-East	62 ppb	12 ppb	80.6 %
	South	60 ppb	20 ppb	66.6 %
	South-West	58 ppb	12ppb	79.3 %
	West	52 ppb	10 ppb	80.7 %
	North West	49 ppb	11 pb	77.5 %

Table 8 Pollutant degradation at the surface of the right-side walls

	Wind Direction	Initial Conc of Pollutants	Final Concentration of Pollutants	Percentage of NOx abatement
Left Wall	North	38 ppb	18 ppb	52.6 %
	North-east	32 ppb	20 ppb	37.5 %
	East	28 ppb	8 ppb	71.4 %
	South-East	34 ppb	8 ppb	68.4 %
	South	25 ppb	12 ppb	52 %
	South-West	30 ppb	11 ppb	63.3 %
	West	41 ppb	12 ppb	70.7 %
	North West	42 ppb	20 ppb	52.3 %

Table 9 Pollutant degradation at the surface of the left side walls

From the above table it can be inferred that wind movement has a strong influence on the mass transfer of the pollutants towards the photocatalytic surfaces. On the right wall, the concentration of the pollutants is higher than the left wall and in turn show a higher potential

of NO_x degradation. This phenomenon is seen as a result of the façade surface being located on the leeward side. The vortex effect in the street carries pollutants towards the leeward side of built forms. The change in the concentration of the pollutants are plotted in the diagram below.

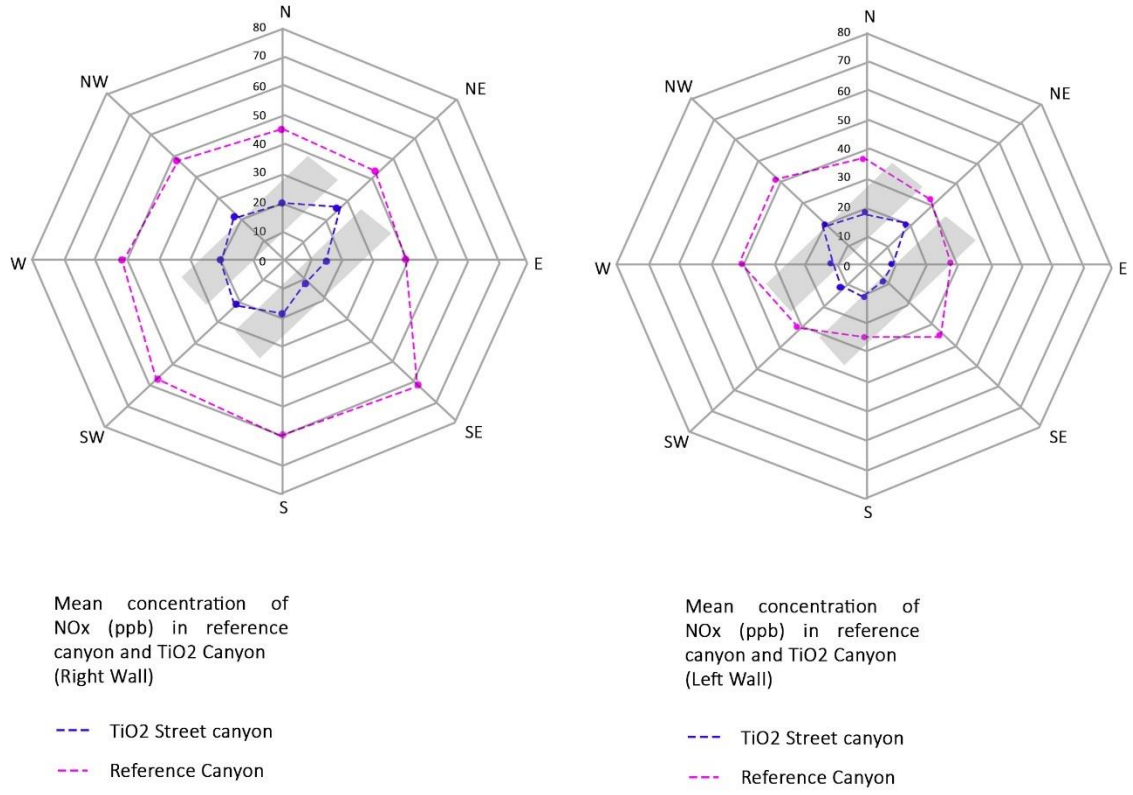

Figure 17 Diagrammatic representation of the pollutant degradation in the street canyon influenced by wind movement

From the above diagram, it can be inferred that when the wind conditions were perpendicular to the built forms, the concentration of the pollutants towards the leeward facades were higher and in turn higher NO_x abatement on that surface.

2.2.4. Case Study: NOx abatement in Umbreto Tunnel - Rome

Lesser demonstration of the photocatalytic ability of these building materials in real environmental conditions has led to restriction in large scale application. However, Umbreto tunnel was one such monitored project which shows the potential reduction of NO_x pollutants after application of the cementitious photocatalytic paint.

The tunnel is situated in the center of Rome under the Qurinale hill and is the busy connecting route Esquilino district and the flaminio district.

Length of the tunnel: 347.7 m; Width: 17 m; Height of the tunnel: 8.5 m

The tunnel had dense vehicular flow of about 1100 vehicles/hour with high amount of pollutants concentrating in the tunnel that are harmful for the pedestrians.

The monitoring of the pollutants was carried out from 8:00 to 18:00 hrs. all five days a week between 7 July 2007 to 23 July 2007. The monitoring devices were placed close to the pedestrian walkways as indicated in the figure below.

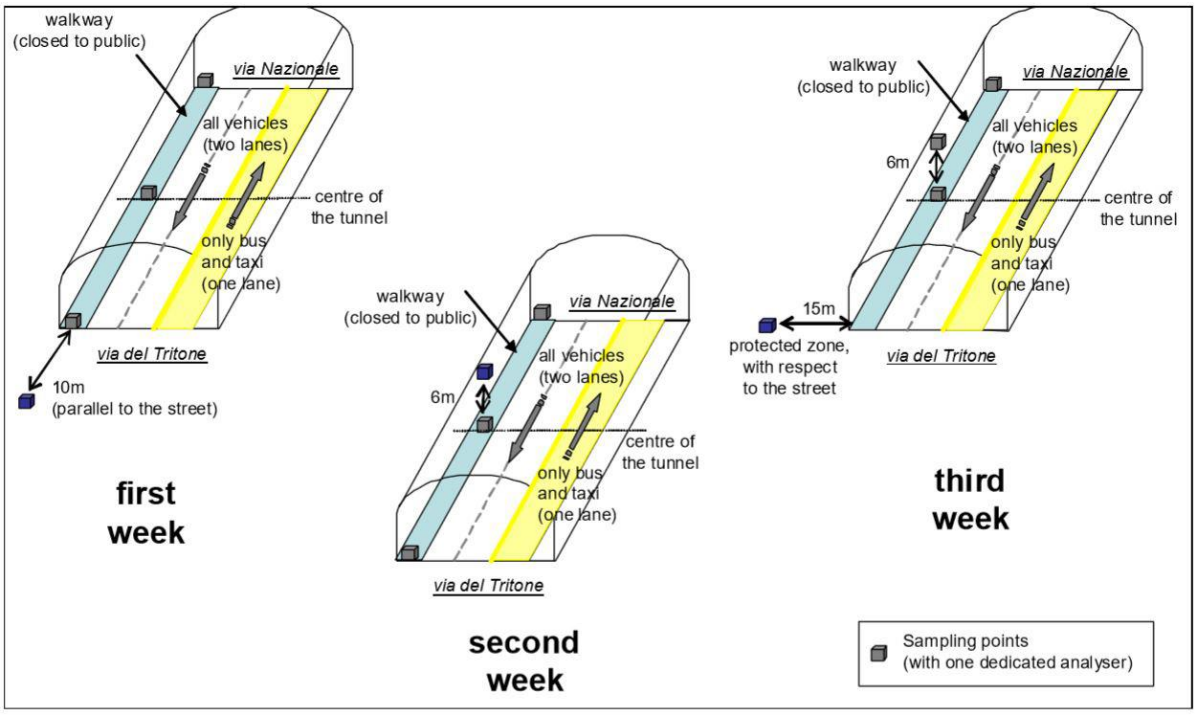

Figure 18 Representation of the positions of the NOx measurement devices

Light Irradiation	Relative Humidity (%)	Wind Speed
20 W/m2 (Artificial light)	10-50 %	0.1 – 1.7 m/s (Avg: 0.38 m/s)

Table 10 Umbreto Tunnel environmental Conditions

The amount of pollutants varied from one end of the tunnel to the other which is the typical distribution of pollutants in a tunnel with natural ventilation due to plug effect. However, in the cross section there was a homogenization of the pollutant concentration at various heights. This was confirmed by the NO_x level measurements at 1m and 6m height from the monitoring devices.

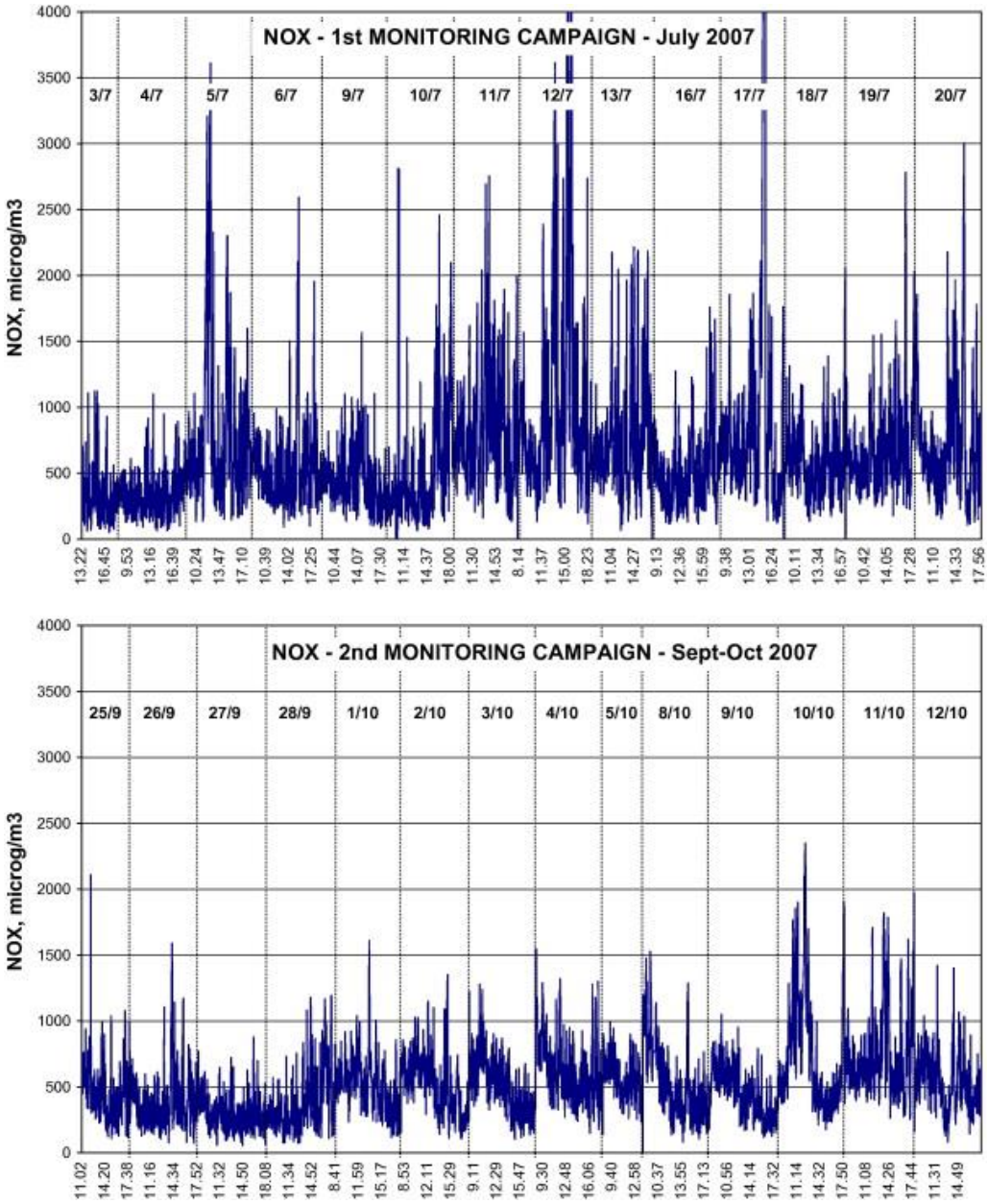

Figure 19 A comparison of the NOx level at the center of the tunnel before (up) and after the renovation (down)

There is a reduction in the mean concentration of nitrogen dioxides after the photocatalytic treatment. From the absolute values calculated, it had been found that there is an overall reduction of 20% of pollutants. However, according to the statistical approach of data evaluation in the study, the study concludes that the abatement range is from 50 – 61% in the center of the tunnel (Guerrini & Luca, 2012). This proves that the NOx abatement potential of photocatalytic material is high in a confined built environment with an average wind speed below 1.5 m/s.

2.2.5. Case study based on the performance of the material – Leopold Tunnel

Leopold II is a tunnel in Brussels that runs between Ghent and Bruges with high traffic density with more than 2000 vehicles per hour. The pollutant concentration in the tunnel builds from 400 - 1000 $\mu g/m^3$ in an average of half an hour. Field campaigns were conducted by PhotoPAQ team to assess the air-purifying effect of cementitious TiO_2 coating on the walls of this tunnel.

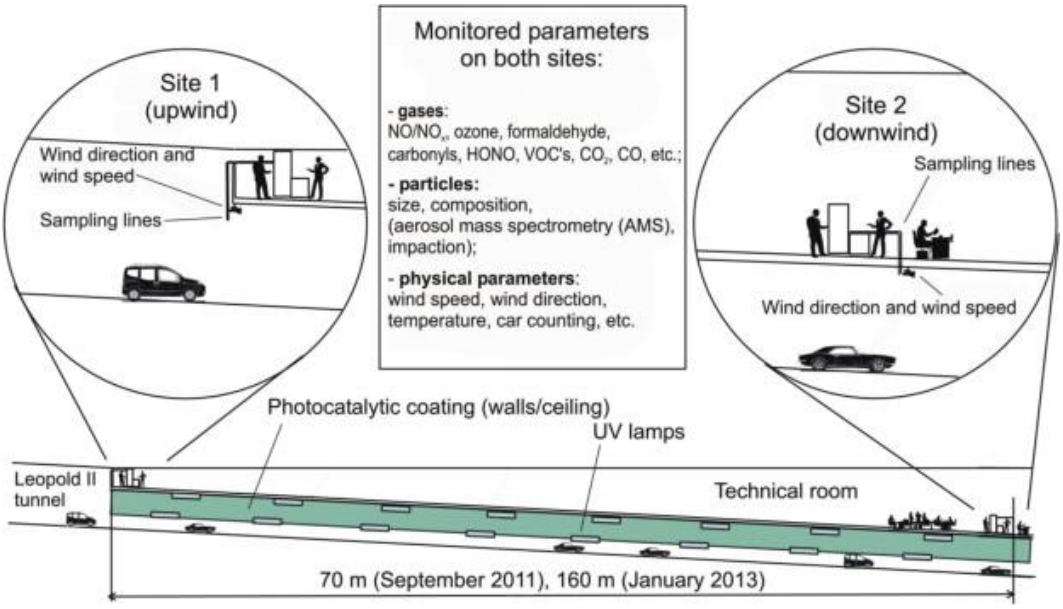

Figure 20 Experimental set-up scheme for Leopold Tunnel II test site in Brussels for NOx abatement

Field campaign was conducted for this tunnel using three testing strategies:

- Measurements before and after the application of the photocatalytic material (has the advantage being applied to both indoor and outdoor sites)
- Upwind and downwind approach (Measuring pollution levels in normal air and comparing with the measurements obtained from the air in contact with active surfaces)
- monitoring air pollution at the downwind site modulated by the UV lamps (1-4 W/m2 – "on/off" approach), to discriminate further between "active" and "non-active" periods of the photocatalytic materials (Gallus, et al., 2015).

On the sampling sites, gaseous pollutants were sampled at a height of 20-40 cm below the tunnel ceiling.

Conclusions from the field campaign:

Although the results indicated less than 2% air purification at the sampling points, certain optimized conditions for future applications were derived to attain good performance in an

urban scenario. Recommendations provided for the proper use of photocatalytic materials were:

- optimized application of the photocatalytic coating on a regular substrate, in order to obtain a low surface roughness to minimize dust adsorption
- high UV light intensity levels ideally around 10 W/m2, to avoid surface passivation
- low average relative humidity less than 60%
- low average tunnel wind speed, for increasing the residence time of the pollutants
- high active surface-to-volume ratio and increased turbulent mixing (Gallus, et al., 2015)

2.2.6. Summary of the Performance of photocatalytic Concrete

The two case studies of the field trials of PICADA and Umbreto tunnel show an improvement in the surrounding air quality. However, photocatalytic surface in these trials has very less specific area and have not been designed for optimal performance. To derive the design principle, the amount of NO_x degradation per square meter of the photocatalytic surface could be a driving factor to calculate the required surface enlargement. The NO_x abatement potential per square meter of photocatalytic concrete is summarized below.

Type of product & Photocatalyst	Humidity (RH)	Type of test	NOx reduction ($mg/m^2/hr.$)	NOx reduction	Reference
Concrete block with P25 (2%)	50 %	Unknown	2.5	Unknown	(Poon & Cheung, 2007)
Concrete block with P25 (10%)	50 %	Unknown	4.0	Unknown	(Poon & Cheung, 2007)
Anatase	50%	ISO	3	Unknown	(Poon & Cheung, 2007)
White cement mortar with P25 (2%)	50%	ISO	6	Unknown	(Guo & Poon, 2013)
White cement mortar with P25 (5%)	50%	ISO	3	30 %	(Guo & Poon, 2013)
P25 spray coating (60 g/m^2) on concrete block	50%	ISO	7	60 %	(Guo & Poon, 2013)
Anatase (5%) in Mortar	50%	ISO 22197-1:2007	18	Unknown	(Hüsken, Hunger, & Brouwers, 2009)

Anatase (5%) in Mortar	50%	ISO	11	20 %	(Ballari, Hunger, Hüsken, & Brouwers, 2010)
Mortar with 5.9 % TiO2	50%	ISO	19	35 %	(Ballari, Yu, & Brouwers, Experimental study of the NO and NO2 degradation by photocatalytically active concret, 2011)
Mortar with P25 (1%)	50%	ISO	11	25%	(Sugrañez, et al., 2013)
P25 spray coating	**50%**	**ISO**	**20**	**45%**	(Yang, Hakki, Wang, & Macphee, 2017)

** measured in accordance with ISO protocol (either 22197-1:2007 or ISO 22197-1:2016)*

Table 11 Summary of photocatalytic NOx abatement activities of TiO2-based concretes in bulk and spray coating for an irradiation of 10 W/m^2

The concrete substrates spray coated with Degussa P-25 photocatalyst gave the highest NO_x abatement even under a cloudy sky (with UV irradiance 10 W/m2) with 20 mg/m^2/hr. Hence, over a period of 7 hours, 1 m^2 of active site could degrade 0.14 grams of NO_x.

2.2.7. NOx abatement of Non-Cementitious TiO_2 coatings

Non-cementitious photocatalytic coatings are paints that contain TiO_2 along with silicates as binders. They are widely applied in both indoor and outdoor applications and tested for air purifying capabilities. A real scale test was done on busy lanes of Manila in Philippines. A 24 km stretch of wall was painted with artwork using paint consisting of PC500(18% Anatase). Five art works each measuring 1000 m^2 have been painted along the stretch of Manila's main roadway with a vehicular density of 13800 cars per day (EDSA, for Epifanio de los Santos Avenue).

The trial monitored by the Manila observatory showed that the surrounding air had a reduced NO_2 levels by 20% that is equivalent to the NO_2 emissions of more than 30,000 cars that passes by the station every day (EIC, 2015).

Figure 21 Photocatalytic paint on the busy lanes of Manila, Philippines

Type of product & Photocatalyst	Irradiation	Humidity	Type of test	NOx reduction	NOx reduction	Reference
Styrene acrylic paint	10 W/m^2	50%	Unknown	0.7 mg.m-2.hr-1	10 %	(Maggos, Bartzis, Leva, & Kotzias, 2007)
VLP7101 KronosTM C-doped anatase (17%)	10 W/m^2	50%	ISO	12 mg.m-2.hr-1	11 %	(Águia, Ângelo, Madeira, & Mendes, 2011b)
PC500 CristalACTiVTM anatase (18%)	10 W/m^2	Variable	ISO	31 mg.m-2.hr-1	28 %	(Ângelo, Andrade, & Mendes, 2014)
StoClimasan	10 W/m^2	50%	ISO	6 mg.m-2.hr-1	3.5 %	(Mills & Elouali, 2015)

** measured in accordance with ISO protocol (either 22197-1:2007 or ISO 22197-1:2016)*

Table 12 Literature summary of the photocatalytic NOx abatement activity of TiO2-based paints

Paint shows a higher abatement of 31 mg/m^2/hr i.e. 0.22 grams of NOx per day. This is twice the capacity of cementitious coating and photocatalytic concrete. Hence, **façade panels would exhibit better performance with adapting non-cementitious coating**.

2.2.8. Case study - Torre de Especialidades Hospital Manuel Gea Gonzales

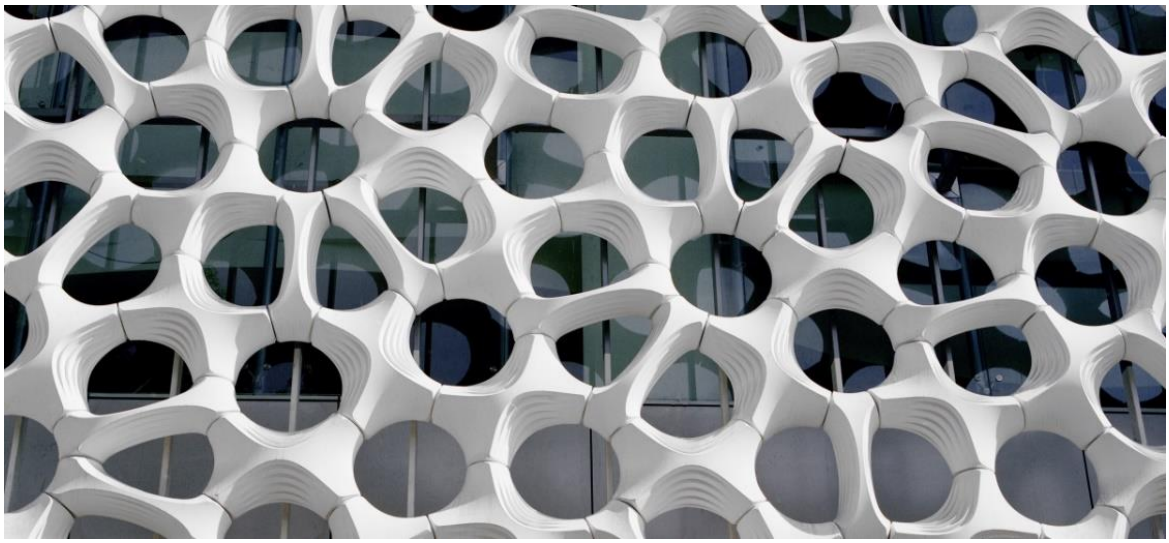

Figure 22 Photocatalytic facade of Torre de Especialidades Hospital Manuel Gea Gonzales, Mexico

Project name: Prosolve370e
Project type: Depolluting Quasicrystal Façade Structure
Façade area: 2500 m^2

This façade system is the world's largest passive urban air-purifying system installed in Southern and Western façade of a Mexican hospital. The concept of this project was to develop a secondary sculptural façade that could be retrofitted onto the existing buildings and installed as independent sculptures in urban areas.

Design goals of the project:

- To reduce the wind speed close to the façade and increase the turbulence
- To increase the surface area available for photocatalytic reaction by maintaining visual comfort.

Design of the façade tiles:

The mesh façade is designed with a balance between the porosity to allow light and achieve maximum surface area to trap pollutants and omnidirectional light. The resultant design is a biomimicry of coral that is morphed into a quasi-crystalline geometry to create two repetitive modules that weave a pattern with indefinite possibilities. The design maintains an inherent synergy between the design form and molecular technology (Depolluting facades, 2013).

To understand the strategies involved in surface enlargement and change in the resultant irradiance pattern, a rough module of 390 series was modelled in Rhino.

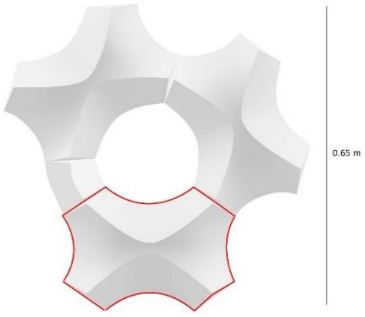

Figure 23 Modelled X-shape Prosolve370e module (Red highlighted portion is analyzed for irradiance)

Method of surface enlargement: Two types of X-shaped modules are arranged along the quasi crystalline grid. The depth of the relief in each module and doubly curved surface help in maximizing the surface area to 200%.

The module is not optimized for a specific sun angle or orientation. The curvature of the surface captures maximum radiation throughout the day from sunrise to sunset (Figure 24).

Fixing method: The modules are attached to a steel substructure with pentagonal brackets to which the X-shaped modules are attached. Each of these modules are interconnected using inter-tie joints to keep the light-weight structures in place (Figure 25). The complicated and non-repeating pattern requires trained labor to assemble the system at site.

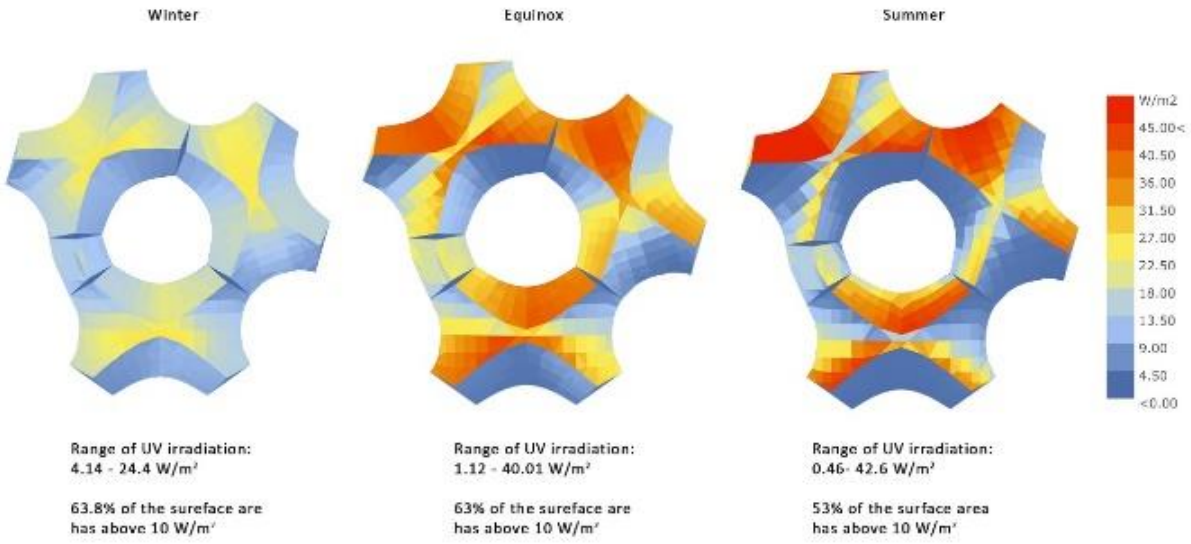

Figure 24 Average Irradiance analysis for three different sun altitude angles in a year on a module of Prosolve370e

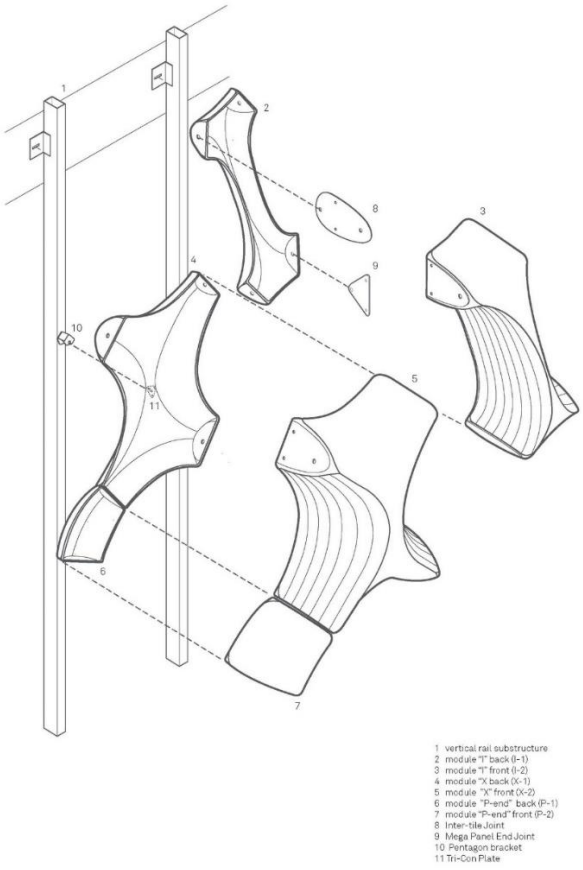

Figure 25 Fixing detail of Prosolve370e

Material:

The 3-dimensional tiles are produced using thermoformed Acrylonitrite butadiene styrene (ABS) plastic shell which lightweight and fire-resistant. The tiles were then coated with nano-

photocatalytic TiO_2 as a pigment suspended in the paint which is known for its self-cleaning and germicidal capacities. Small amount of UV radiation in combination with the surrounding humidity is enough to reduce the air pollutants. For optimum performance, it is necessary that these systems are located closer to the source of pollutants to neutralize NOx (Nitrogen dioxides) and VOCs (Volatile Organic Compounds).

Resultant design of the façade area: 5000 m^2 (Façade area multiplied with the surface enlargement factor)

Amount NOx removed: 0.26 gram/m^2/day

Maintenance: Replenishment of TiO_2 Paint once in 5 years

The façade modules are installed on the south and west facades of the hospital to cut down on the solar gain for the interiors while the outer surface performs for the urban environment.

Although, the façade has been performing for over 5 years, fields tests have not been conducted to understand its influence on the surrounding air quality as it requires intensive monitoring over months with expensive equipment inputs.

2.2.9. Case study 2 - TiO2 panel

The case study discussed below depicts another approach to design the photocatalytic façade panels to have maximum annual exposure to irradiation on the south orientation. The same strategy could be applied to the west and east orientations of the facades.

Design goals of the project:

- To increase the amount of incident irradiation onto the façade panel

Design approach:

The goal of this design is to increase the maximum annual radiation on the façade panel much higher than the incident radiation on a flat panel. Parameters like geographic coordinates, design test day, and a panel orientation from North are utilized to analyze the daily incident solar radiation amounts and determine the highest amount of radiation over a day (sunrise to sunset) that would fall on a plane with a normal vector, n_{MAX}, at 174.58° azimuth, n_{AZ}, and 79.52° elevation, n_{EL}. The surface of the panel is constrained by the face's normal angles (Nikolov & Fox, 2015).

Test Location Latitude:	40°36'16.46" N
Test Location Longitude:	75°21'38.85" W
Test Date:	07/26/13
North Angle:	22.5°

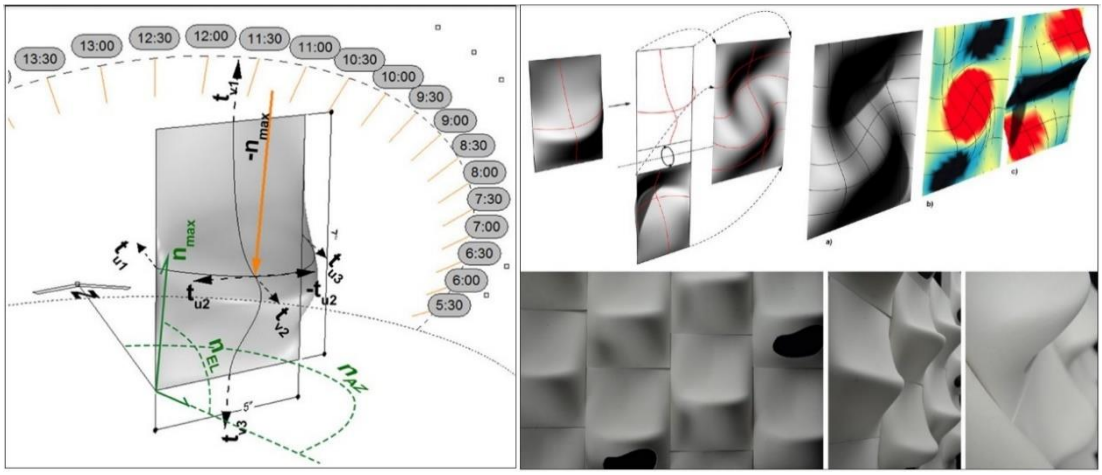

Figure 26 Design Parameter and panel generation (Red spots: Zones of maximum annual irradiation)

Surface enlargement: 1.136 times (113 %) compared to that of a flat panel of same dimensions. In addition, 76.45% of surface area of the proposed panel has higher exposure to radiation than the flat panel of equal overall dimensions. **13.58% of the proposed surface is exposed to 75% of total accumulated daily radiation** (Nikolov & Fox, 2015).

Figure 27 Perspective and elevation of the panels by elimination of low irradiation zones form the panel

2.3. Pollution in Urban areas

The issue of air pollution, its causes, consequences and environmental regulations related to these had been briefly discussed in section 1. The first part of this section elaborates about the different types of air pollutants, their sources and allowable concentrations in urban scenario.

The second part describes about NOx pollution in major cities of the world, site selection, dispersion pattern of pollutants and their variations over heights in different urban scenarios.

2.3.1. Air Pollutants

Pollutants can be classified as primary and secondary based on their origin. Primary pollutants are particulate or gaseous matters that are released from sources like industries,

automobiles and buildings. While secondary pollutants are products formed by the reaction of two or more primary pollutants in the presence of light and heat.

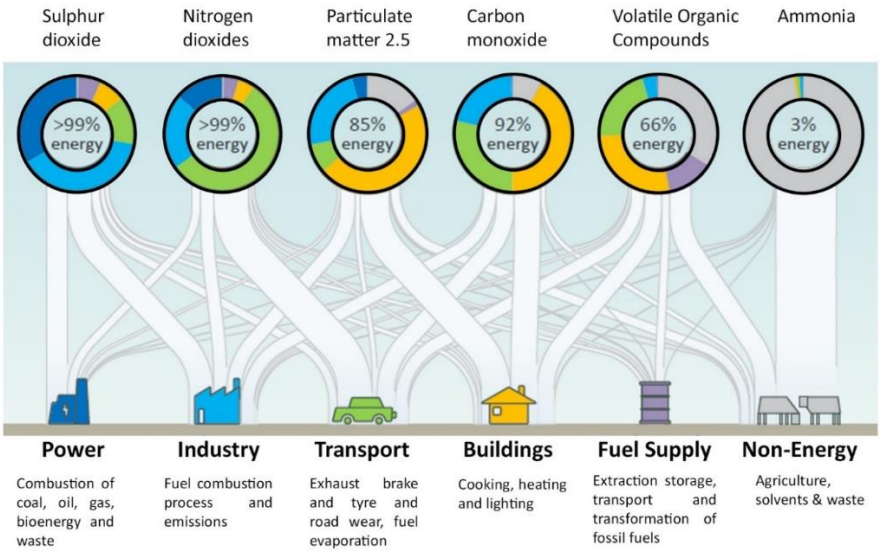

Figure 28 Primary air pollutants and their sources (IEA, 2015)

Particulate matter and carbon monoxide are primary pollutants which retain their state as emitted from the sources. While oxides of Sulphur and nitrogen (NO_x) and Volatile Organic Compounds (VOC's) transform themselves into ground ozone and photochemical smog during high temperature and light conditions. Hence, primary pollutants that transform into harmful secondary pollutants need much more attention. And photocatalytic building materials have reducing capabilities of these transformative primary pollutants.

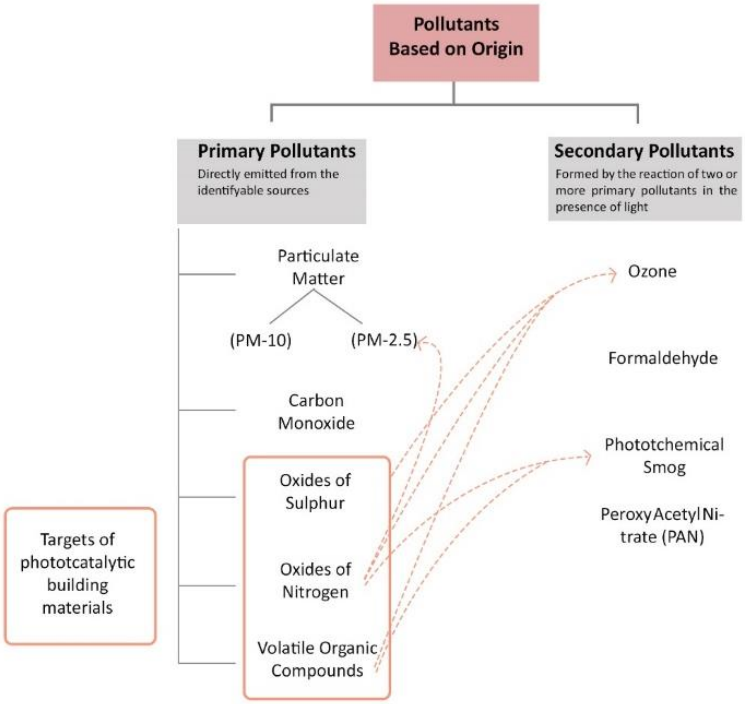

Figure 29 Types of Pollutants and their transformation to secondary pollutants

The table below indicates the health effects caused by SO_2 and NO_x along with the permissible levels in urban scenario.

Pollutant	Health effects of the pollutant	Regulatory levels in urban air
Oxides of Sulphur (SO_2)	-Inflammation of the respiratory tract -Aggravation of asthma and chronic bronchitis -Cardiac diseases	20 µg/m^3 24-hour mean 500 µg/m^3 10-minute mean
Oxides of Nitrogen (NO & NO_2)	-Bronchitis -Reduced lung function growth	40 µg/m^3 annual mean 200 µg/m^3 1-hour mean

Table 13 Target pollutants and their regulatory limits in urban policies

2.3.2. Built forms and Pollution dispersion:

The figures below show two extremes of an urban scenario where there is a high dispersion of pollutants and high accumulation of pollutants.

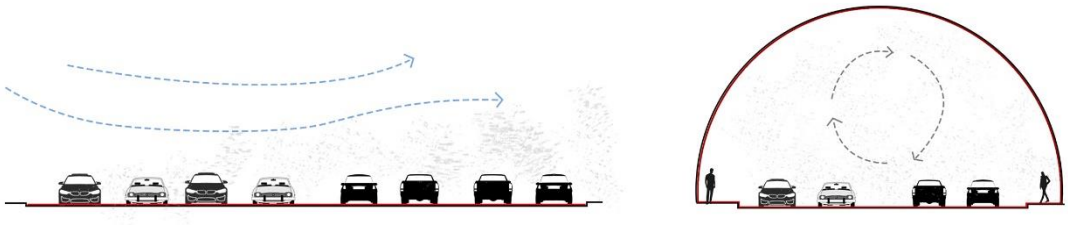

Figure 30 Quick dispersion of pollutants with wind in urban sprawls like highways (left) & Circulation of Pollutants inside a Tunnel (right)

An intermediate scenario would be street canyons where there is a simultaneous phenomenon of wind movement and accumulation of pollutants. The microclimate of the street canyon is influenced by micro-meteorological effects of urban geometry. High pollution levels have been observed in street canyons, which is a term frequently used for urban streets flanked by buildings on both sides. The classification / dimensions of a street canyon are expressed by its aspect ratio. Aspect ratios is height of the building divided by width of the street (H/W). Most common street aspect ratios are 0.5, 1 and 2.

Wind conditions above the influence the air flow within the street. Hence, there is a clear distinction between the wind over the roof and flow within the canyon. Three main dispersion conditions could be identified for the below mentioned prevailing synoptic winds at roof levels:

- At low wind condition for synoptic wind speeds lower than 1.5 m/s.
- Perpendicular or near perpendicular wind speeds over 1.5 m/s blowing at an angle more than 30 degree to the street canyon axis

- Parallel or near parallel wind flow over 1.5 m/s.

In the case of perpendicular flow, the upwind side of the canyon is usually called leeward, and the downwind windward. A t wind speeds greater than 1.5 to 2 m/s, perpendicular to the built form, three types of wind flow regimes can be noticed based on the aspect ratio of the streets: a) isolated roughness flow, b) wake interference flow and c) skimming flow.

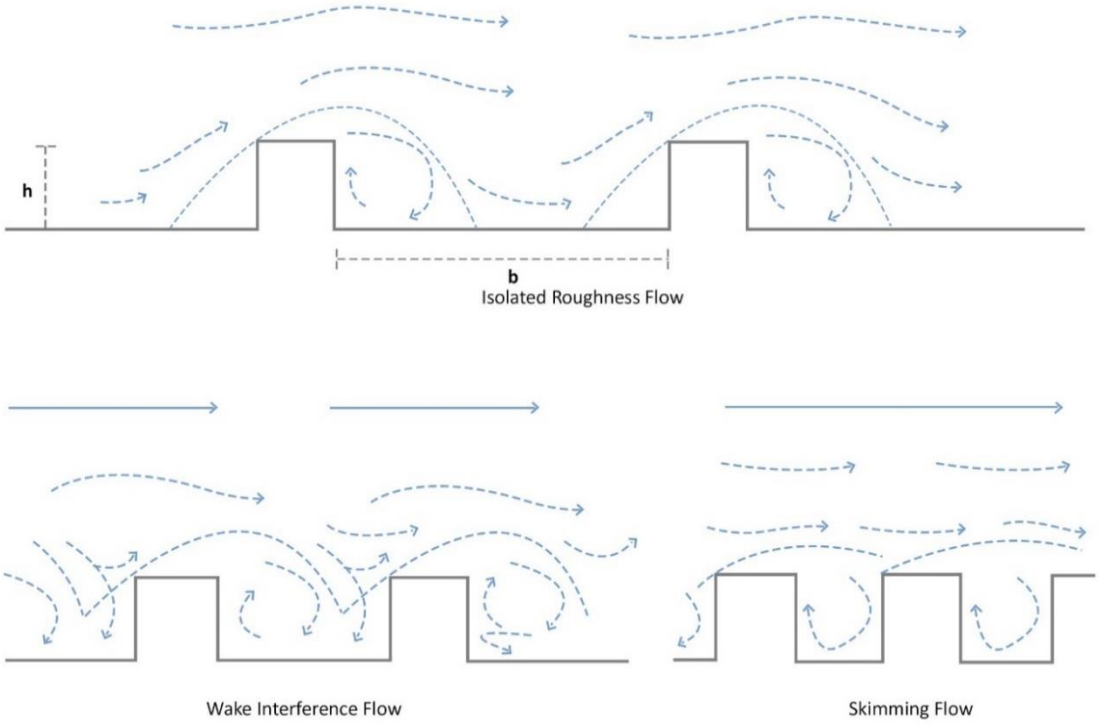

Figure 31 Wind flow pattern within the canyon for winds greater than 1. 5m/s perpendicular or almost perpendicular to the built forms

In wide canyons (H/W $<$ 0.3), air travels enough distance downwind before the next building acts as an obstacle. This isolated roughness flow results in good ventilation flushing out the pollutants from the street. There is a disturbance in the air flow as the buildings get more closely spaced.

For streets with aspect ratio 0.5, the disturbed air has insufficient distance to readjust itself before the next obstacle which results in wake interference flow. Though the ventilation rates are not sufficient, they still have less accumulation of pollutants (Vardoulakis, Fisher, Pericleous, & Gonzalez-Flesca, 2003).

For regular and narrow canyons with H/W $\sim$ 1 or greater than 1, the roof wind produces a skimming effect in the canyon that results in single vortex. In such situations, the leeward side of the canyon becomes the pollutant receptor. Within these streets, pedestrians, cyclists, drivers and residents are likely to be exposed to pollutant concentrations exceeding current air quality standards.

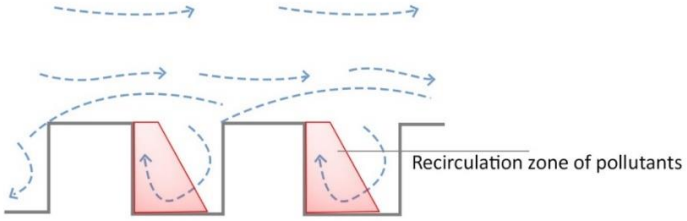

Figure 32 Pollutant recirculation on the leeward side of the street canyon (T.-B. Ottosen, 2015)

Since the wind conditions vary over different times of the year, there is a high potential of the pollutant accumulation on various parts of the streets.

Hence street canyons with aspect ratio 1 or greater than 1 needs innovative measures for the reduction of pollutant concentration. From the above it can be seen how aspect ratio play a critical role in accumulating pollutants. Similarly, length of the streets also adds to such effects which can be seen in the figures below.

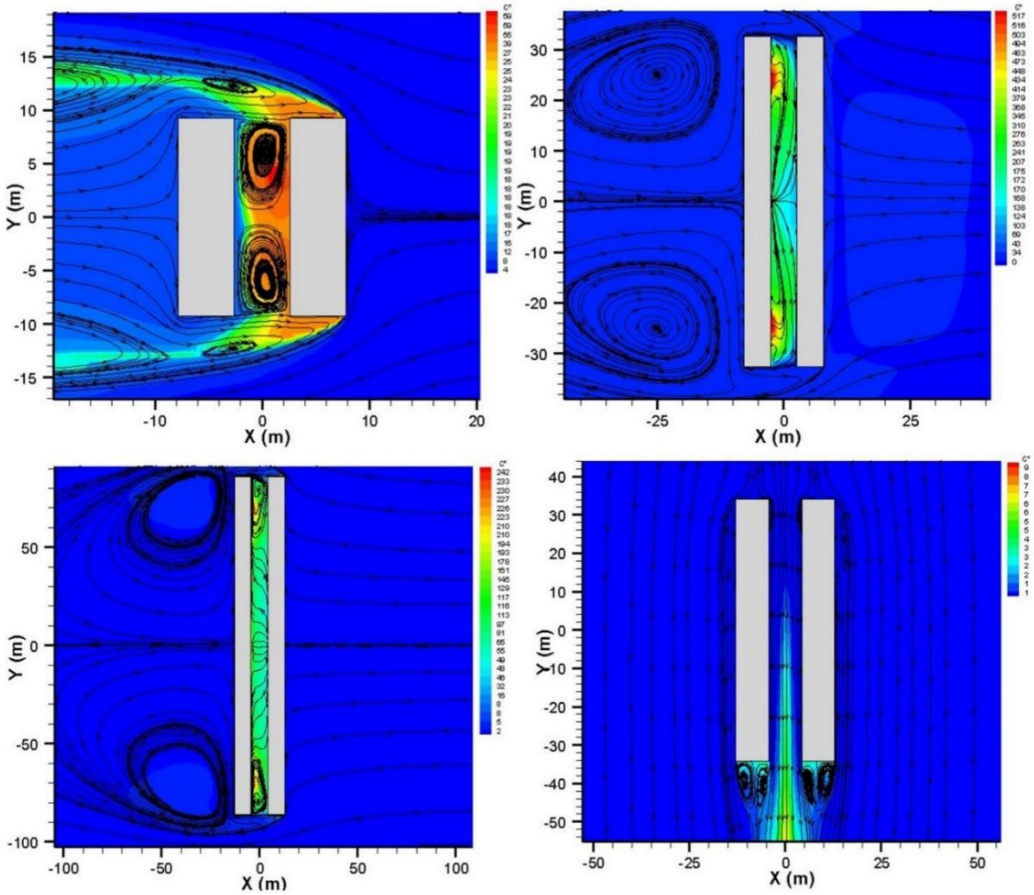

Figure 33 Pollutant dispersion fields for perpendicular and parallel wind flow in a street canyon measured at 0.5H of the street canyon for different lengths of the street (Wind speed = 4 m/s & aspect ratio 5)

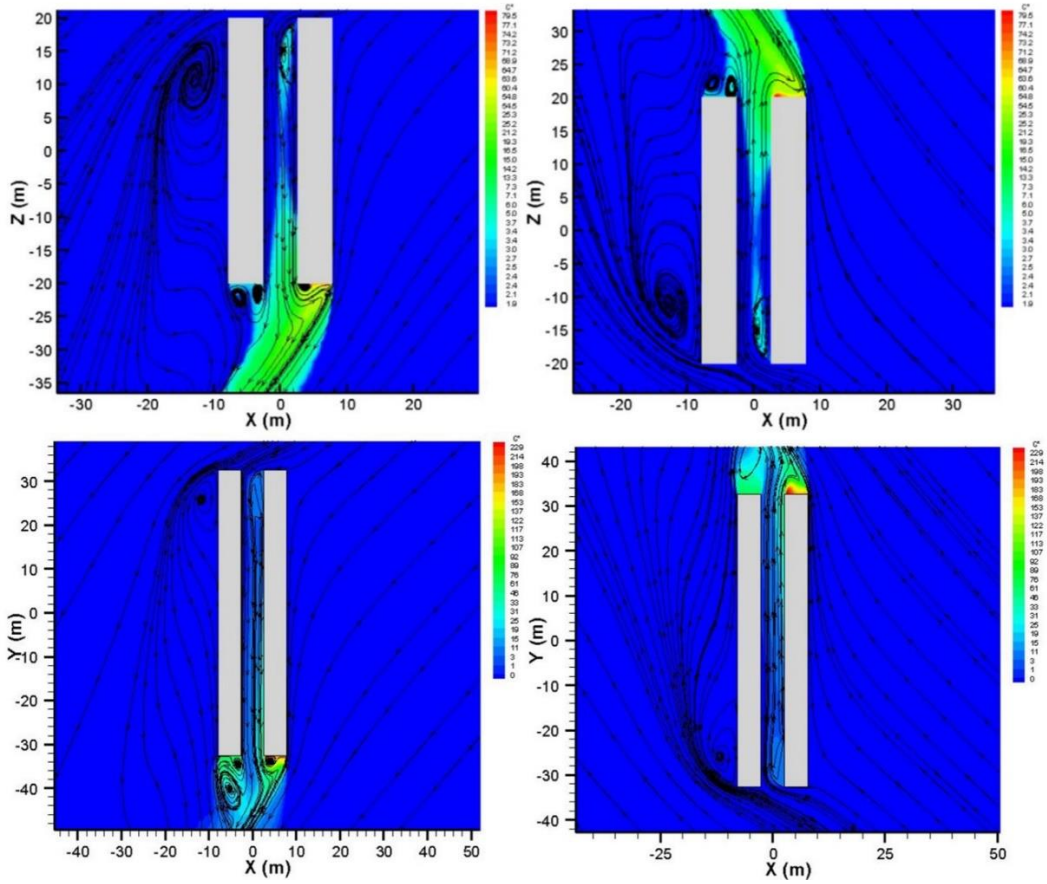

Figure 34 Pollutant dispersion fields in the street canyon at 0.5H for wind flow at an angle between 0 to 90° to the street (Wind speed = 2.0 m/s & aspect ratio 3); (Barmpas, Moussiopoulos, & Vlahocostas, 2006)

The pollutant dispersion fields for perpendicular winds accumulate the pollutants within the street canyon for length of the street ranging from 20 m to 175 m. In the situation when wind flow is parallel to the façade or at an angle, the pollutants are quickly flushed out of the streets and the pollutants accumulate at the ends of the streets on the shorter side of the building (Figure 34 & Figure 35).

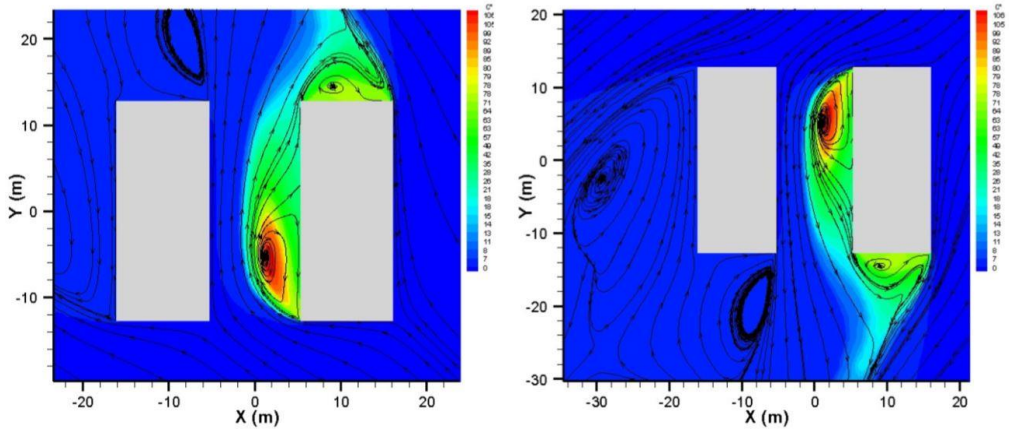

Figure 35 Pollutant dispersion field for wind velocity of 2.0 m/s at an angle of 45° (aspect ratio 1)

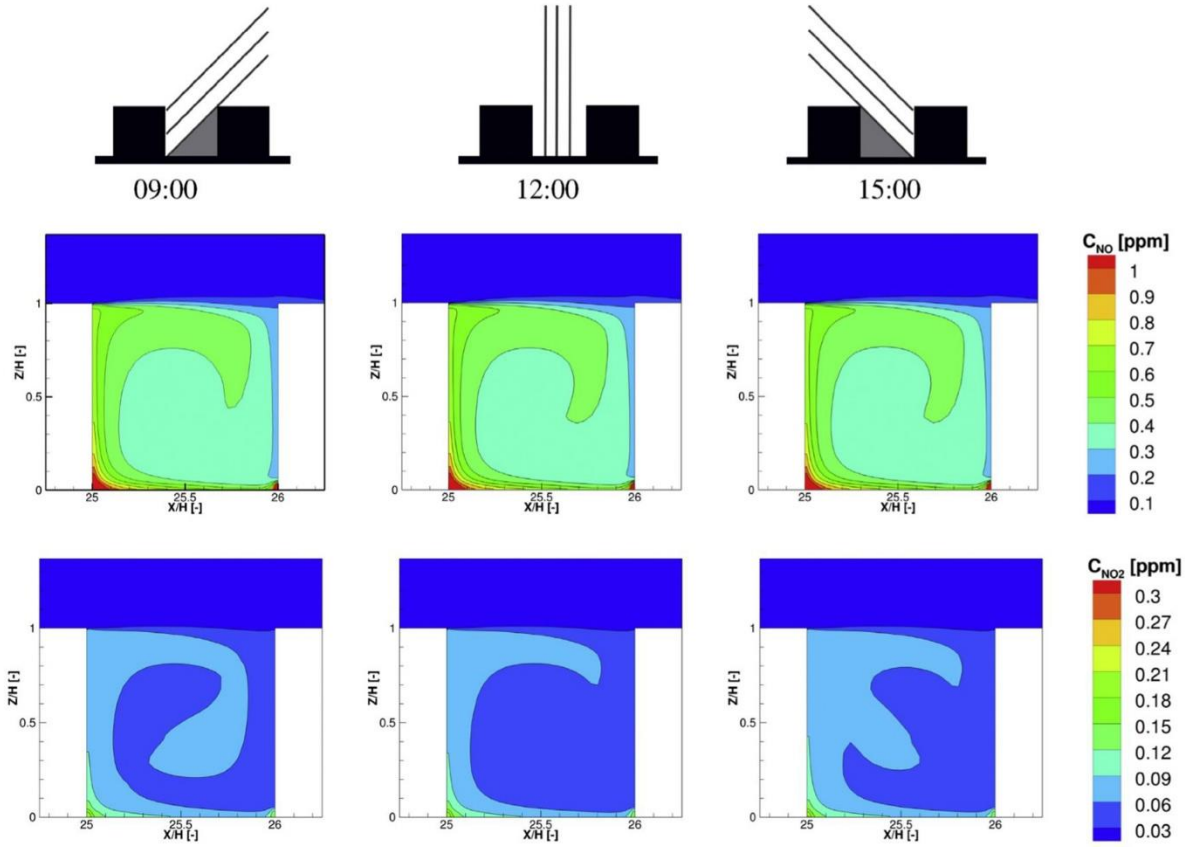

Figure 36 Pollutant dispersion along the section of the street with an aspect ratio of 1 ((Muilwijk, Schrijvers, Wuerz, & Kenjeres, 2016)

Figure 36 shows the dispersion field over the cross-section of the street canyon with perpendicular wind flow. The pollutants recirculate within the street canyon.

In most of the cases depicted above, the accumulation of pollutants is along the leeward facades of the building. This shows the potential of integrating photocatalytic coating onto the façade surface for efficient pollution abatement.

The semi-confined nature of the street canyon, tendency to accumulate pollutants makes it an ideal situation to evaluate the façade panels for its pollution abatement performance. Hence, in the final part of this thesis, to evaluate the performance of the flat photocatalytic panel and the designed façade panel, this situation of a street canyon with aspect ratio 1 is chosen.

2.3.3. Variation of Pollutants over heights

The concentration of pollutants varies with different heights. Several studies have been conducted to model the concentration profile of NO_x over a ranging height. One such design firm is WSP | Brinckerhoff that collected data of air quality monitoring undertaken at different heights from the local authorities in London. The measurement sites were zones classified as "roadsides" and urban background". The sample points for roadside were located between 1 to 5 meters from the edge of the roads. While the urban background concentration was at a distance more than 20 meters away from the emission sources. The data collected is plotted in a graph from the bottom of the building up to a height of 27 m.

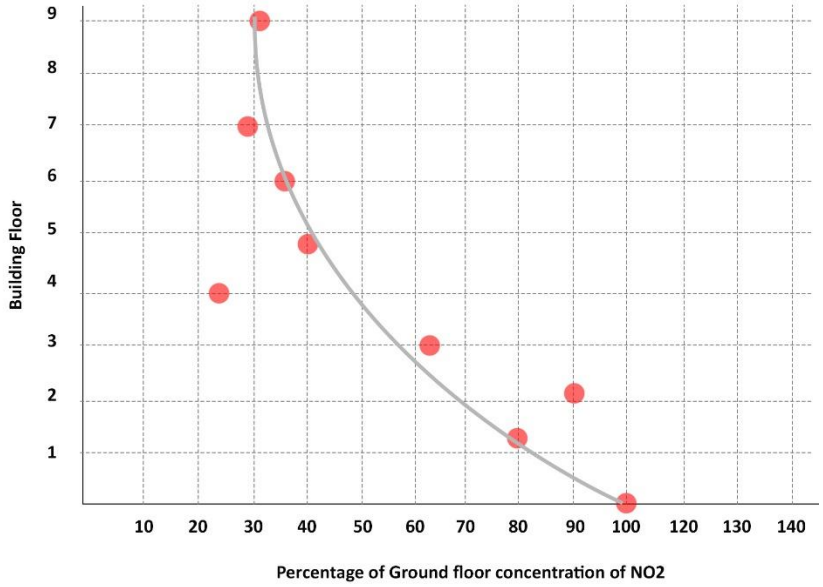

Figure 37 Variation of pollutant concentration over the height of a building in London while concentration at ground floor level is considered as 100%

From the graph, it can be inferred that the amount of pollutants that meet the façade decreases with heights. In another study, it was predicted that pollution levels the height of 17 m was critical (Wang, Bosch, & Kuffer, 2008). Hence, **this necessitates the high surface enlargement for the façade panels that are in the lower floors (up to 12-17m height) of the building than on the upper floors.** However, for buildings located in high emission zones this argument may not be valid as the background concentration of pollutants is high even at heights above 17m.

2.3.4. NOx pollution in Urban areas

The target pollutants of the photocatalytic building materials are the Nitrogen dioxides in the urban scenario. Hence, it is important to target the major cities where there is a potential to use them on the built form to achieve an improvement in the quality levels. According to Europe Environmental Agency, annual mean for NOx levels is 40 $\mu g/m^3$. From the chart below, it is clear how the annual limits have been breached by more than 25% in London, Paris, Delhi and Beijing.

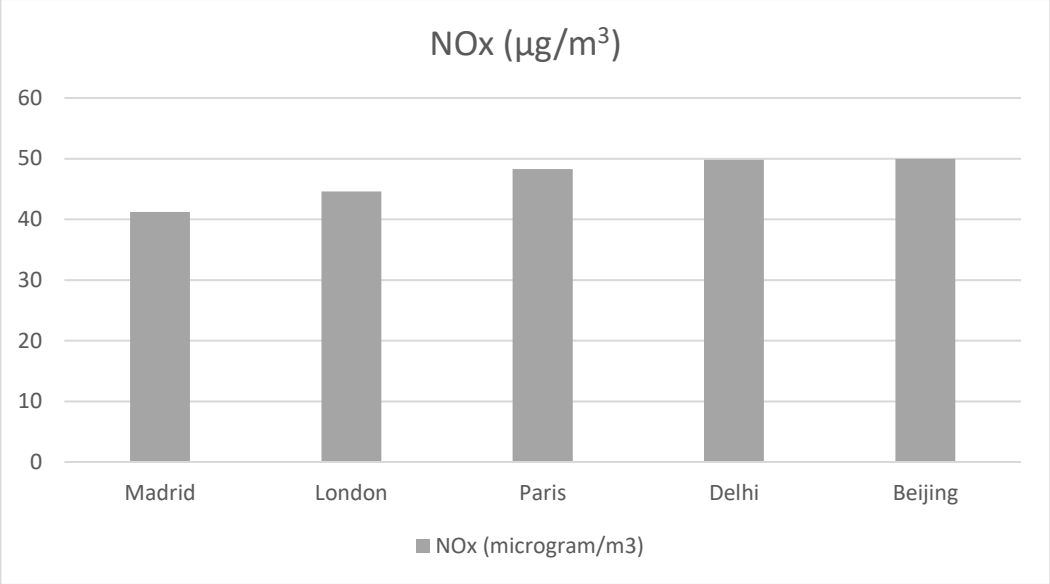

Figure 38 Most polluted cities with vehicular traffic (Annual mean NO_x level = 40 µg/m^3); Source: EEA, Aerosol and Air quality Research; Central Pollution board

Though, the overall pollution limits in London have been exceeded by 20%, a closer look into the streets show an exceedance of the annual limit by at least more than 2.5 times.

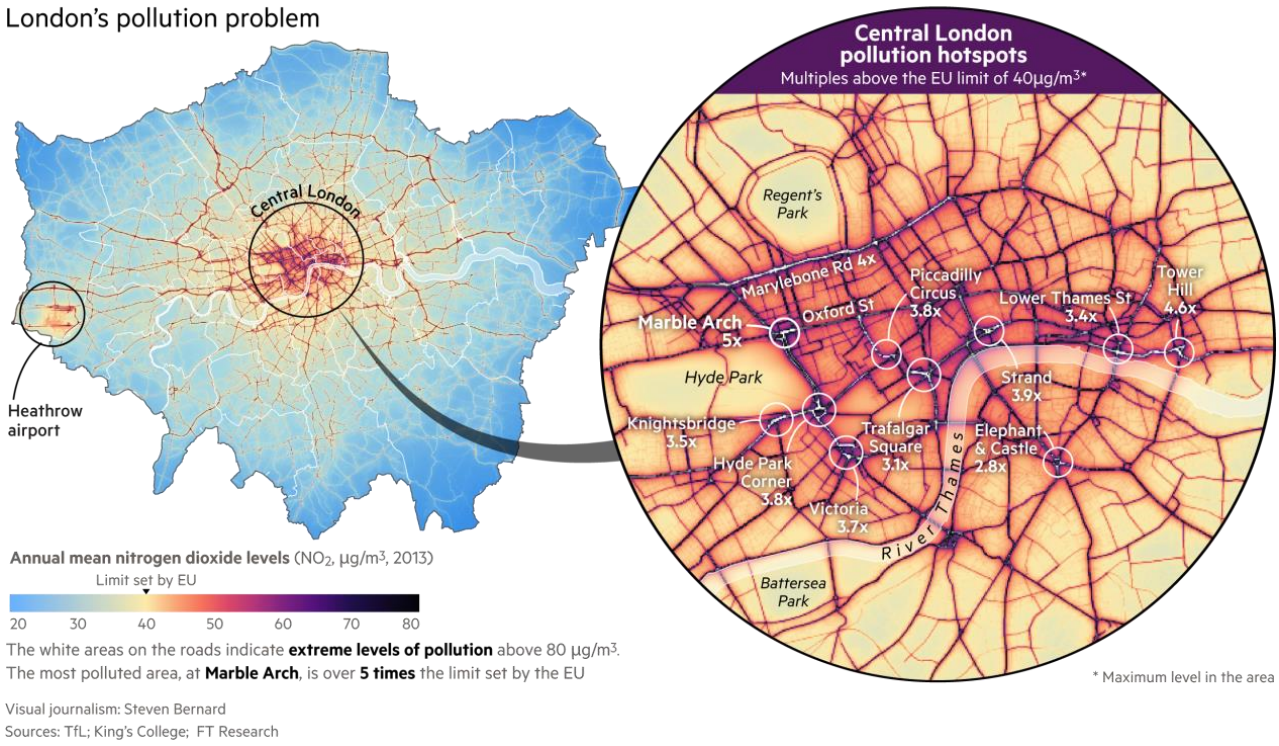

Figure 39 NOx Pollution in London and exceedance of annual limits

High pollution rates and breaching regulatory limits is seen in the denser part of the city. This is a clear indication of how urban built form and wind movement highly influences the residence time of pollutants in a zone. With supporting urban policies for photocatalytic building materials and presence of NOx pollution issue, London is chosen as the context.

2.3.5. NOx emission calculation in reference street

To frame the design requirements, it is necessary to pick a real situation with prominent NOx pollution to calculate the amount of nitrogen oxide emissions from vehicles. Hence, based on existing studies of Emission source department by the transport research laboratory, Putney high street, London has been chosen as the reference street canyon as a real situation that is close to the street aspect ratio of 1.

Putney high street is one of the many sites in London that broke the annual mean for NO_x record with 120 $\mu g/m^3$ in 2016. Based on the number of vehicles passing through the street on each day and type of vehicles, NOx emission is calculated below.

Vehicular density of Putney high street: 20,000 vehicles per day

Vehicular Emissions in Putney high Streets					
		Cars	Taxi	LGV	
		13385	1457	2686	
Total no:of Vehicles				17528	
				Light Duty	
Emission (g/km)	Vehicle type	% of vehicles	No:of Vehicles	Emissions (grams)	
	Pre Euro	1%	175	77	
0.44	Euro I	2%	351	154.6	
0.22	Euro II	9%	1577	346.94	
0.15	Euro III	32%	5608	841.2	
0.08	Euro IV	40%	7012	560.96	
0.06	Euro V	16%	2805	168.3	
			17528	4130.8	
				6.502	Kg/day
Putney Street Length		0.6 Km			
		Heavy Duty Vehicles			
		HGV	Bus	Coach	
		398	1930	9	
Total no: of Vehicles				2337	
				Heavy Duty	
Emission (g/km)	Vehicle type	% of vehicles	No:of Vehicles	Emissions (grams)	
23	Pre Euro	0%	0	0	
8	Euro I	1%	24	192	
6.5	Euro II	2%	47	305.5	
5	Euro III	68%	1589	7945	
4	Euro IV	14%	327	1373.4	
1	Euro V	15%	350	350	
			2337	10165	
				10.16	Kg/day
			Total NOx	16.6	Kg/day

Length of Putney High Street	0.6 Km			

Table 14 Emissions in Putney high Street (G.J.M.Velder, 2013) (Savage & Turpin, 2011)

In this scenario, it would be required to reduce the pollution by at least three times to satisfy the regulations. The obtained data is carried forward for the calculation of emission flux that will be used to simulate the situation of a street canyon in COMSOL in section 7.4.2.

2.4. Theory for Evaluation of photocatalytic façade

Langmuir – Hinshelwood model is used to describe the photocatalytic process which is governed by the kinetics of the heterogeneous reaction shown in Figure 6. This model allows formulation of the photocatalytic oxidation rate equation.

Assuming a general irreversible reaction:

$$A + B \rightarrow C + D$$

The reaction rate constant "r" for this reaction is given by:

$$r = k\Theta_A\Theta_B$$

Where Θ_A and Θ_B are given by the equations respectively:

$$\Theta_A = \frac{K_A X_A}{1 + K_A X_A}$$

$$\Theta_B = \frac{K_B X_B}{1 + K_B X_B}$$

Where K_A and K_B are adsorption equilibrium constants;

X_A and X_B are the concentrations of reactants in gaseous phase (Herrmann J. , 2010)

This model has been used by several authors to describe the photocatalysis of NO on semiconductor surfaces and they have obtained similar results. The experiments described by Wang et al. 2007 and Folli et al., 2011 had similar results for the kinetic constant k and adsorption equilibrium constant.

Also, the model can accommodate the influence of experimental conditions such as UV irradiance, relative humidity and reactor size which are important to translate the convective flux to a large volume of space like a street canyon. The kinetic equation for NO degradation rate and the extension of the model for UV irradiance is explained in the next section.

2.4.1. Kinetic equations for the air purifying panel:

NO degradation refers to reaction of NO with water vapor to form nitrates as the end products. Langmuir-Hinshelwood rate model is the most widely used approach to model the degradation rate of a photocatalytic surface as described by (Hunger, Husken, & Brouwers, 2010). Following this as a general model, the disappearance rate of the reactant could be described respectively:

$$\boldsymbol{r_{NO} = -1 \frac{kK_{NO}C_{g(NO)}}{1+K_{NO}C_{g(NO)}}} \qquad (1)$$

Where r_{NO} is the reaction rate at the active surface for NO [mol/m^3/s]

k is the reaction rate constant for the degradation of NO [mol/m^3/s]

K_{NO} is the adsorption equilibrium constant for NO which is a function of RH at 50 % [m^3/mol]

C_{NO}
is the concentration of NO in the air over the active surface [mol/m3]

Predicting the performance of the photocatalytic panels is influence by large number of variables in the urban environment. To obtain a comprehensive modelling, it is necessary to include at least two external influences like the concentration of water vapor (expressed as RH) and irradiations into the model to account for the impact of the changing weather conditions (Hunger et al, 2010). The Relative Humidity (RH) for the analysis is kept at a constant of 70%.

2.4.2. Extension of the model for UV irradiation:

The performance of the surface photocatalysis is not only affected by the wavelength, but also by the intensity of the irradiance. Experiments by Hunger et al, 2010 prove that there is a strong dependence between reaction rate constant of NO and intensity of UV irradiation. Photocatalytic activity increases with increase in irradiation levels. For UV irradiation E<250 W/m2, the degradation rate increases proportionally while for E>250 W/m2, photocatalytic activity increases with the square root of E for the value of irradiance. In the designed panels the range of UV irradiation falls between the range 0.3 W/m2 as the lowest value and 45.9 W/m2 as the highest incident irradiance on the facade panel.

The dependence of reaction rate constant of NO on UV irradiation for both linear and non-linear dependencies can be expressed as:

$$\boldsymbol{k = \alpha_1 \left(-1 + \sqrt{1 + \alpha_2 E}\right)} \qquad (2)$$

Where k is the reaction rate constant for the degradation of NO [mol/m3/s]

α_1 = 0.03 mg/m^3 and α_2 = 9.1 m^2/W are the correction factors used to fit the formulation with the experimental data.

E is the UV irradiation in W/m^2

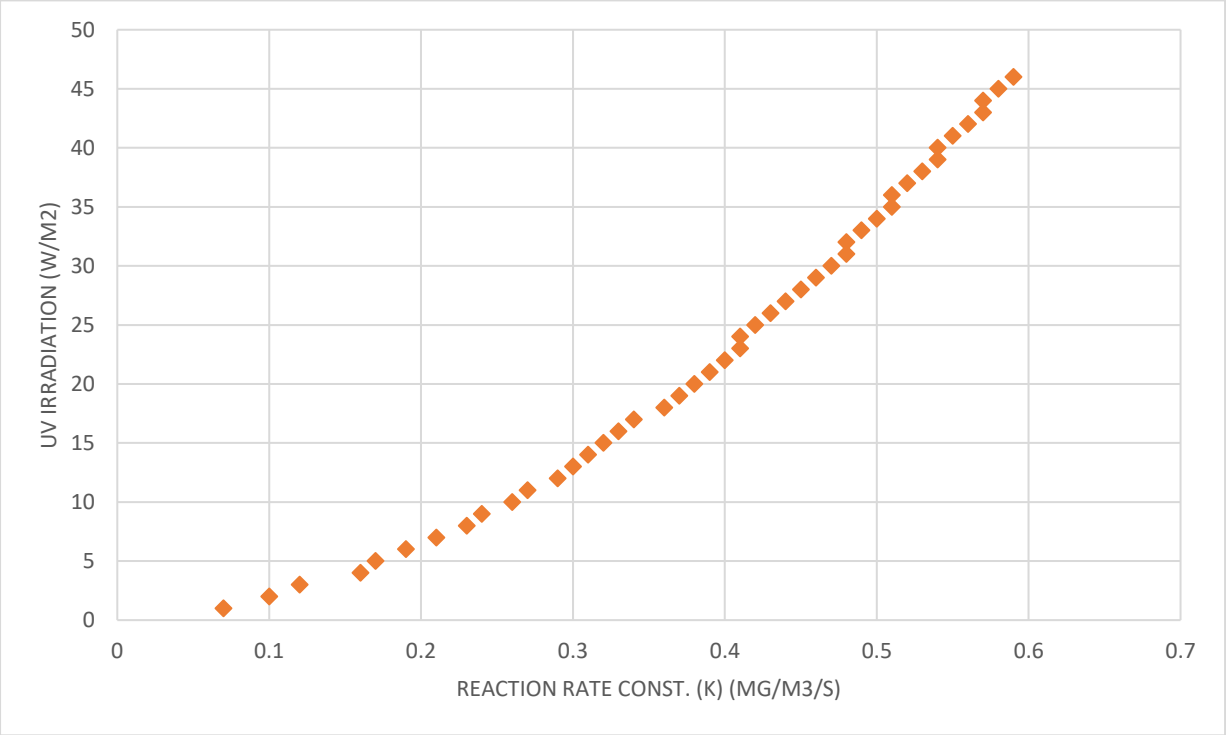

Figure 40 Dependence of reaction rate constant of NO as a function of irradiation

The experiments by Hunger et al, 2010 clearly the states the strong influence of relative humidity on the degradation of NO. The water molecules from the air is absorbed on the surface of the substrate. With increase in RH levels in surroundings would lead to high competition between NO and water molecules which in turn reduced that absorption equilibrium constant of NO. Accommodating the influence of humidity in the form of K_d (Effective adsorption equilibrium constant) and the irradiance levels into the **disappearance rate constant of NO** would give:

Combining Equations 1 and 2:

$$r_{NO} = -1\frac{kK_dC_{g(NO)}}{1+K_dC_{g(NO)}}\alpha_1\left(-1+\sqrt{1+\alpha_2 E}\right) \quad 3$$

$K_d = K_{NO}/(1 + K_{H_2O}\, C_{g(H_2O)})$ where $K_{(H2O)}$ is the absorption equilibrium constant of water.

This equation is used to model the photocatalytic façade as flux in COMSOL model.

2.5. Conclusion:

In the literature review, various research papers have proved the benefits of application of photocatalytic coating on pavements and facades in urban environments like the example in Castorweg, Netherlands where they had seen a difference of 18-45% in NO_x concentration in the immediate surroundings compared to the control street.

Various factors affecting the performance of photocatalytic coating are inferred from the controlled situation of laboratory experiments. These dependent variables affecting the performance are incident UV radiation, contact wind speeds, relative humidity and material properties like the type of coating and substrates onto which they are applied. These factors discussed above needs to be correlated with the urban climatic context to frame the appropriate design parameters.

A flat panel coated with TiO_2 may not be the most optimum way to integrate onto building facades which can be seen in studies of Umbreto tunnel and Leopold tunnel that highlight the dysfunctionality of these coatings in less lighting levels and high wind speeds. Case study of Prosolve370e shows the potential of design in surface manipulation to achieve surface enlargement and turbulence generation. Hence, it is assumed that an appropriate design of the panel would be necessary to implement them for better results in urban scenarios before being tested for their performance.

Their application would prove to be feasible and economical only when they are applied in the right context. With increasing height of built forms, the concentration profile of the pollutants decreases with heights. In dense built environments, the vehicular plumes are concentrated at the façade surfaces up to the height of 3m in streets with aspect ratio of 1. It would be more appropriate to integrate the photocatalytic façade panels on low rise structures (up to a height of 10m) which is chosen as the boundary condition for the further analysis.

03 DESIGN PARAMETERS & SITUATIONS

Chapter Overview

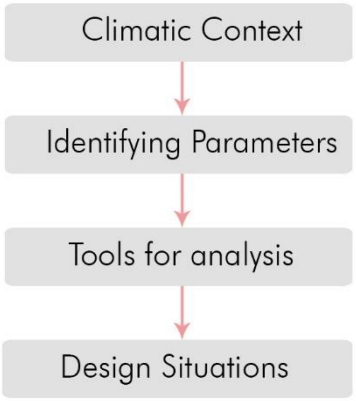

This chapter deals with the study of London's climatic factors that affects the performance of photocatalytic materials like relative humidity, precipitation and irradiation potential of facades.

The second part of this chapter explains about identification and evaluation of parameters determining photocatalysis in urban situations followed by the tools used to analyze the parameters.

The last part of this chapter presents the design situations where the concept must be applied and evaluated.

3.1. Climatic Context: London

The policy framework in London and constant breaching of NO_x levels in various streets has led to selection of this city as the reference context to extract climatic parameters. Wind speed, relative humidity and irradiation levels are the most critical factors affecting photocatalytic materials. The climatic data that needs to be applied in the further analysis are inferred from the following section.

Wind speed: Wind speeds are critical in deciding the amount of residence time (flow rate) of the pollutants over the façade. In the figure below, it shows that 72 % of the year the winds speeds range between 3-5 m/s. The highest wind speeds are between 5-9 m/s which are for 11% of the time in the year. And for 1 % of the time in the year, the wind speeds are lesser than 2 m/s. **The highest velocity for most of the time in the year is 5 m/s which is used in CFD analysis for analyzing the wind velocity field over the façade for perpendicular and parallel flows.**

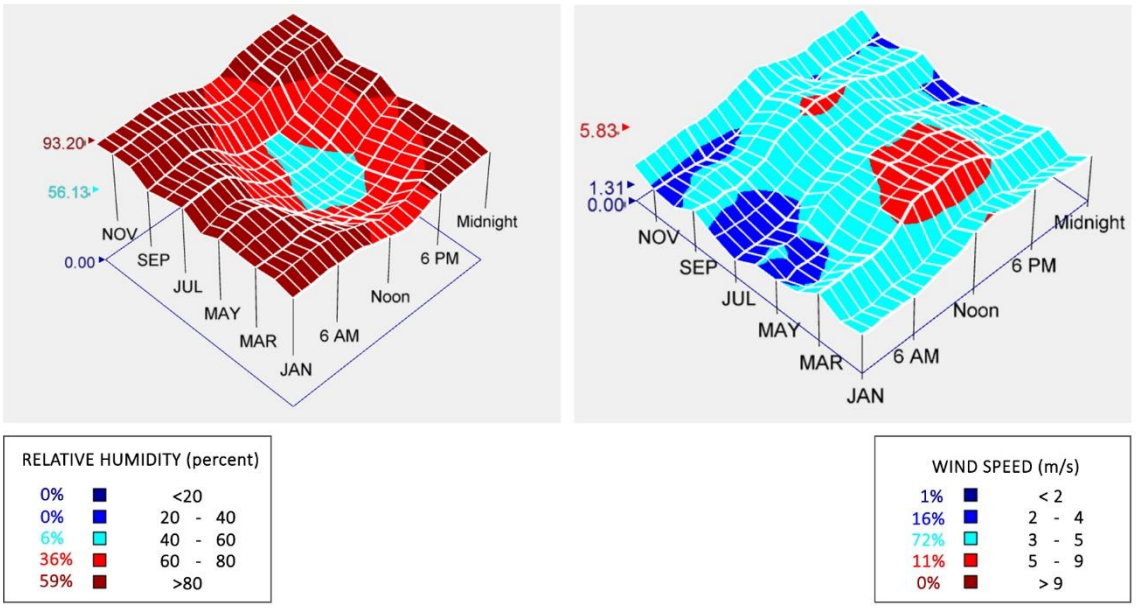

Figure 41 Yearly average humidity levels (left); Yearly average wind speed (right) (Climate Consultant 6.0)

Relative Humidity: For more than 90% of the year, relative humidity is above 60%. The most favorable condition for a good photocatalytic reaction is 10-50%. Humidity conditions in London may not be most favorable for the best performance of photocatalysis. However, this climatic parameter does not affect the geometry of the panel. But, a value of 70% RH is used to calculate the effective absorption equilibrium constant in section 7.4.2.

Rainfall: London has a precipitation of 263.0 days with January receiving the highest amount rainfall (13.5 days of rain) and July receiving the least amount with 6.5 days. The average range of precipitation is 500-2500mm and 5000mm for the local totals.

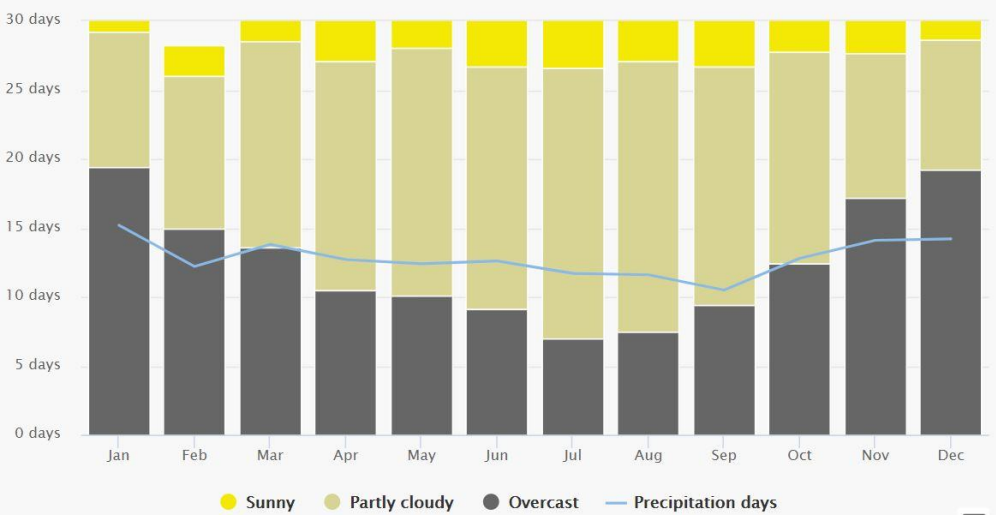

Figure 42 Number of precipitation days for various months in a year (Source: Meteoblue)

Figure 42 shows that there is at least 10 days of precipitation in a month. Literature studies suggest a washing of photocatalytic surface once in two months helps in replenishing the photoactivity of the catalyst. Hence, **frequent showers on site helps in cleaning the façade surface and replenishes the photocatalytic activity by washing away the byproducts like nitrates that are accumulated on the surface of the panel without special needs for maintenance.**

Solar irradiation: Amount of incident radiation on the building surfaces varies with the orientation of the façade. The average radiation levels are higher during equinox and summer for all the orientations and lower during winter. South façade has the highest amount of incident radiation throughout the year. The hierarchy of the orientation based on the amount of incident radiation is: South > West > East > North. Hence, **the design strategies discussed further are applied to the south façade for deriving the concept and then tested for its performance.**

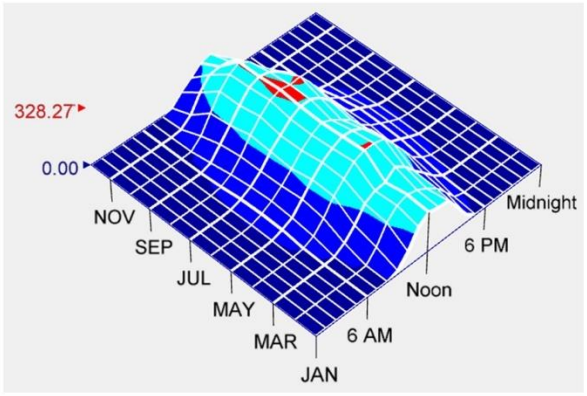

Average solar irradiation on South facade, London

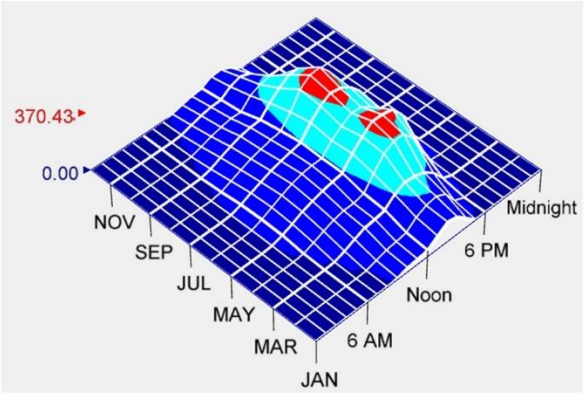

Average solar irradiation on West facade, London

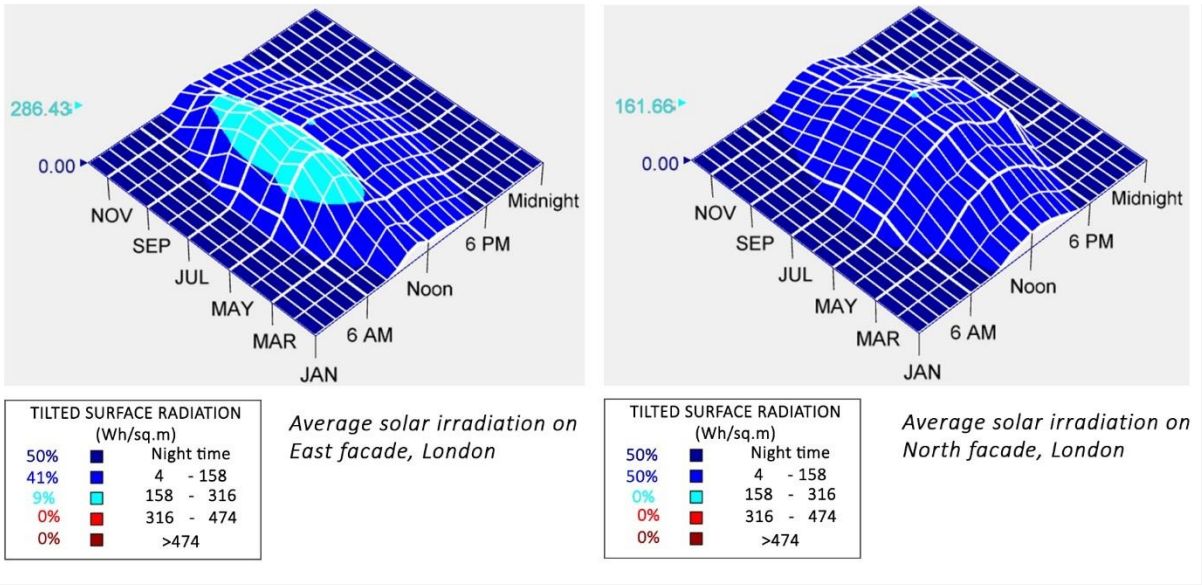

Figure 43 Incident solar radiation on the vertical built surfaces

3.2. Translation of Parameters to urban scenario

From the literature review, irradiance levels and flow rate are the determining factors for photocatalysis. Most of the studies had specified radiation requirements in terms of UV irradiance and not solar irradiance. Hence, the first part of this section talks about the proportion of UV irradiance in the solar spectrum. While the flow rate is correlated to the wind velocity field.

3.2.1. Extracting UV irradiance from Solar Spectrum:

The Solar spectrum is composed of electromagnetic waves which are classified into three categories (Figure 44) based on their wavelength. Electromagnetic waves with larger wavelength have less energy (infrared) and the one with shorter wavelength have more energy (Visible light or UV).

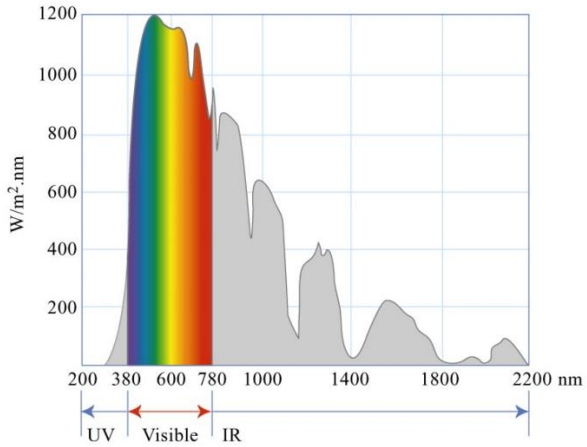

Figure 44 Solar spectrum and its energy composition (Source: WE forum)

Photocatalysis requires the UV-A with a wavelength range of 315-400 nm for the electrons to get excited and create a hole pair. The percentage of UV irradiation varies with places ranging from 2-5%. In a study of solar irradiation at higher altitudes by lumthaler & Ellinger, 1997, various measurements of total incident radiation and UV-A irradiation were measured during different seasons of the year for Innsbruck in Austria and Jungfraujoch in Switzerland (Summer solstice, winter solstice and equinox). The study also indicates increases in the amount UV radiation with increasing heights. The measurements of proportion for incident UV irradiation are presented in the table below:

	Daily total global irradiance ($MJ/m^2/day$)	Daily total UV-A irradiance ($MJ/m^2/day$)	Percentage of UV irradiance in solar irradiance (%)
Innsbruck, Austria (577 m a.s.l)			
Summer Solstice	29.45	1.48	5.02
Autumn Equinox	16.45	0.82	4.98
Winter Solstice	5.09	0.24	4.72
Spring Equinox	18.36	0.8	4.35
		Average % UV	4.76
Jungfraujoch, Switzerland (3576 m a.s.l)			
Summer Solstice	36.50	1.89	5.17
Autumn Equinox	22.55	1.16	5.14
Winter Solstice	7.39	0.32	4.33
Spring Equinox	22.70	1.17	5.15
		Average % UV	4.89

Table 15 Maximal daily total global irradiance for sunlight and UV-A (lumthaler et al, 1997)

From Table 15, it can be concluded the difference in altitude has a difference of only 0.13% in UV light composition for a 3000 m altitude difference. Though the range of UV irradiance varies over different seasons, **a proportion of 4.5 % of the total incident solar irradiation is assumed for further analysis.**

3.2.2. Surface wind velocity field:

Reduction of wind speed over the photoactive façade surface. Surface roughness of the building envelope helps in modifying the wind flow field on the building. It has been proved that effects of reduction of wind pressures are considerable for walls with surface roughness such as balconies, louvers, canopies and any kind of appurtenances. Adding textural elements to the building envelope can reduce the local forces on the building façade (Lignarolo, Lelieveld, & Teuffel, 2011).

A CFD analysis of smooth façade versus rough façade by Lignarolo et al. 2011 shows the difference in the velocity fields for wind flowing parallel to the façade (Figure 45). The values of velocity are taken along a plane located at 0.5 meters away from the façade surface which corresponds to the plane at the center point of the roughness elements. Along the

smooth facade (case a), velocities are within the range 5 – 9 m/s and up to 15 m/s close to the top and the upwind corner. Alternating roughness elements in the vertical direction provides uniformity of the flow field by avoiding stagnation of air and enough turbulence. From this, it can be inferred that surface texture offers big resistance to the wind by decreasing the velocity of wind close to the façade. And measurement of wind velocity field at the surface of the façade panels would provide information about the flow rate of air close to them.

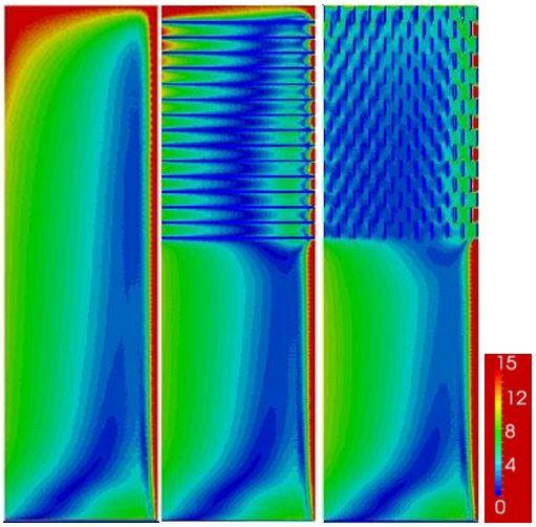

Figure 45 Influence of surface roughness on the velocity field on the façade of a building 100m tall; from left case a, case b and case c

3.2.3. Tools for analyzing the parameters:

Maximizing the total radiation and understanding the UV irradiation pattern on the geometry is necessary to enhance the light capturing potential of the panel. And wind velocity field needs to be analyzed over the roughness elements to decide their sizing. To interconnect the workflow in a single interface, plugins of rhino only were selected. Ladybug (component of grasshopper plugin) is the tool that was used for studying the irradiance patterns while Rhino CFD plugin was used to analyze the wind flow field over the geometry. Apart from these octopus is used to optimize the identified parameters for the design. Each of these tools and their method of usage is explained below:

Ladybug: The incident radiation results for a geometry can be obtained using the weather data input for the reference context (London). Two types of data sets were extracted. They are:

- The output from the radiation analysis component as irradiation (Whr/m^2) which is the sum of irradiance over a time period (in this case it would be sum of irradiance over the analysis days per m^2).
- Irradiance (W/m^2) is the instantaneous intensity of solar radiation on a unit area per unit time (hour). To ease the comparison of UV irradiance for summer and winter,

shortest day in the year is chosen. All the irradiance levels of UV are a measured for an 8-hour average from 8:00 (sunrise) to 16:00 hours (sunset).

The faces of the façade panel must be maximized for incident irradiation throughout the year. Once maximized for irradiation, the geometries need to be compared with each other based on the incident UV irradiance. UV levels required for photocatalysis are described as irradiance in most of the literature studies and not as irradiation. Hence, the average UV irradiance is measured as an average over 8 hours for each of the analysis days.

Analysis period: To simplify the year-round calculation and comparison of radiation and incident irradiance, the analysis is done for three differ sun altitude angles:

- 21 December (Winter solstice)
- 21 March (Equinox) and
- 21 June (Summer solstice)

Rhino CFD: In a computational domain shown in Figure 46, the façade panels are mounted on a building of 10 m height with wind flowing parallel to the façade.

- Boundary conditions: The inlet has a velocity of 5 m/s in logarithmic profile which is the wind speed for 70% of the time in London. The velocity profile changes with height from the ground. The walls of the domain are modelled with open boundary condition.
- The wind velocity at the surface of the facade panels for various arrangements are measured using probe points at the middle of the building's height and compared with the velocity field on a flat panel at the same height. The projection length of the panels manipulates the wind speed over the façade surface.

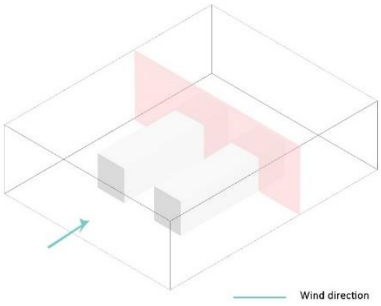

Figure 46 Computational domain for Wind velocity field analysis for perpendicular flow (left) and parallel flow (right)

Optimization tools: Galapagos (for single objective) and octopus (for multi-objective) are the two tools opted for optimization. For the conceptual justification, the geometries are optimized for only summer as the maximum amount of self-shading is reached in summer for the south façade. The starting geometry shortlisted after this process is optimized for three objectives namely; surface enlargement, maximum irradiation during summer and winter. Having more than one objective requires a multi-objective optimization plugin that has led to the choice of octopus.

3.3. Design Situations:

A good design roots from its context and it must respond to its immediate environment to stay relevant. In this situation of applying a photocatalytic building material whose performance is highly dependent on the surrounding environmental phenomenon, it is important to study and understand the situations in which the panels would be performing.

Urban environments are different from one place to the other. The buildings differ in their orientations, they may be present in densely built surroundings or they may be free standing. Such characteristics of their location determines the influence of the environmental factors over the built forms and the surrounding phenomena associated with them like transportation of pollutants, incident radiation etc.

Two contrasting design situations of free-standing building and a street canyon are chosen to understand their pros and cons in terms of implementing photocatalytic surface onto them. The performance inhibiting factors need to be understood for each of these situations which would frame the design requirements for the façade panel.

3.3.1. Case 1: Standalone building

Irradiance: Standalone building typologies considered here are built forms away from the city in high emission zones or near highways where the surrounding concentration of pollutants are high. Such a building receives ample amount of unobstructed radiation throughout the year on its façade surfaces. The figure below indicates the incident 8-hour average UV irradiation (between 8:00 and 16:00 hrs.) for three different positions of the sun in a year.

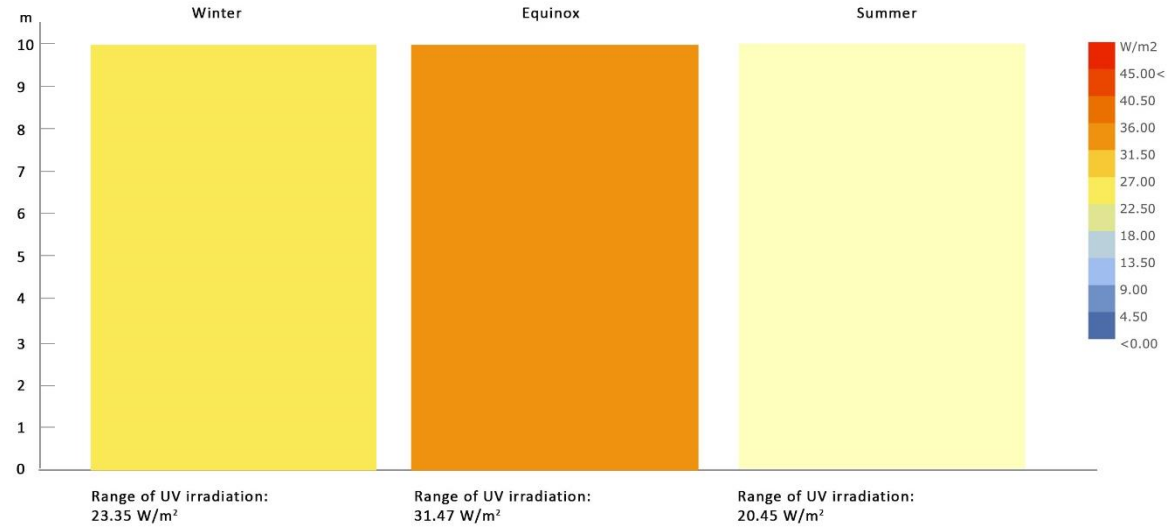

Figure 47 UV-irradiation (7-hour average) on the South facade of a stand-alone building (10 m height)

In Figure 47, the south façade depicted has an ideal UV irradiation available for a good photocatalysis reaction where all the facades have UV irradiation greater than 10 W/m^2 with summer having the least value of 20.45 W/m^2.

These buildings are subjected to high-speed wind due to no surrounding obstructions. Wind hits the façade with highest velocity when the direction is perpendicular to the façade. For such wind flow, velocity field over the façade was studied.

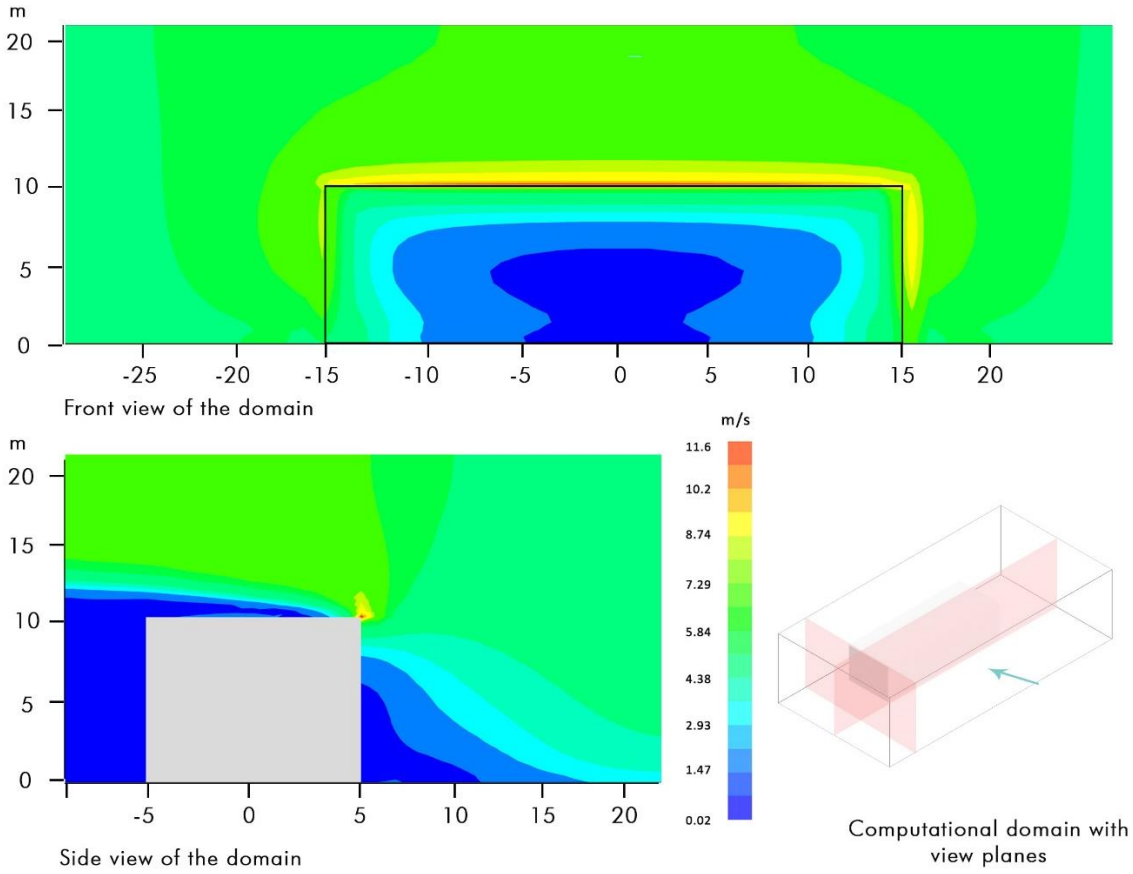

Figure 48 Wind velocity-field over the surface of the facade for perpendicular flow with velocity 5 m/s

In Figure 48, the velocity field towards the corners of the building have high velocity, while maximum part of the façade is in the low velocity zone (<2 m/s). Hence, perpendicular winds may not be strongly influential in analyzing the geometry.

3.3.2. Case 2: Street Canyon

Secondly, highly polluted urban situation would-be a high-density traffic route bounded by buildings on either side (street canyons).

The façade receives the least amount of radiation at the bottom of the street at any season. Lighting levels increases gradually in the streets from bottom to the top. Winter season has 67% of the facade surface below 10 W/m^2 while autumn/spring has 8% of surface area below 10 W/m^2.

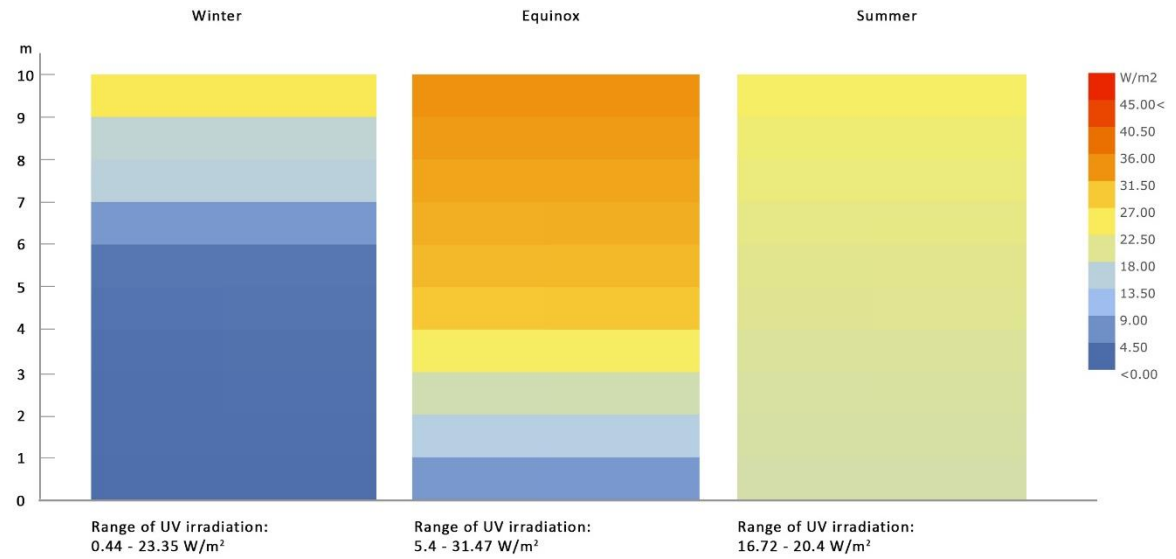

Figure 49 UV irradiation (8-hour average) over the south facade in a street canyon of aspect ratio 1.

The incident winds blowing perpendicular to the façade will not strong influence on the façade surface. However, the effect of wind direction parallel to the façade was analyzed and shown in the figure below.

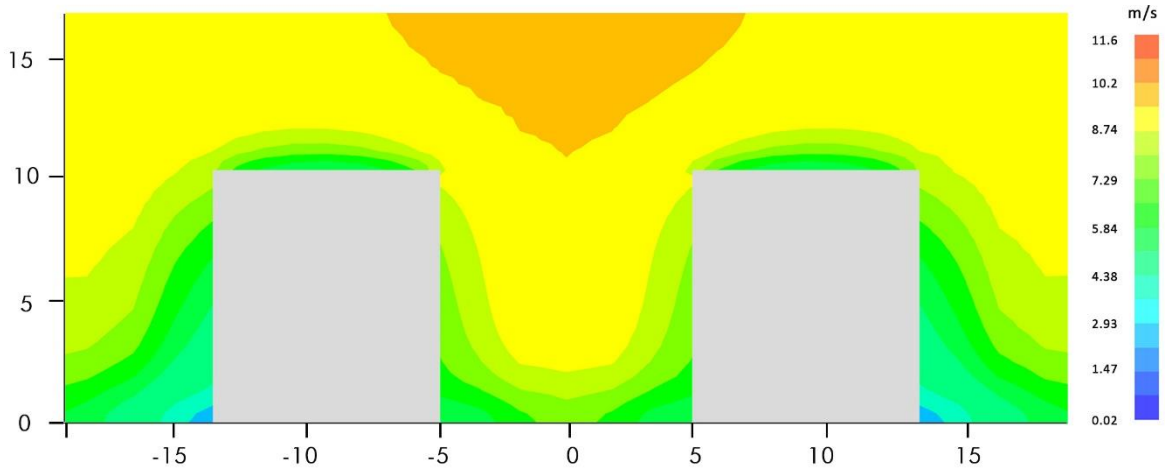

Figure 50 Wind velocity field between the street canyon for wind flow parallel to the street

From both the cases of built form in urban environment, the winds move faster and have less residence time over the façade when the wind orientation is parallel to the facade. Figure 50 shows the wind speed profile over the façade. From the bottom of the building to the top, they have incident velocities higher than 2 m/s.

Case 1 and Case 2 are two generalized situations extracted from the urban environment showing variations in the lighting levels and contact wind speed on the façade.From these two cases, two issues can be identified in urban areas in correlation with photocatalytic surfaces that are further used in justifying the design:

- Zones with low penetration of light (< 10 W/m^2)

- Zone with faster movement of wind (> 2 m/s)

The benchmark values for irradiation and velocity are picked from the literature review of Leopold tunnel.

Environmental Factors	Stand-alone building	Street canyon
Wind	Perpendicular wind and parallel winds are a concern.	Parallel winds are faster and flushes out the pollutants faster without enough residence time on the photocatalytic surface.
Irradiation	100 % of the surface with irradiation more than 10 W/m^2 throughout the year.	Winter has more than 60% of the surface area with irradiation less than 10 W/m^2 of UV irradiance.

Table 16 Summary of the design situations in urban environment

The designed geometries should be tested for parallel winds over them and for irradiation levels in street canyon during the conceptual phase.

04 DESIGN STRATEGIES

Chapter Overview

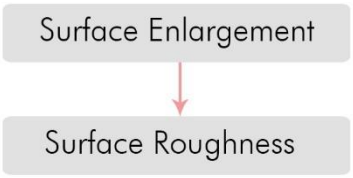

The first part of this chapter deals with experimental strategies for enlarging surface. Pros and cons of each strategy is discussed, and a strategy is chosen for developing the concept.

The second part of this chapter explains the influence of roughness elements in manipulation of wind velocity fields with a test concept. This helps in concluding the minimum size of the roughness elements for starting point to develop the concept.

4.0. DESIGN STRATEGIES

Integrating the facade panel into various urban situations and orientations would require them to receive light from multiple directions. Enhancing the incident irradiation is possible by modifying the cardinal angles of faces of the panel with respect to the sun vector. Photocatalytic surfaces can perform in both direct and diffused solar radiation for breaking down the pollutants. Hence, optimization of these panels for a sun angle is not necessary.

The surface enlargement should be designed such that the panel receives ample amount of radiation throughout the day and the year. The figure below shows the variation in cardinal angles of the façade panels face in response to suns position.

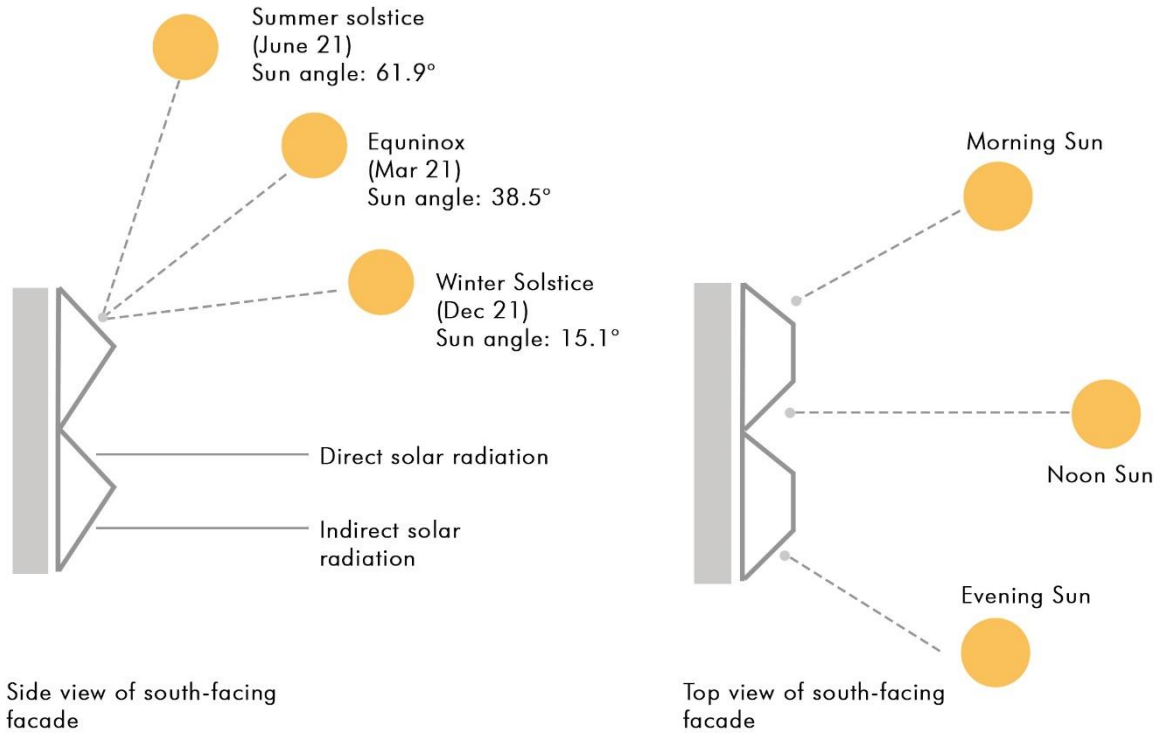

Figure 51 Surface enlargement design principle for south façade

4.1. Strategies for surface enlargement:

The surface enlargement factor that will be discussed hereafter is calculated as the final surface area after manipulation divided by the original area of the flat façade panel.

In the initial stages of the design, three methodologies were experimented to frame the strategies which are discussed below:

Method 1 - Splitting the volume: First method discussed is splitting the volume/cuboid into a grid and alternating them with solids and voids. The same process was repeated for

triangular and hexagonal grid with a resulting geometry that has a depth of 0.3 m having surfaces inaccessible for light and rainwater penetration. They could also lead stagnation of air in the deep pockets of the modules reducing its pollution abatement efficiency.

Method 2 - Sinusoidal manipulation: Such patterns are inspired from the heat transfer modules that use sinusoidal patterns to increase the ratio of surface area to thermal mass. From Figure 52, a range of surface enlargement from 1.6 times to 3.5 times is possible. The surface area of these panels can be increased by morphing the surface with sinusoidal curves along different axis of the panel. The resultant pattern is however like the previous case obtained by splitting method with inaccessible areas for light and rainwater penetration. This could lead to deposition of by products on to surface for longer time creating surface passivation and would require manual maintenance to restore photoactivity.

Method 3 - Pyramidal extrusion: Capturing omnidirectional light is the most essential part for this panel. Developing a pyramidal surface would help in capturing light from various orientations at different times of the day with surface enlargement not compromising on the smoothness of the surface.

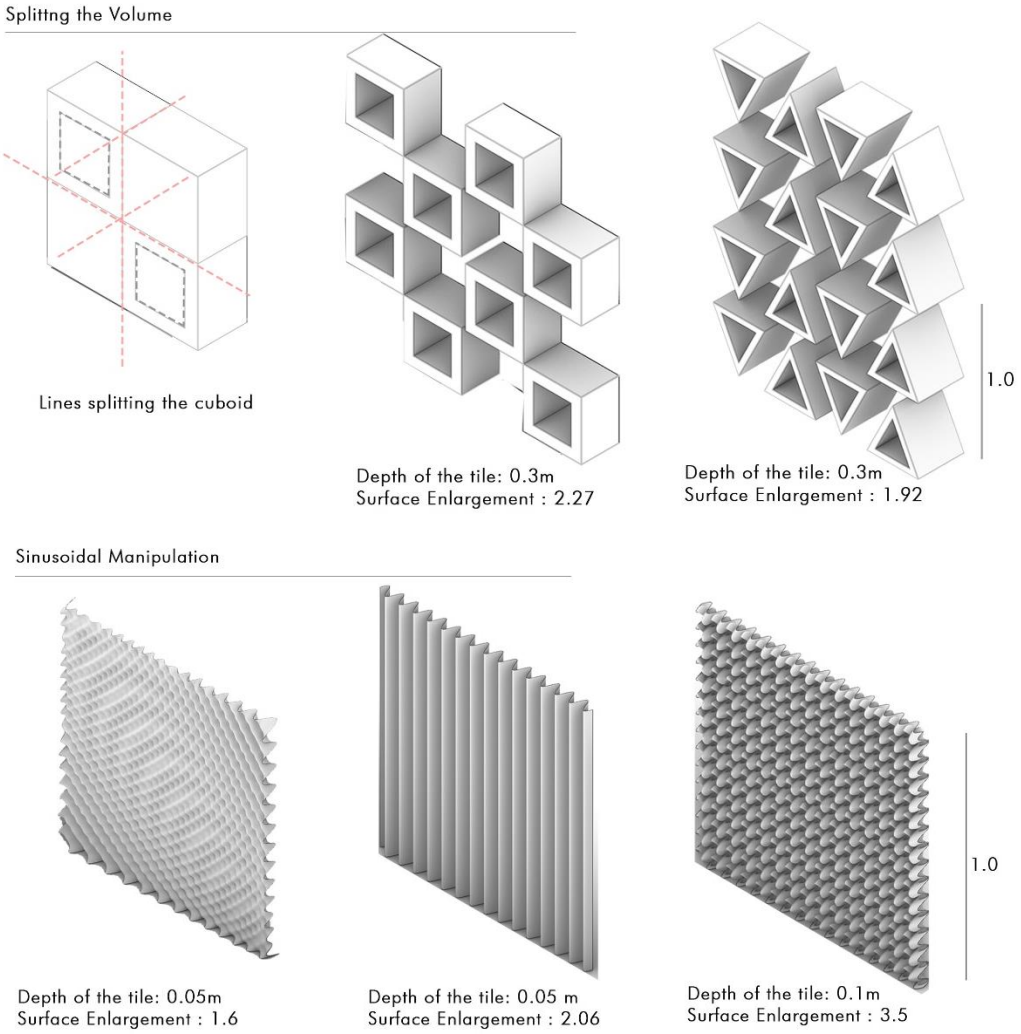

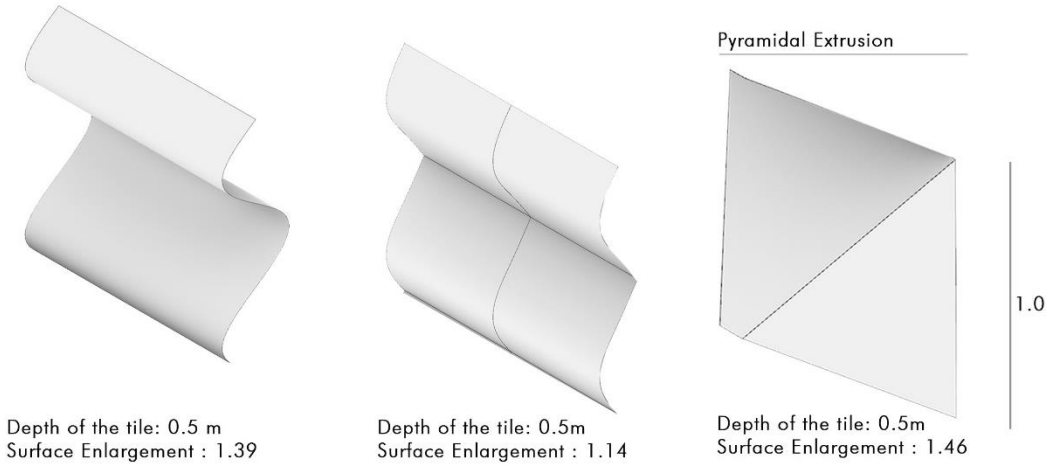

Figure 52 Conceptual surface enlargement strategies of 1 x 1 m facade panel

4.1.1. Effect of surface enlargement strategies on irradiation levels:

Surface manipulation can vary the range of incident irradiance over the surface for different zenith angles of the sun. The Highest amount of radiation over the panels is received during summer and the least amount during winter. However, a panel has maximum surface area with average irradiation of at least 10 W/m^2 during winter followed by equinox and summer. Maximum amount of self-shading on a façade geometry is possible during summer. Following this, the conceptual phase design is done with the goal of minimizing the shading on the façade panel for summer. The above conclusions are made from the analysis of the panels discussed below which are conceptual models for a 0.5 x 0.5 m module. Panel 2 with better irradiation is taken forward to see the effect of wind over it.

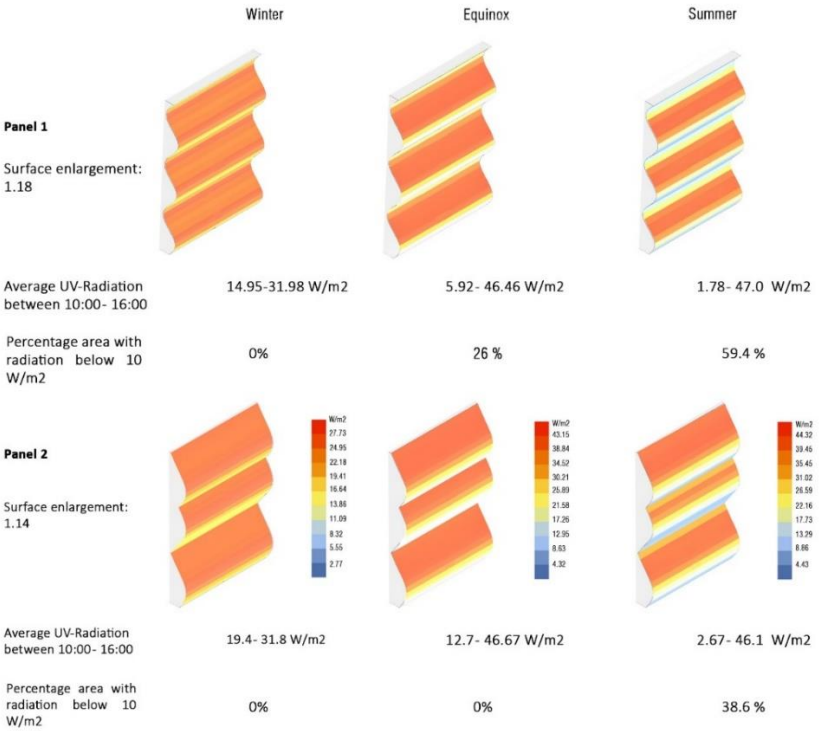

Figure 53 UV irradiation level on a sinusoidal test panel (not optimized for irradiation)

4.2. Strategies for reduction of contact wind speed:

As previously discussed in section 3.2.2, roughness elements help in reducing the contact wind speed at the surface of the façade. These elements can vary in size and shapes and there are various ways to create the texture from:

1. Arrangement of a geometry; or
2. Manipulating the surface geometry

To understand the effect of arrangement geometry on the wind velocity field over the façade panel, two situations are analyzed for one type of panel;

1. Alternating the arrangement of a sinusoidal panel
2. Arrangement of panels with voids

4.2.1. Roughness Strategy 1:

Alternate arrangement of panels had two projection lengths 0.1 m and 0.2 m. The range of velocity field in 0.2 m projection zone is much lesser than 2 m/s for a larger area compared to the projection zone with 0.1 m.

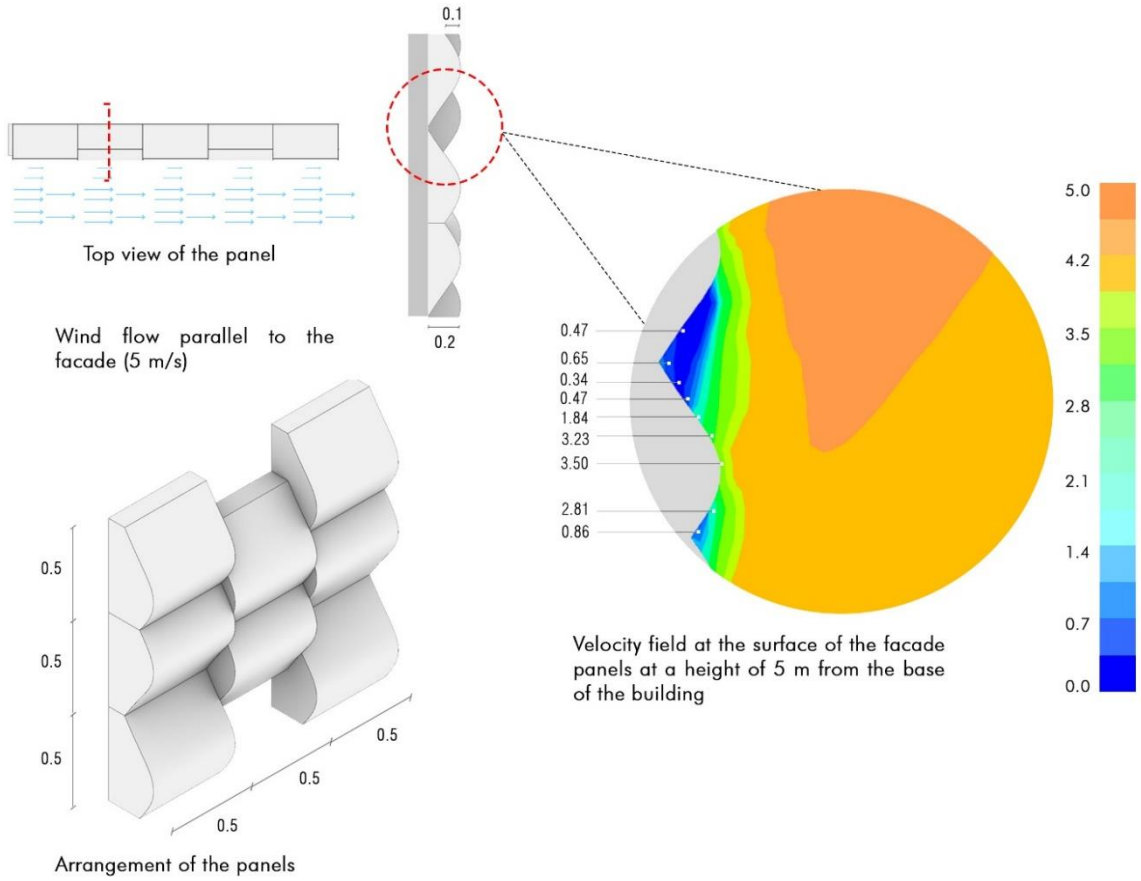

Figure 54 Wind velocity field measured for surface with projection elements at a height of 5m for a 10 m tall building (Computational domain 2 (right) is used from Figure 46)

The velocity field measured at the same height for a flat façade surface is about 4 m/s (Figure 50). Hence, the resultant average velocity on façade surface with projection elements of 0.2 m has a value of 1.8 m/s which is twice lesser than the value at the flat façade for the same point. Very small regions of the surface are exposed to larger wind speeds.

4.2.2. Roughness strategy 2:

From the previous geometry, every alternate panels were removed to create voids. The velocity in the voids are in the range of 0.65 – 0.84 m/s much lesser compared to the velocity on the projection. However, the velocity field on the sinusoidal panels are higher than 1.5 m/s. There is an alternation of higher and lower contact wind speed field.

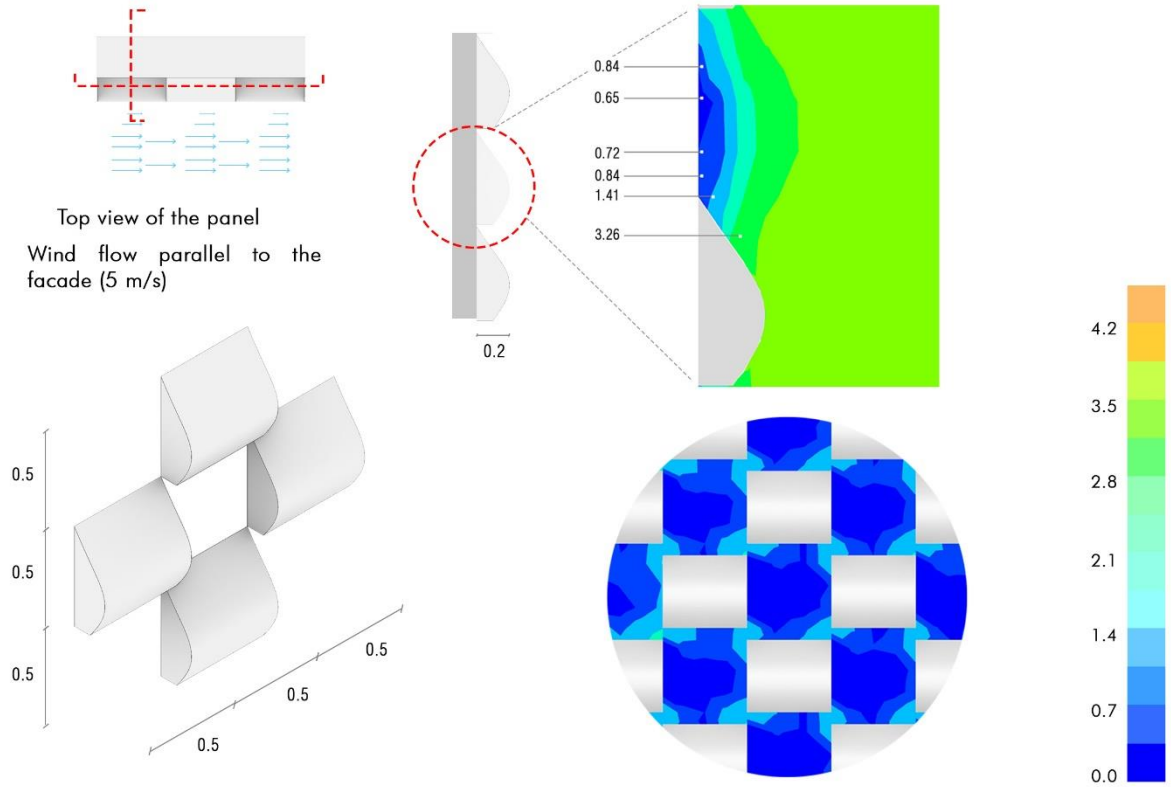

Figure 55 Wind velocity field measured for surface with voids at a height of 5m for a 10 m tall building (Computational domain 2 (right) is used from Figure 52)

4.2.3. Conclusion:

Comparing the two cases, the change in the roughness texture has a better impact in the reduction of the wind speeds. Case 1 has wind velocity range of 0.3 – 0.6 m/s at the undulations which is lesser compared to case 2. Hence, the varying the surface texture would be enough to slow down winds than having deep projections like case 2.

For projection length of the panel being a variable, a minimum of 0.2 m depth is chosen from case 1 for a module height of 0.5 m.

05 DESIGN METHODOLOGY:

The design strategies are experimented on various shapes packed together in a grid in the first part of this chapter. Comparing all the concepts, the most efficient shape is further analyzed to check for the wind velocity field over the geometry.

The selected shape is modified into an architectural concept from a tessellation pattern as the starting point and optimized for maximum irradiation for the year with surface enlargement.

The result is implemented into the street canyon to check for irradiance levels on the optimized panel.

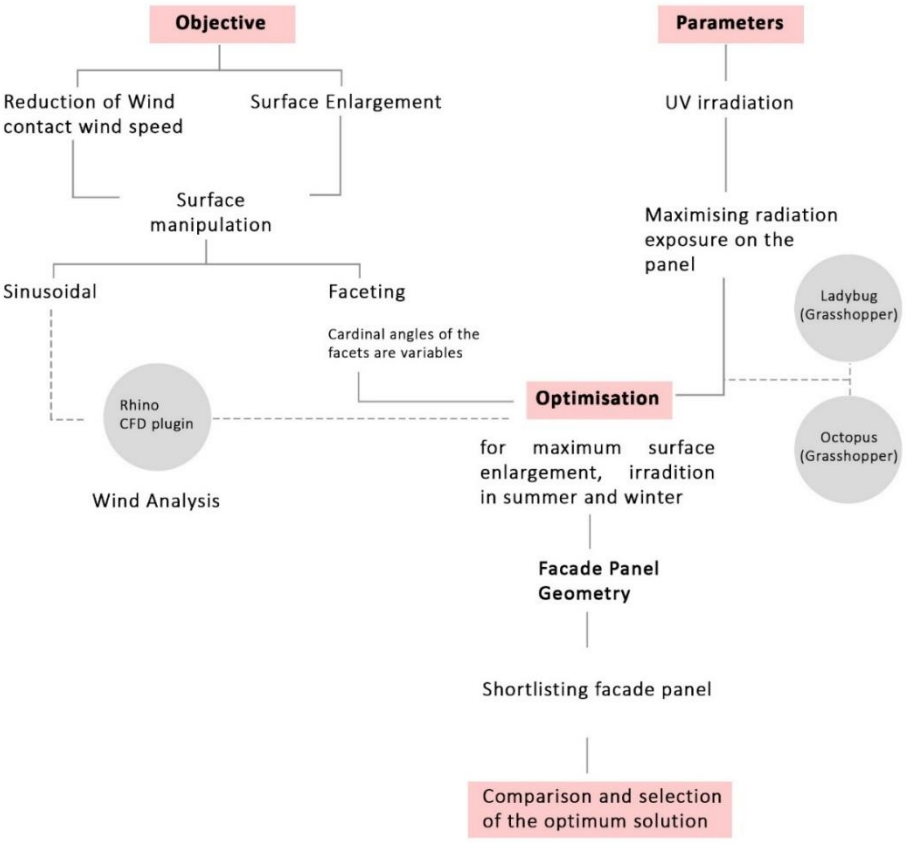

Figure 56 Methodology of design and tools used to achieve the objective

5.1. Conceptual Design:

The strategies discussed in the previous section need to be combined considering other aspects like modularity, mass manufacturing and aesthetics of the panel.

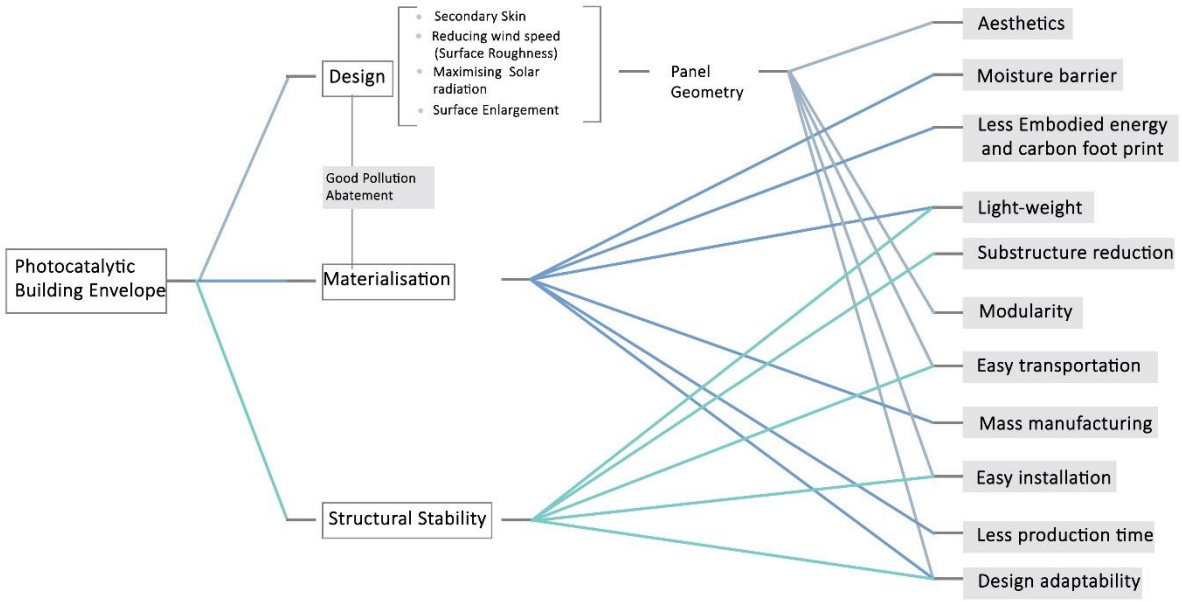

Figure 57 Chart depicting the considerations accounted for the conceptual phase

Keeping modularity as the starting point, closely packed grid patterns of triangle, square and hexagons were chosen to apply the discussed strategies.

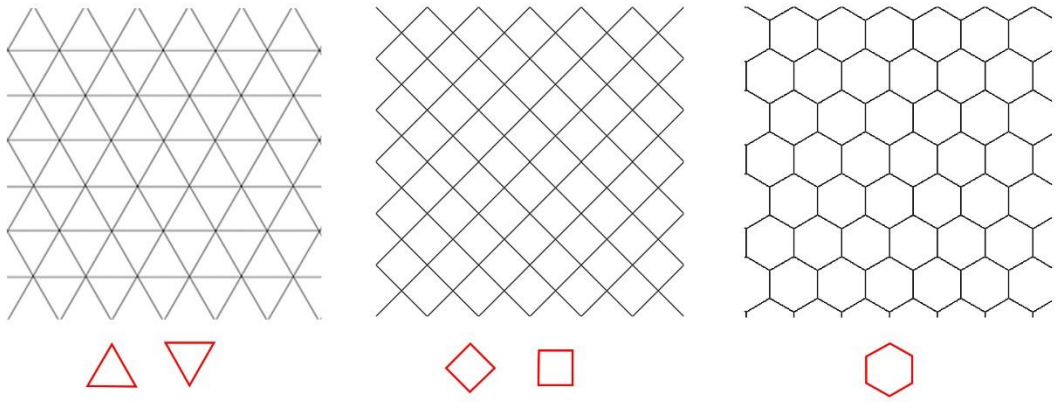

-

Figure 58 Grid patterns chosen to apply design strategies

Each of the shape (0.4 m wide and 0.4 high) in the grids were manipulated as pyramidal forms by changing the variables mentioned in Figure 59 to maximize the surface enlargement factor and incident irradiation for summer in Galapagos. The elite geometries with highest surface enlargement factors and irradiation for the analysis period are filtered

for each shape. For comparison of the outputs from the different shapes, geometries with highest surface enlargement factors were shortlisted which are analyzed for the incident the UV irradiance.

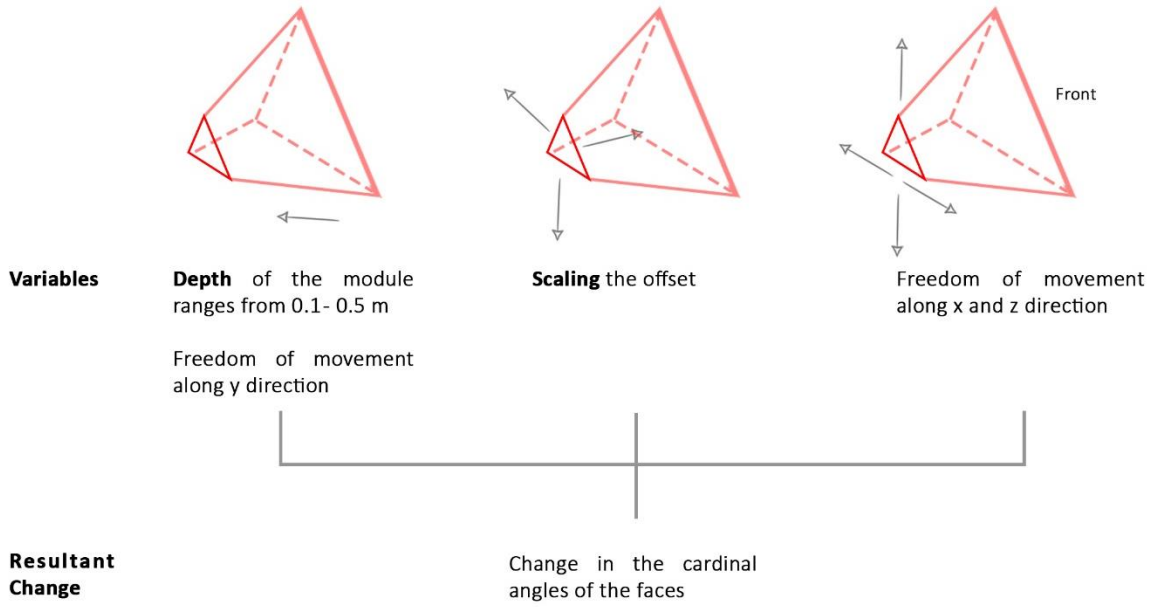

Figure 59 Variables to modify the surface enlargement and roughness factors

Comparison of Concepts:

The output and irradiance analysis for each of these shapes in Figure 58 are depicted in Appendix A.

- The surface enlargement factor was highest for the square pyramids with 1.96 followed by triangle and the lowest for hexagon (1.65).

- The depth of the panels was highest for the square pyramids (0.18m) followed by hexagonal pyramids. The higher the projection length, more would be the wind speed reducing effect.

- The geometries used for further comparison were shortlisted with the criteria that they would have least amount of surface area under an average irradiation of 10 W/m^2.

In the figure below, Modules with similar surface enlargement factors were chosen for the UV irradiance analysis.

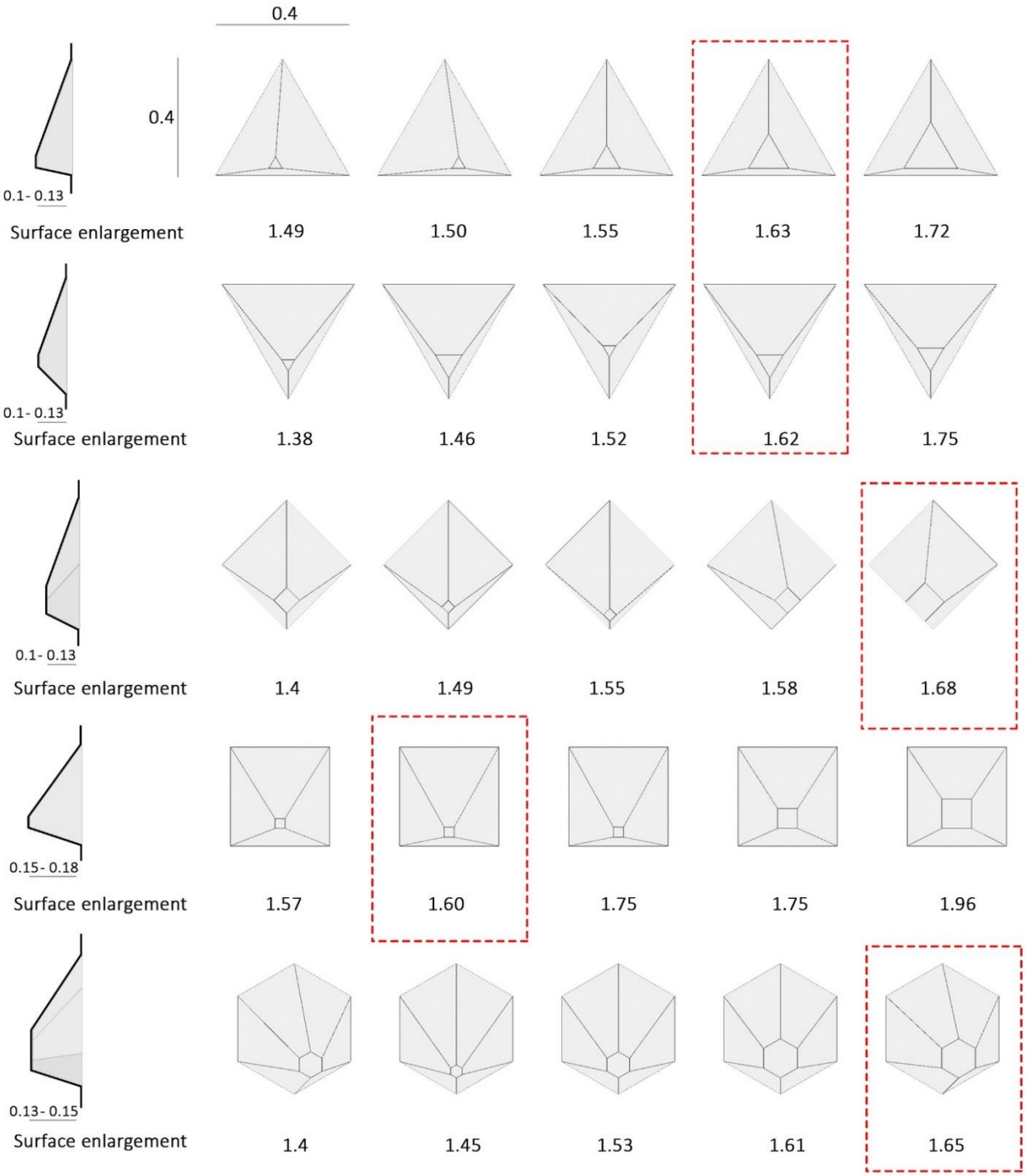

Figure 60 Comparison of output on surface enlargement for various shapes and selection of ones with similar enlargement values

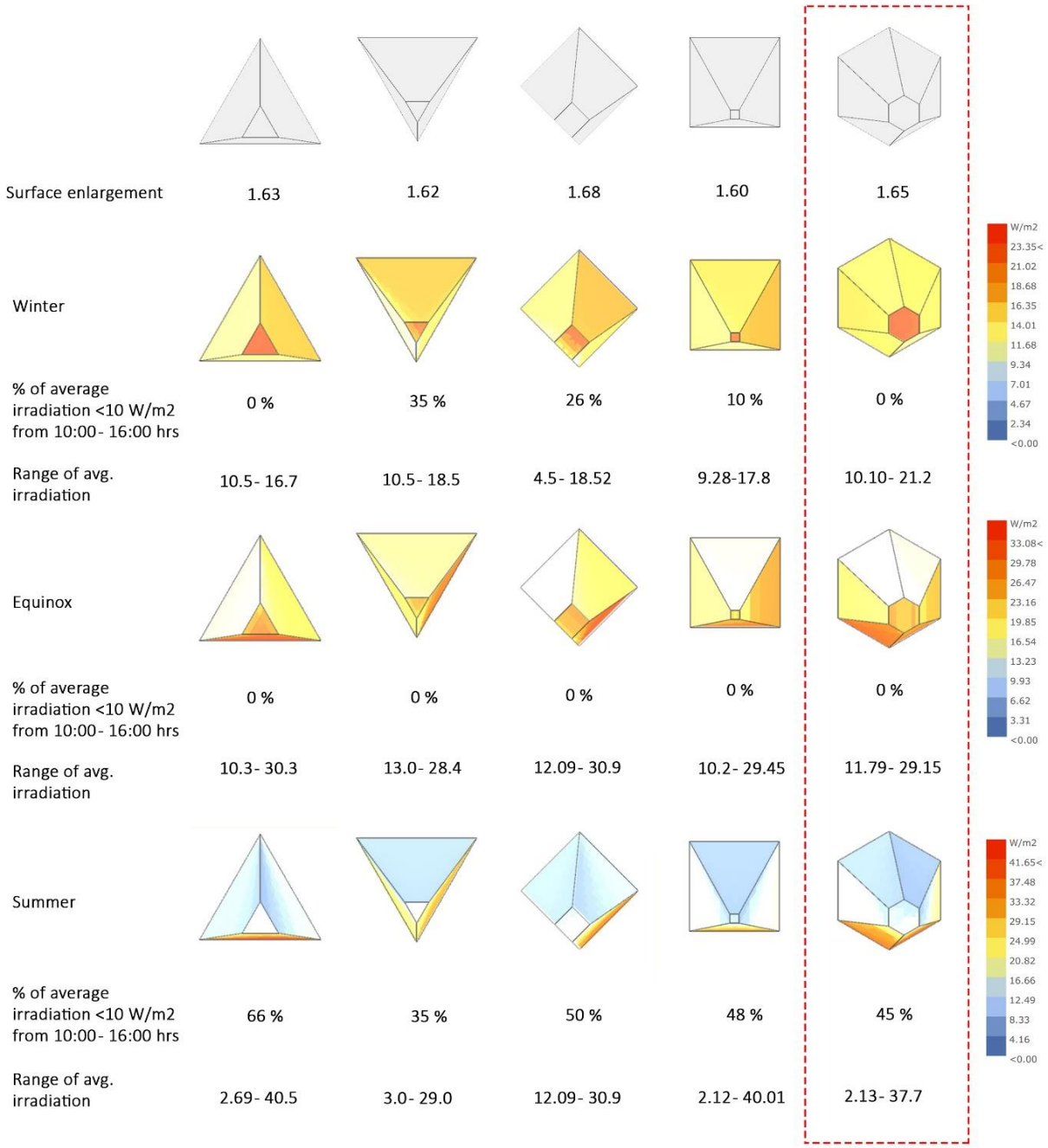

Figure 61 Comparison of UV irradiance for the analysis period for the outputs

Triangular and hexagonal pyramids have 0% of surface area under 10 W/m2 during winter and equinox. Also, hexagonal pyramids have the highest range of irradiance during winter and least amount of shaded surface during summer. Compared to the shapes analyzed, hexagonal forms proved to be more efficient in capturing omnidirectional light.

5.1.1. Wind velocity field on the finalized concept:

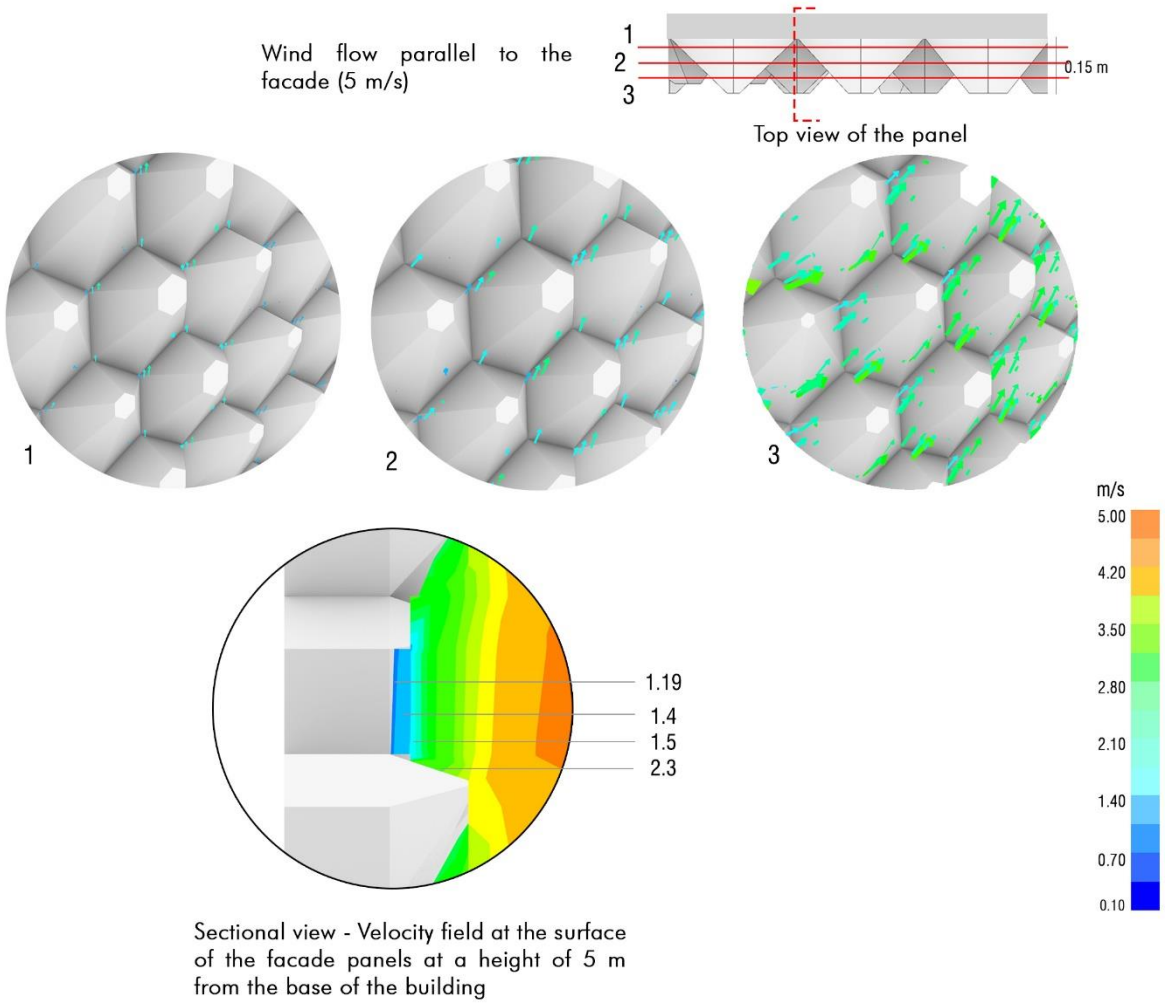

Figure 62 Wind flow path and velocity field over the facade surface of the concept with flow parallel to the façade

The velocity field between two adjacent tiles are lesser than 2 m/s. However, the velocity at the tapering faces are higher. The wind flow over the panels take a longer path due to the alternating pattern that provides higher residence time over the active surface.

5.2. Conceptual development:

The shape of hexagon shows better light capturing abilities. And this is chosen as the starting point for the design. From the architectural perspective, it is required to break the visual monotone of the façade panel.

Hence, A tessellation pattern of hexagon was chosen where the hexagon in rotational motion of 120° forms a pattern. Repeating the shape to form a pattern gives a potential to manufacture the design as a module of tile or as a panel for larger applications.

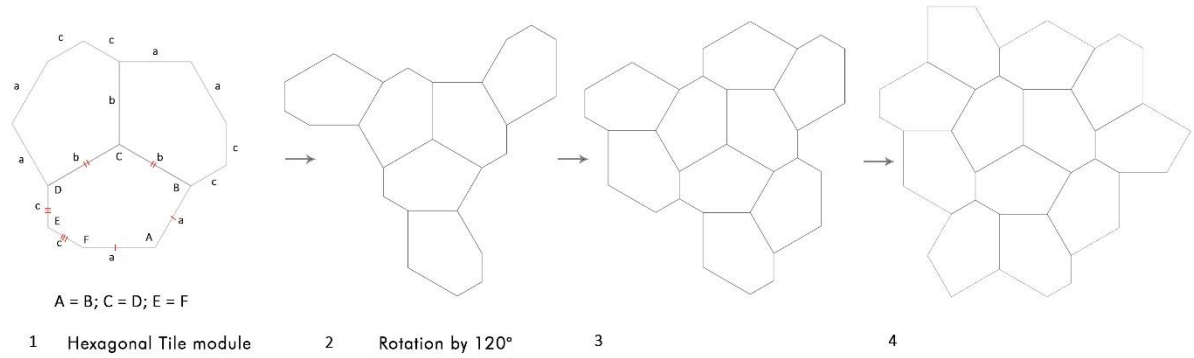

Figure 63 Growth of the hexagonal tessellation using rotation as the principle

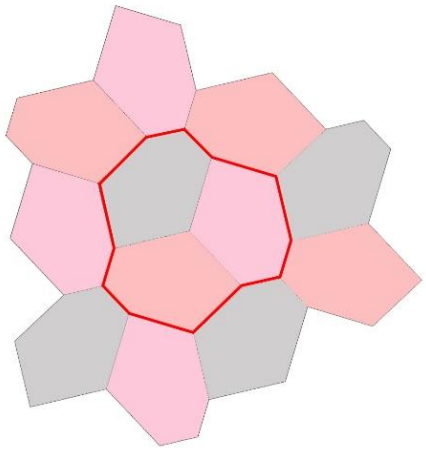

Figure 64 Hexagons indicated using same colors have same variables for the optimization process

The central tile module is the single repetitive unit that forms the pattern. To account for the shading effect by the adjacent geometries, surrounding modules are also considered for the optimization process. The variables and methodology explained in Figure 59 are used on the pattern. The objectives for the geometry are maximum surface enlargement, maximum irradiation for summer and winter.

5.2.1. Optimization results and comparison:

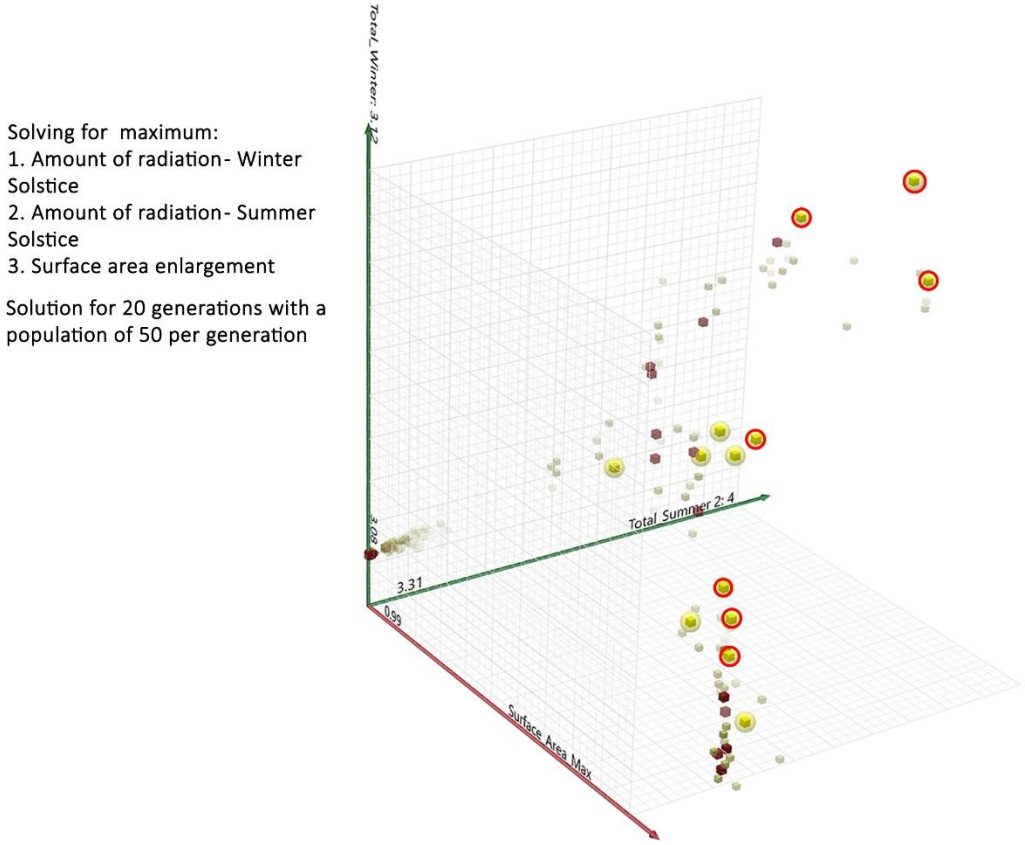

Figure 65 Graph from Octopus plugin plotted with the optimized results

The result from the optimization gave three distinct solution groups:

- Maximized radiation levels with least surface enlargement
- Intermediate radiation levels and surface enlargement
- Maximized surface enlargement and lesser irradiation levels

From each of these groups, the optimum solution was sorted for comparing the UV irradiance levels on their surface.

There is a linear increase in incident irradiation with increase in surface area.

Surface area with average irradiation levels greater than 10 W/m^2 provide best active areas. In figure 67, no clear pattern in the change of active surface area is noticed. However, **the criteria for selecting the geometry is that they should have maximum active surface area during winter, equinox and summer.** This means that this geometry would have the maximum amount of active surface area available for photocatalysis in a year. The selection made is indicated in the figure below This concept is further developed into a panel.

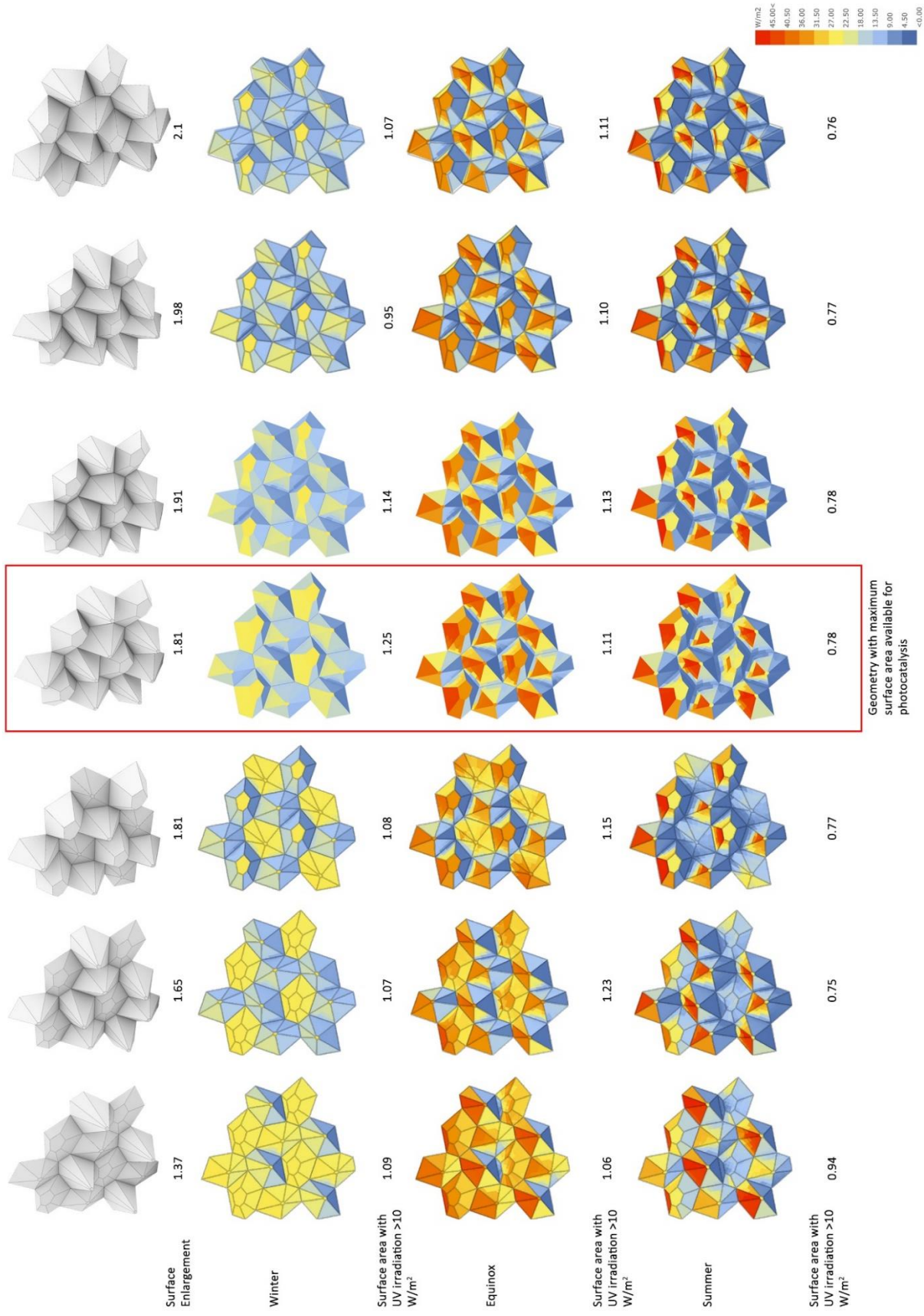

Figure 66 Comparison of Optimized geometries for year-round irradiation for South facade

5.3. Application in Street Canyons:

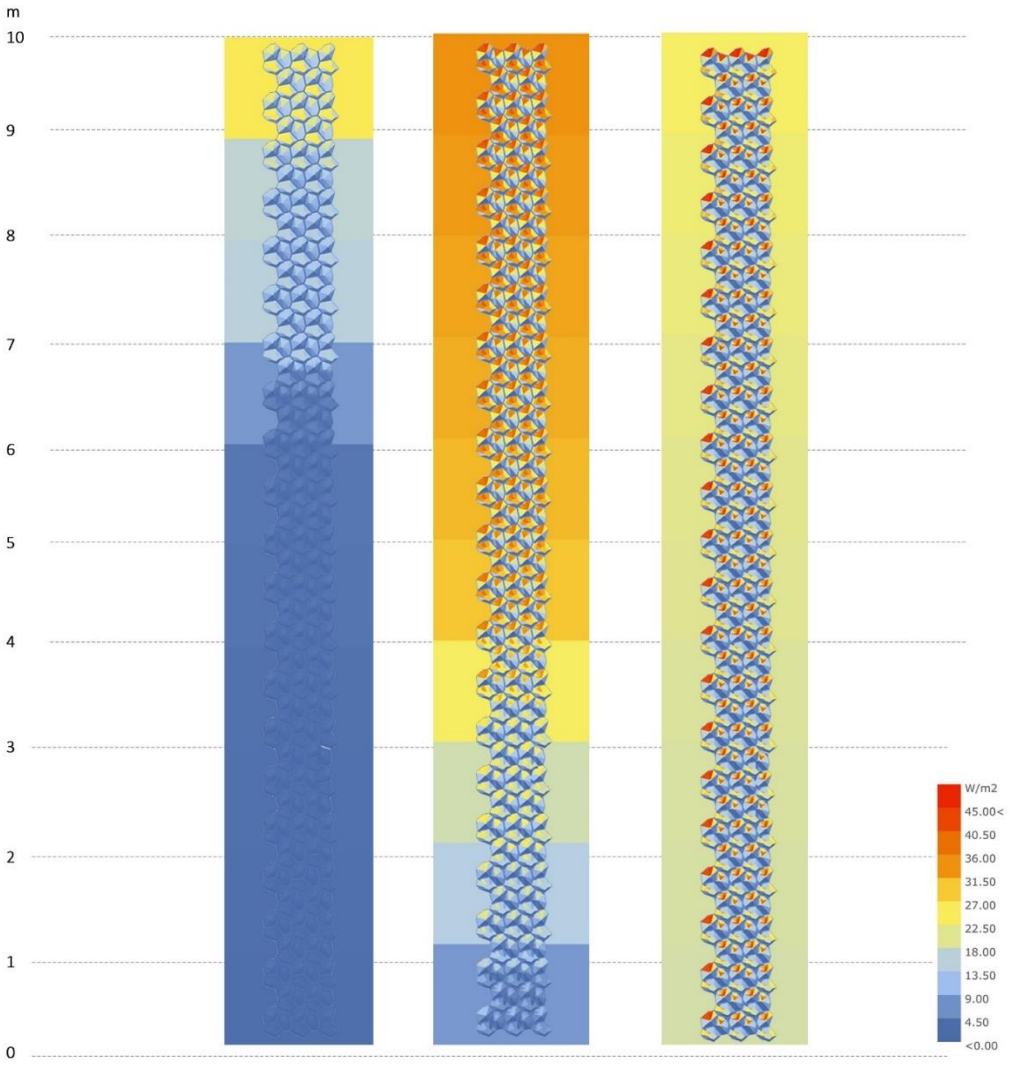

Figure 67 Variations in level of Irradiance on the designed panels in a street canyon of a south façade of aspect ratio 1

5.4. Conclusion:

A flat panel receives even amount of radiation exposure at the different times of the day. The designed panel has zones of high irradiation and less irradiation. The amount of UV irradiance on high irradiation zone is twice higher in summer and equinox compared to irradiation on flat panel. In winter, the irradiance levels are not higher than a flat surface. But they have twice more of active surface available for photocatalysis with irradiation of at least 10 W/m^2.

In street canyons where there is lesser penetration of light at the bottom of the street, 35-40% of the panel area gets twice more irradiance than a flat panel at the same height.

06 DESIGN DEVELOPMENT

Chapter Overview

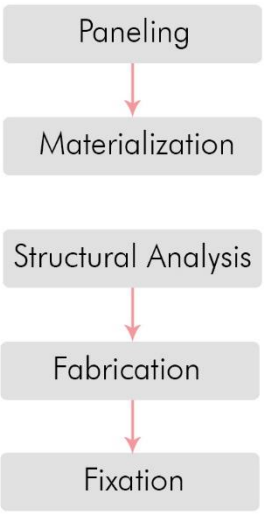

The concept needs to be developed into a product based on modularity and sustainability. For mass manufacturing the panels and easy installation, it is required to simplify the geometry as repeatable panels. This chapter deals with the paneling the façade panels as repeatable modules and selection of a modular concept. The second part of this chapter highlights the criteria defined to select the material and selection methodology validated by structural analysis. A brief description of the selected fabrication method is also explained after materialization. The last part of this chapter has the explanation of the fixing method adopted to mount the façade panels.

6.0. DESIGN DEVELOPMENT

Currently, TiO_2 coated panels have been designed as secondary façade panels in examples like Palazzo Italia pavilion in Milan and Hospital Manuel Gea González in Mexico (Prosolve370e). In Milan project, every panel manufactured was of a unique pattern (750 unique panels) requiring high economical and material input for production process. Prosolve370e is composed of two repetitive ABS plastic modules which favors mass production. But, their visual complexity of design requires specialized installation team as they do not fit into the conventional technique of assembly. Hence, an intermediate solution that bridges the gap between design and widespread application requires modularity and integration with conventional implementation techniques.

The pattern of the designed façade cladding is a repetitive module of a tile cluster that could be repeated as can be seen in Figure 68. The size of each of these modules are 0.29 x 0.3 m with a tile depth of maximum 0.13 m. The smaller dimensions, undulating geometry and the depth of the tiles offers very few support points for mounting with shorter grid of support system. Consecutively, it also increases the number of components required to assemble this system. Hence, increasing the size of these panels would help in minimizing the required number of supporting components and attaining more support points.

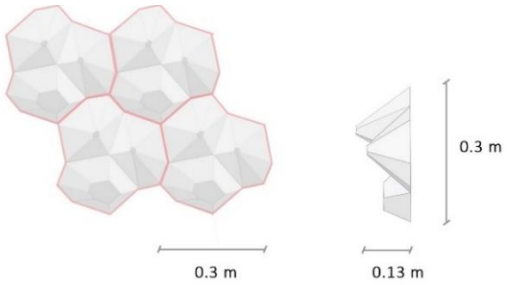

Figure 68 Basic module that repeats to create the facade pattern (left); side view of the tile module (right)

The end points from each of the hexagons were picked and connected such that they are packed in triangles. The scale of the packing was magnified in size by creating hexagons over the triangulated pattern (Figure 69). It reflects the simplification of this pattern into larger modules compared to the initial tile module.

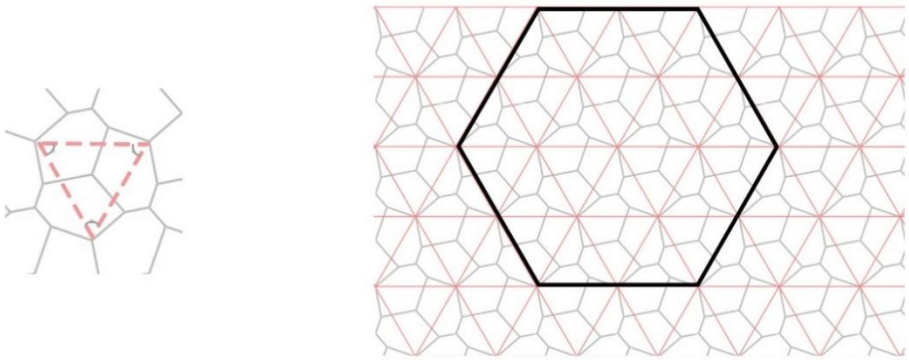

Figure 69 Step 1: Triangulating the facade pattern; Step 2: Magnifying the scale of the panels into hexagonal patterns

6.1. FAÇADE MODULES

Paneling concepts experimented using the hexagonal packing of the pattern as described in Figure 69 are explained below. This has led to four modular concepts which are illustrated with their advantages and disadvantages before the selection of the final panel based on modularity and easy fixation.

6.1.1. Façade Module 1:

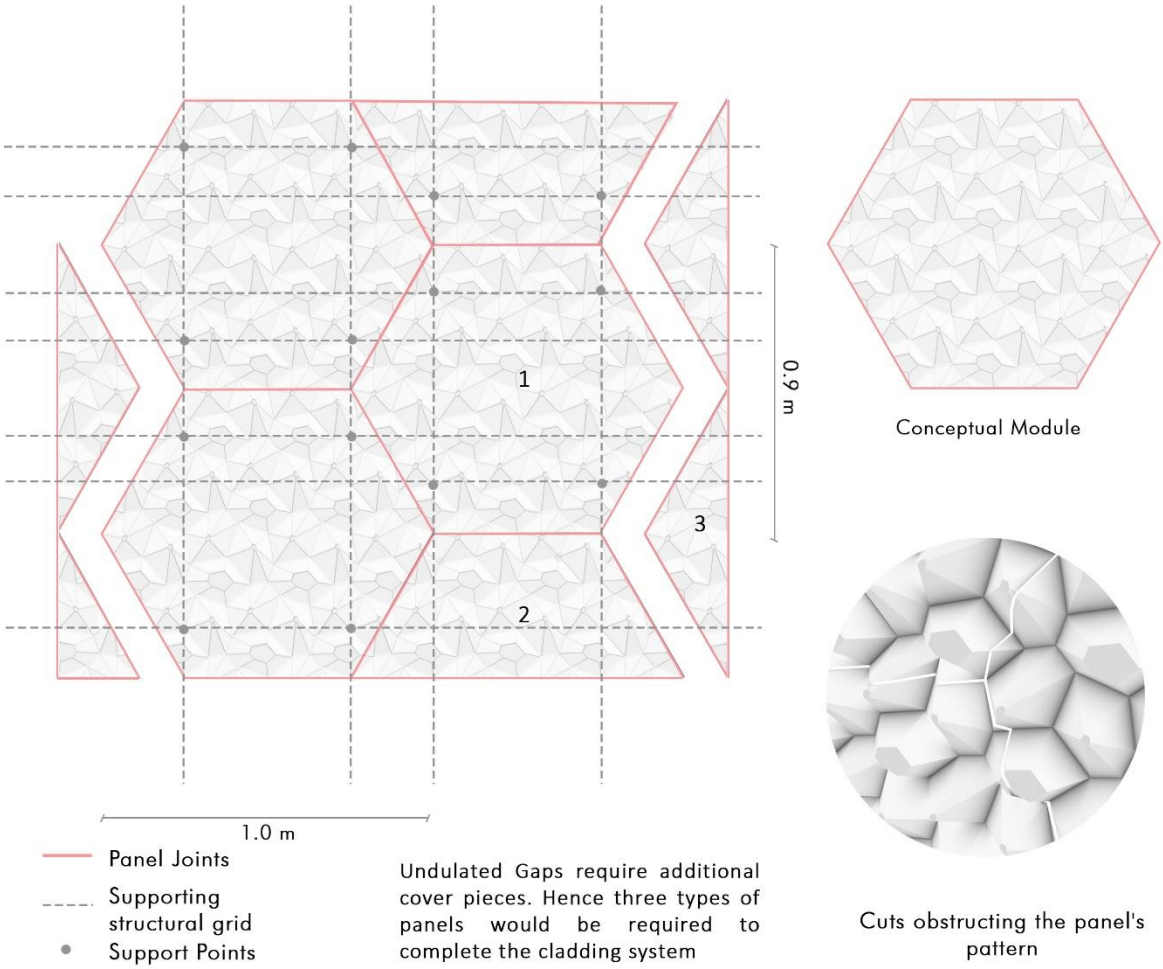

Figure 70 Hexagonal facade modules

The façade pattern can be created with one type of hexagonal module. However, they would require additional types of cut panels at the top, bottom and the sides to complete a rectangular face. The supporting grid is a simple alternate pattern of rectangles. However, the edges of these panels have irregular levels and breaks the pattern's visual continuity (bottom right Figure 70).

6.1.2. Façade module 2:

To avoid the irregular and abrupt panel edges, the profile of the pattern is followed along the hexagonal shaped in the previous module. The advantage of this paneling type is that the visual interruptions are avoided.

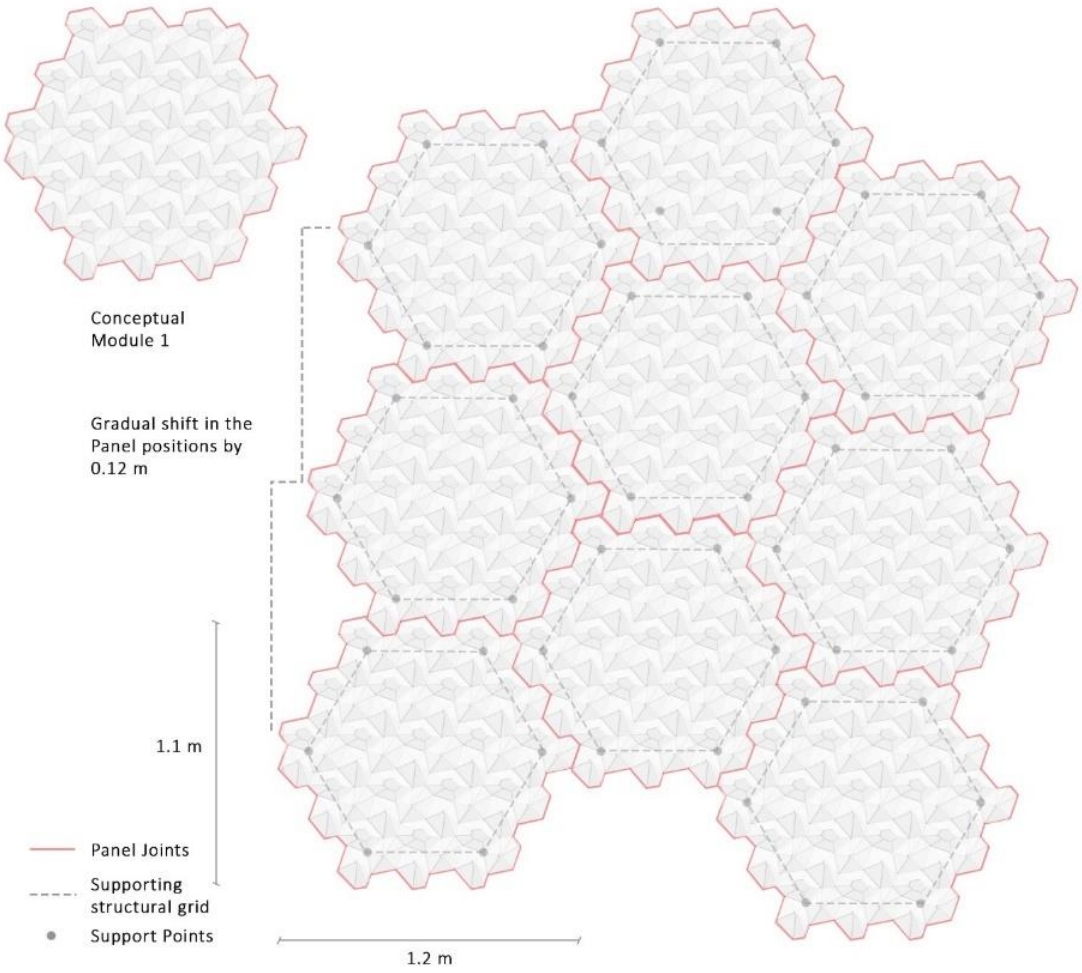

Figure 71 Modularizing along the profile of the panel as an extension of the hexagonal packing

However, it would have the following disadvantages:

- The panels are not aligned to each other and they keep shifting with increasing heights that would make it unsuitable for integration onto existing buildings.
- Non-uniform supporting structural grid as a result of the misalignment.
- The undulation of the façade panels edge profile makes the installation methods harder as the panels cannot be slid from top to bottom or from right to left side.

6.1.3. Façade module 3:

The third approach was to modularize façade pattern into rectangular panels as they can be accommodated into conventional fixing methods. The hexagonal packing was further subdivided into rectangles which led to a singular facade panel system.

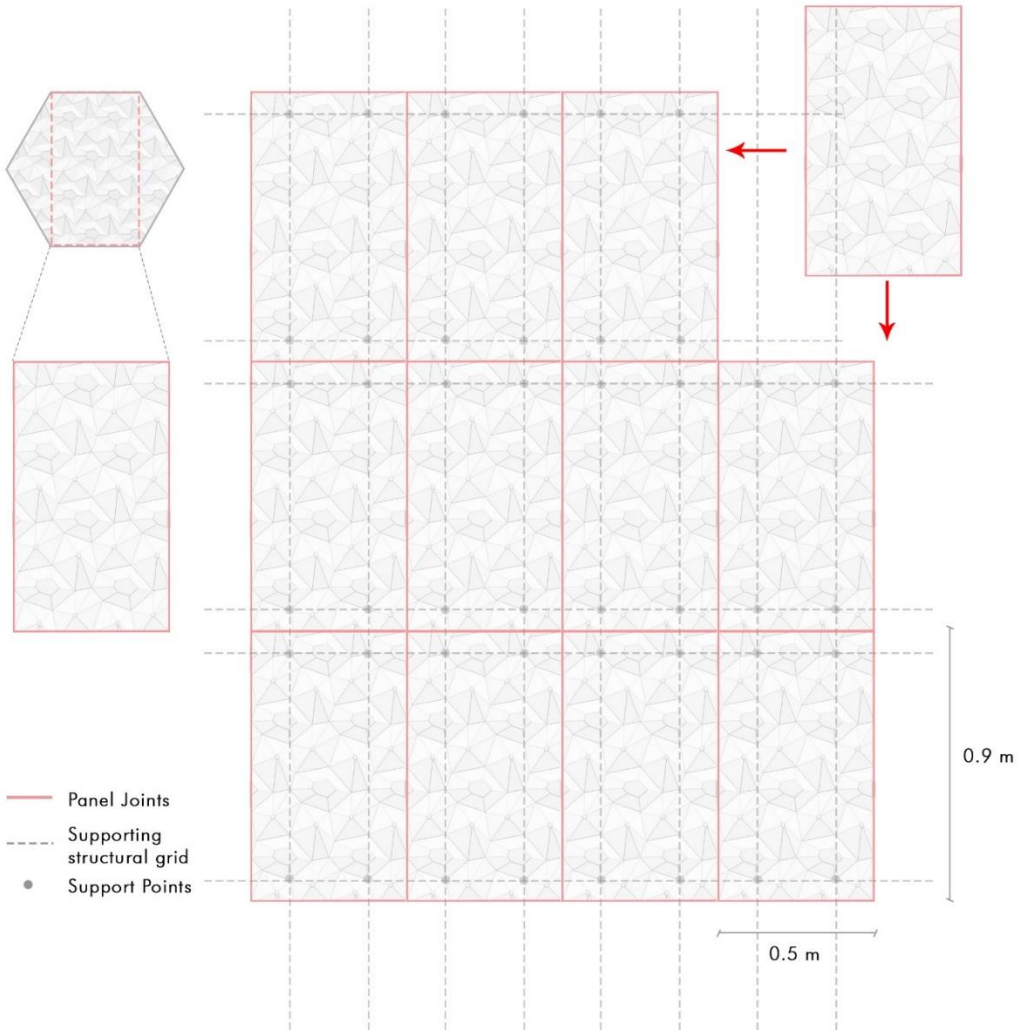

Figure 72 Simplified rectangular paneling

The major advantages of this paneling are that:

- They have a simplified and uniform grid of supporting structure.
- They could be integrated onto various existing buildings as they follow a grid of 0.5 m.
- Conventional installation methods using invisible rail sub frames or anchors can be adopted as they can be slid from either direction.
- Highly suitable for seismic regions as these panels (like rectangular panels) can move with the structural frame onto which they are mounted and in turn accommodate lateral drifts.

The only disadvantage is like that of façade module 1 which is abrupt joints of the panel.

6.1.4. Façade module 4:

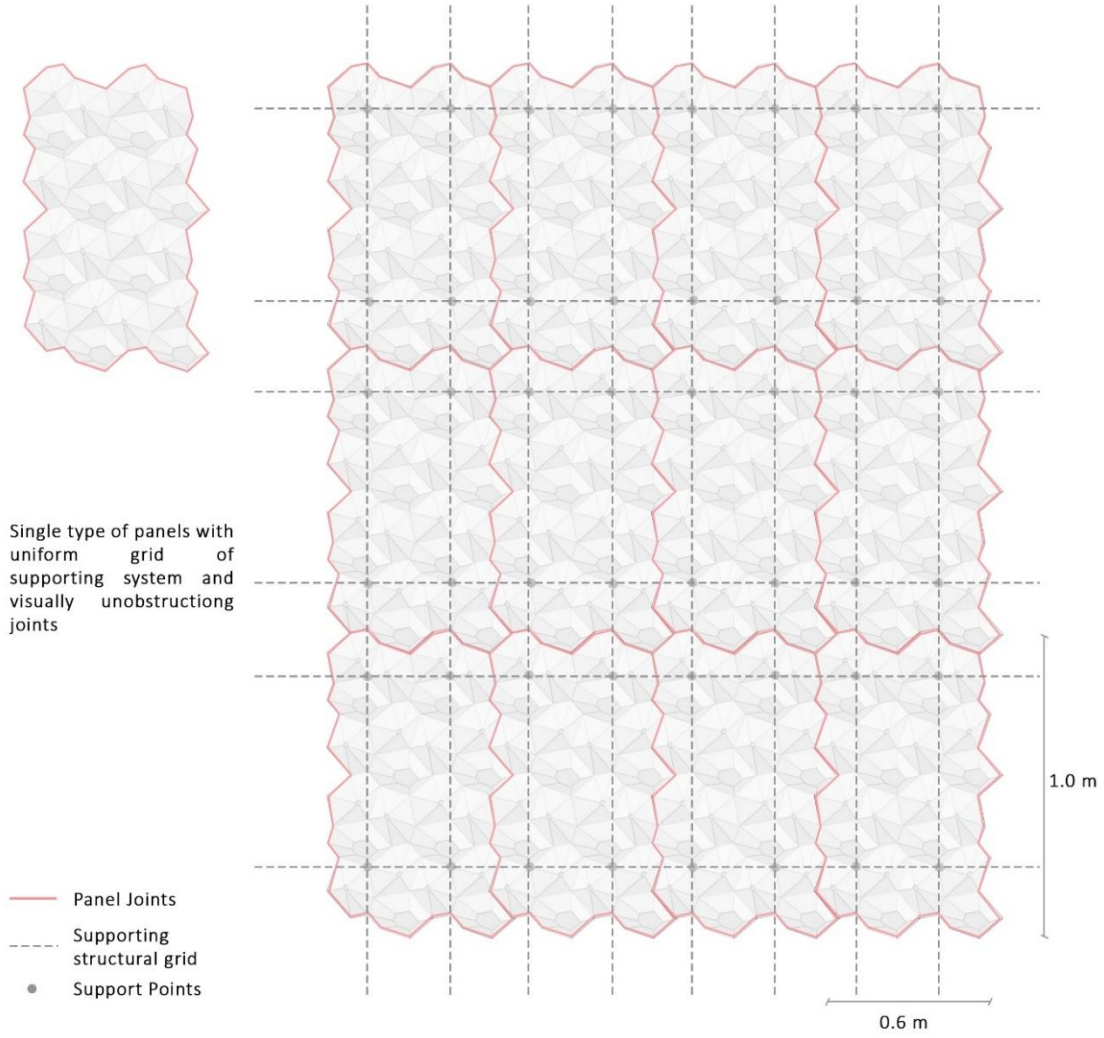

Figure 73 Final module of the facade

Concept 3 has been evolved by tracing the closest profile of the pattern running about the rectangular grid to eliminate abrupt panel edges. The simplified grid supporting structure is retained and the size of the panel could be integrated on to existing buildings and other urban infrastructure.

The disadvantages of this system are that:

- These panels are not suitable for seismic region as the undulated edges of the panel cannot accommodate lateral drift unless large joint gaps are given.
- The panels must be mounted at an angle perpendicular to the wall. Conventional rail sub frame system or anchors may not be suitable, and connections must be designed by modifying the existing ones to suit this profile.

Façade module 3 & 4 are both suitable for easy and widespread implementation. However, module 4 has been taken forward for detailing in section 6.3.

6.2. MATERIALIZATION

6.2.1. Criteria for material selection and methodology

Careful choice of material is necessary for the expected benefits of air purification to outweigh the negative environmental impacts of the façade panel. To simplify the design intent and material selection process, three major criteria are framed for the decision matrix:

- Criteria 1 - Pollution abatement performance: Substrates are important in supporting the photocatalysis reaction. The factors determining the potential of a substrate are:
    - Good absorption capacity
    - Method of immobilization and
    - Photocatalytic activity

- Criteria 2 - Design Performance: The material should also be moldable to achieve the geometry with an adequate panel size (0.6 x 1m) and have a good structural performance for high wind loads. As the panels are more like retrofits on existing buildings, it needs to reduce its load onto the existing structure. This leads to the sub criteria:
    - Design flexibility: It refers to the potential of the material to be fabricated to the required shape and panel sizes.
    - Weight of the panel: For the suitable materials, information on mechanical properties of the material was gathered. The properties are applied for the structural analysis in Karamba (plugin in grasshopper) with wind loads acting on the façade panels to check for the stress levels on them with thickness as the variable. The optimum thickness is selected at the end of this process and weight of the panel is calculated.
    - Durability: It is related to the resistance to the material to environmental factors like weathering and wind loads.
    - Substructure requirement: The spacing of the support system could be predicted from the structural analysis model.

- Criteria – 3 - Environmental impacts: Though the panels could help in purifying the surroundings offering health benefits without a need for constant maintenance regime, there is an intensive amount of energy consumed during the production, transportation and fixing. To achieve a balance between the energy use in realization of the panel and environmental benefits offered by it, material with least of amount of embodied energy and carbon emissions needs to be selected. The quantity of material used is calculated for its embodied energy (MJ/Kg) and carbon emissions (Kg CO_2/Kg) using the data Inventory of carbon and energy (ICE) table as they address context of United Kingdom.

6.2.2. Comparison of substrates:

Façade cladding materials onto which the photocatalytic effect of TiO_2 are tested include metals, stones, terracotta, ceramic, concrete and polymers. Each of these materials are first compared for first pollution abatement performance. The shortlisted materials from this criterion is further analyzed for criteria 2 and the further shortlisted analyzed for criteria 3. The process of comparison for various criteria are described in a brief table below:

Metals - Aluminum panels			
Pollution Abatement Performance	Absorption Capacity	The high density of the metals reduces the absorption capacity of the pollutants.	✗✗
	Method of Immobilization	Spray coating TiO_2 has less adhesion. Hence, thermal spraying would be required that leads to conversion of anatase to rutile form at high temperatures.	✗✗
	Photocatalytic activity	High temperature treatment and poor absorption capacity inhibits photocatalytic potential.	✗✗
Stone			
Pollution Abatement Performance	Absorption Capacity	High porosity is observed in soft stones (up to 42%) that supports absorption	✓✓
	Method of Immobilization	Spray coating at room temperature	✓✓
	Photocatalytic activity	Good photocatalytic performance -Stones like marble and limestone showed 90% degradation of methylene blue and Rhodamine B after 7.5 hrs of UV irradiation in daylight. (Kapridaki et al, 2014)	✓✓
**Stone is avoided in further analysis. Though they have good pollution abatement performance compared to the metals, they are unsuitable for fabricating the façade geometry.*			
Terracotta			
Pollution Abatement Performance	Absorption Capacity	Good absorption capacity helps in trapping pollutants.	✓✓
	Method of Immobilization	Spray coating cementitious paint	✓✓
	Photocatalytic activity	- Application of the coating at less temperature prevents phase transition from anatase to rutile form. - NOx degradation up to 90% in 50 min under irradiation of 30 W/m2 (Bianchi, et al., 2016)	✓✓
Design Performance	Weight of the panel (Kg/m^2)	30 – 60 (assuming a thickness of 15 mm)	✓
	Durability	Good resistance to weathering. But, the brittle nature of the material reduces its service life.	✓
	Flexibility of design	Like concrete, terra-cotta can be molded virtually into any shape, it is fireproof and strong. It has less resistance to compression which limits the sizing of the panels. Hence, they are	✗✗

		more suitable for manufacturing tile modules in Figure 68.	
Ceramic			
Pollution Abatement Performance	Absorption Capacity	Porosity of the material could be controlled during manufacturing.	✓✓
	Method of Immobilization	Sol-gel Method with thermal treatment (No replenishment of the coating is required)	✓✓
	Photocatalytic activity	- Good photocatalytic activity - NOx degradation up to 90% in 50 min under irradiation of 30 W/m2 (Bianchi, et al., 2016)	✓✓
Design Performance	Weight of the panel (Kg/m2)	Unknown	
	Durability	Excellent abrasion and impact resistance.	✓
	Flexibility of design	-Fabrication of complex geometries is challenging. -Manufacturing large panels is impossible as they are highly brittle (This limits sizing of panels.)	✗✗
Polymers - PVC (Poly Vinyl Chloride)			
Pollution Abatement Performance	Absorption Capacity	Good Absorption Capacity	✓
	Method of Immobilization	Spray coating (Paint) (Requires periodic replenishment once in 5 years)	✓✓
	Photocatalytic activity	High Photocatalytic activity	✓
Design Performance	Weight of the panel (Kg/m2)	5.9 (Panel thickness: 5 mm)	✓✓
	Durability	Excellent abrasion and impact resistance against weathering. However, a barrier layer is required to prevent the degradation of the polymer due to TiO_2	✓
	Flexibility of design	-Complex geometries with thinner panel sections can be manufactured. -Has potential for varying size of panels	✓✓
Polymers - Acrylonitrile-butadiene-styrene (ABS Plastic)			
Pollution Abatement Performance	Absorption Capacity	Good Absorption Capacity	✓
	Method of Immobilization	Spray coating (Paint) (Requires periodic replenishment once in 5 years)	✓✓
	Photocatalytic activity	High Photocatalytic activity	
Design Performance	Weight of the panel (Kg/m2)	5.77 (Panel thickness: 5 mm)	✓✓
	Durability	Excellent abrasion and impact resistance.	✓
	Flexibility of design	-Higher stiffness of the material allows for fabrication of complex and thinner shells with high strength. -Has potential for varying size of panels	✓✓
Polymers - Acrylics			
Pollution Abatement Performance	Absorption Capacity	Good Absorption Capacity	✓
	Method of Immobilization	Spray coating (Paint)	✓✓

		(Requires periodic replenishment once in 5 years)	
	Photocatalytic activity	High Photocatalytic activity	
Design Performance	Weight of the panel (Kg/m2)	5.2 (Panel thickness: 5 mm)	✓✓
	Durability	Excellent abrasion and impact resistance.	✓
	Flexibility of design	-Higher stiffness of the material allows for fabrication of complex and thinner shells with high strength. -Has potential for varying size of panels	✓✓
Concrete -	Lightweight concrete panels: UHPC/GFRC/FRC panels (UHPC is considered as panels as thin as 10 mm could be designed)		
Pollution Abatement Performance	Absorption Capacity	These panels have 2-6% porosity that helps in better adhesion of the photocatalytic coating and adsorption.	✓
	Method of Immobilization	Spray coating cementitious paint	✓✓
	Photocatalytic activity	• Application of the coating at less temperature prevents phase transition from anatase to rutile form. • Studies show 80% degradation of pollutant (methylene blue) at the surface. ((Fontana, et al., 2016)	✓✓
Design Performance	Weight of the panel (Kg/m^2)	35.49 (Panel thickness: 15 mm)	✓
	Durability	Excellent resistance against environmental impacts demonstrates feasibility and increased service life.	✓✓
	Flexibility of design	-Complex geometries with thinner panel sections can be manufactured. -Wide range of panel sizes could be designed ranging from small to large panels.	✓✓

Table 17 Comparison of materials for facade panels

From the above tables, polymers and UHPC are the most suitable materials in terms of design flexibility. Hence, the next step is to calculate the environmental impacts of these materials for which the quantity of each of these materials required need to be calculated. The method of determination is explained under the section 6.2.3.

6.2.3. Fabrication of the Panels

Polymers and UHPC were the most suitable materials to fabricate the façade geometry. The spacing of the supporting structure and thickness of the panel is decided based on the stresses developed in the panels. Fabrication method is chosen after the selection of the material based on its weight and embodied energy calculated after structural analysis of the panels in Karamba – a plugin in grasshopper (Appendix).

The geometry of the panels has been modified by creating spaces for support points as indicate din the figure below.

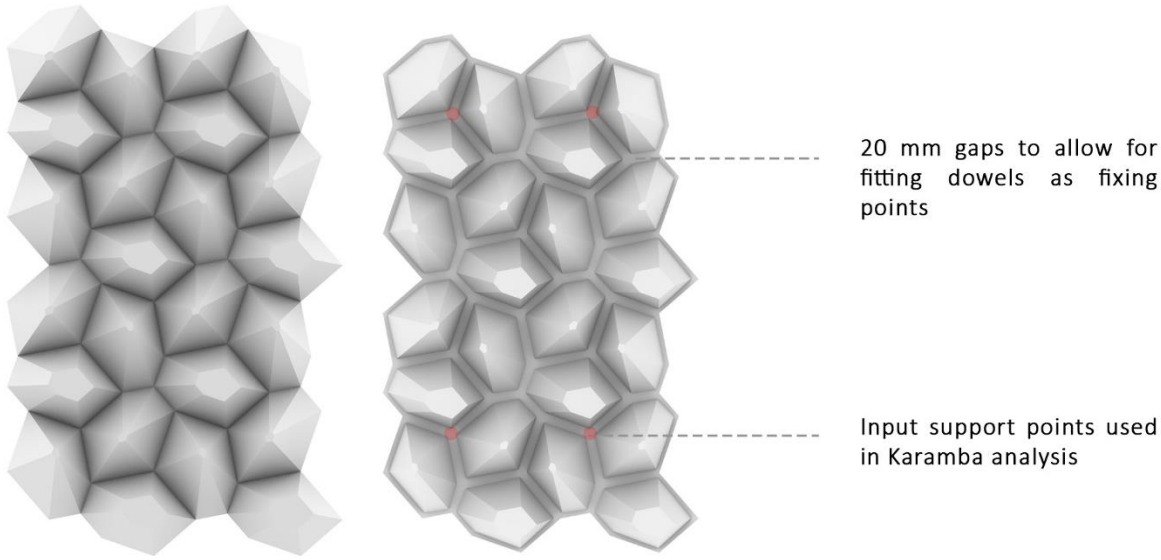

Figure 74 Spacing between the pattern is introduced to accommodate the support.

	UHPC	Polymer -ABS
Young's Modulus (GPa)	53	2.58
Specific Weight (Kg/m$^{3)}$	2450	1050
Tensile Yield strength (MPa)	9	5.5
Reference	(R.B.Holland & Kahn, 2016)	(Material data book, 2003)

Table 18 Material properties used in Karamba for structural analysis of UHPC and ABS polymer panels

The thickness of the panels and their embodied energy calculated based on weight is listed below:

Thickness (mm)	Maximum tensile stress in the panel (N/mm2)	Yield Tensile Stress utilization (%)	Weight of the Panel (Kg/Panel)	Embodied Energy (MJ/Panel)	Carbon Emissions (Kg CO_2/m^2) (0.45)
5	0.87	107.1	11.25	87.41	5.06
10	0.27	34. 7	23.66	183.83	10.65
15	0.14	16.4	35.49	275.75	15.97
20	0.08	9.3	47.33	367.75	21.29
25	0.06	6.1	59.16	459.67	26.62
30	0.04	4.5	70.99	551.59	31.9

**The highest stresses on UHPC panels are developed on the backside at the middle of the panel, due to deflection of the panel in this zone. They are however in permissible limits within 9 N/mm^2.*

Table 19 Calculation of weight of UHPC Panels and analysis of stress developed in the panels

Structural analysis of UHPC panels shows a potential thickness from 10 mm. However, most of the panels in practice are manufacture with a thickness of 15 mm and 20 mm. 15 mm panels have 50% less embodied energy compared to the ABS panel of same surface area.

UHPC panels above 25 mm thickness exceeds the embodied energy of the ABS plastic panels. Complying to the practicalities, a 20 mm panel is chosen.

Thickness (mm)	**Maximum tensile stress in the panel (N/mm2)**	**Tensile Stress utilization (%)**	**Weight of the Panel (Kg/Panel)**	**Embodied Energy (MJ/Panel)**	Carbon Emissions (Kg CO_2/m^2) (3.6)
0.5	0.19	43.1	5.55	527.25	19.98

Table 20 Calculation of weight of ABS Panels and analysis of stress developed in the panels

Of all the materials discussed above, plastic panels have the least amount of weight making it suitable for a very light weight retrofit. However, the embodied energy and carbon emissions of these are the highest. Hence, UHPC is selected as the façade panel substrate for coating with TiO_2. However, to realize the concept and implement the geometry, it is necessary to further research the feasibility of this geometry in fabrication. For panel thickness more than 20 mm, it would be environmentally feasible to opt for ABS plastic panels.

The requirement of the complex geometry in a thinner section is a challenge. The sequence of casting the architectrual UHPC panel should be planned in such a way that the fibres have appropriate orientation. Various methods of fabrication considered includes:

	Spray casting	Displacement casting	Injection casting
Method	The surface geometry of the mold could be sprayed with UHPC and manually brushed until the thickness required is achieved.	Precise volume of concrete required to fabricate the panel is deposited on to the positive mold. The negative mold is introduced over the top portion	The negative and positive molds are clamped together with infill point for pouring the UHPC. Molds need to be filled slowly to prevent entrapment of air and avoid vibration.
Advantages	Single mold is required	Less control over the distribution of material	Accurate casting method
Disadvantages	-Surface finish is good only on one side -Labour Intensive	- Two types of molds are required	- Two types of molds are required (positive an dnegative molds)

Figure 75 Fabrication techniques considered for casting UHPC Panels

Injection molding has been chosen to fabricate the façade panels as they give highly accurate castings irrespective of elements complexity.

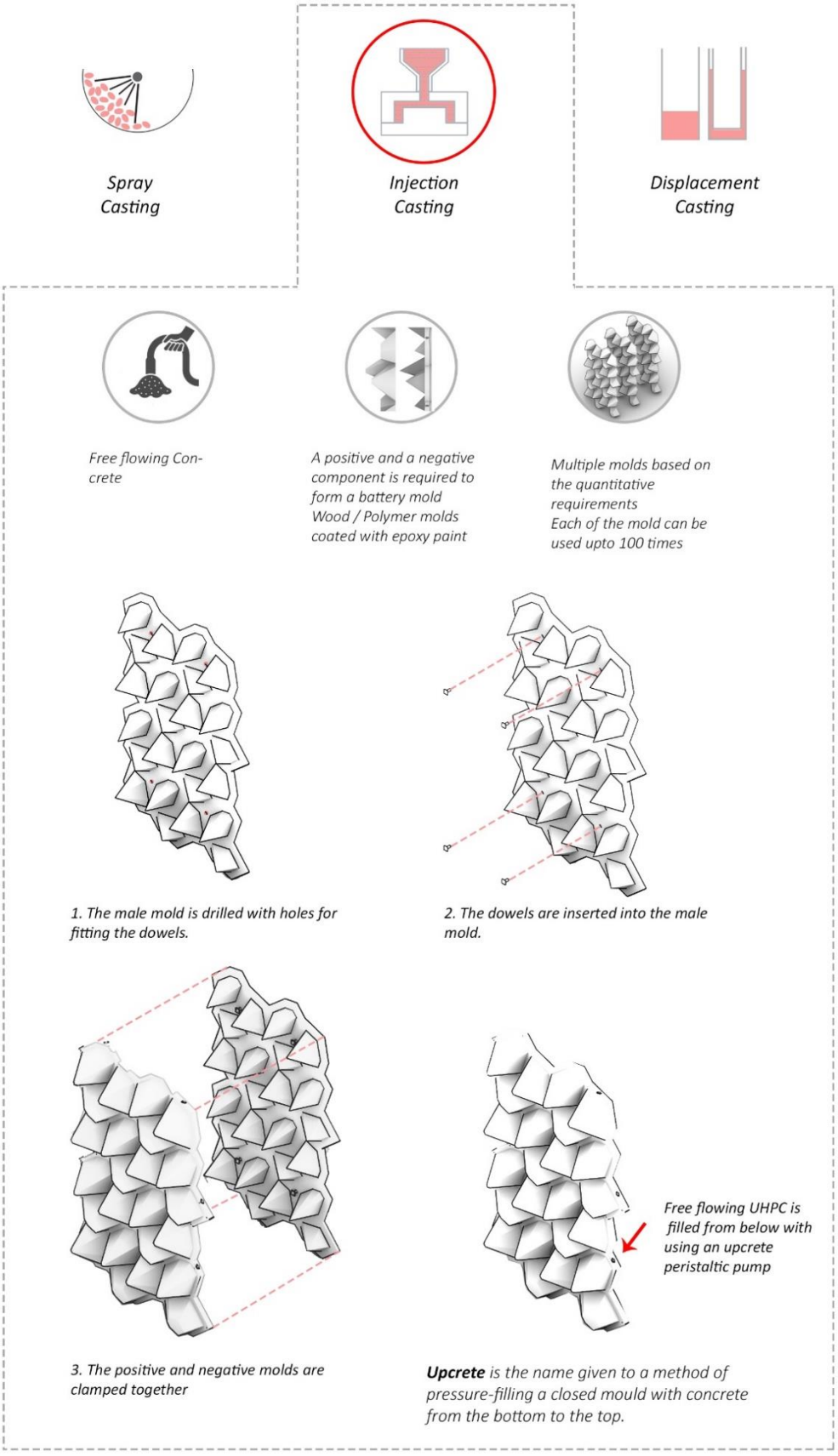

Figure 76 Process of Injection casting of UHPC using a male and a female mold for the façade panel.

6.3. Fixing System of the panels:

Conventional anchors have been chosen to mount the panels onto a load bearing structure. Factors like buildability, eventual removal of the panels with safety and possibility of replacement are considered. Moreover, thermal movement of the panels and mounting methods have been considered to design the joints of the panels.

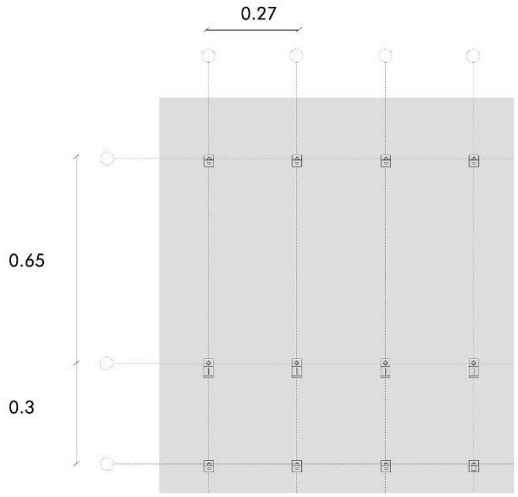

Figure 77 Supporting structural grid for the facade panels on a loadbearing wall

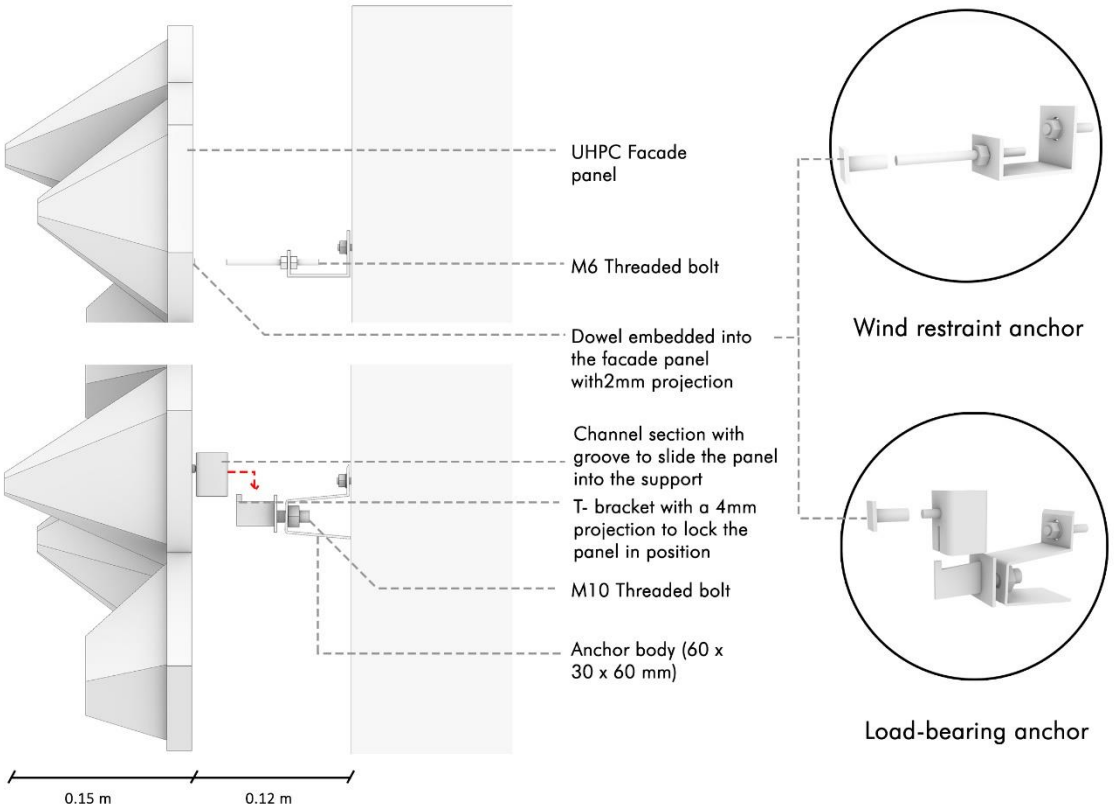

Figure 78 Fixing detail of the facade panels

Movements of UHPC panel:

Thermal movement can occur due to the change in the dimension of a flat panel which is calculated by:

$$\Delta L = \alpha . \Delta T . L$$

where ΔL = change in length

α = coefficient of linear expansion

ΔT = change in temperature and

L = length over which ΔL is being measured.

Assuming a rise in temperature (ΔT) of 30 °C and a value of coefficient of linear expansion (α) of 18 x 10-6/°C

- a 1.0 m long panel will expand by (18 x 10-6 x 30 x 1.0 x 1000) mm = 0.54 mm
- a 0.5 m long panel will expand by (18 x 10-6 x 30 x 0.5 x 1000) mm = 0.27 mm

Apart from this, mounting the panels need a minimum vertical movement space of 6 mm. In total, a 8 mm joint gap is left between the panels.

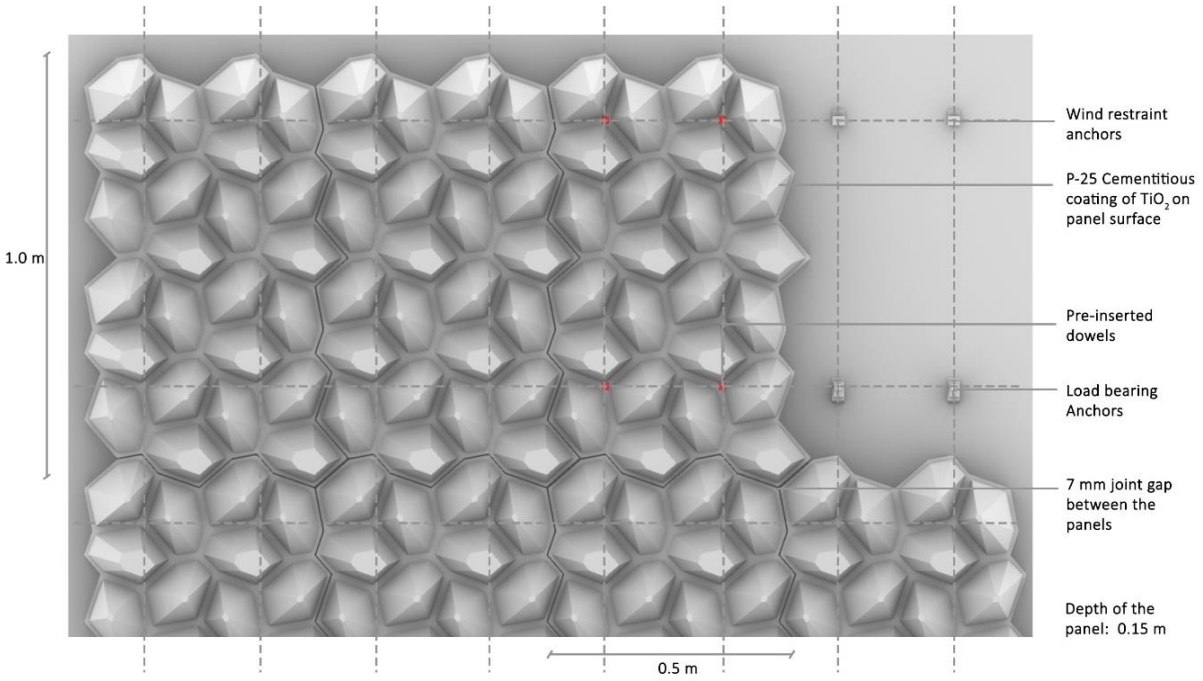

Figure 79 Layout of the Facade system mounted over a wall

6.4. Application in urban scenarios

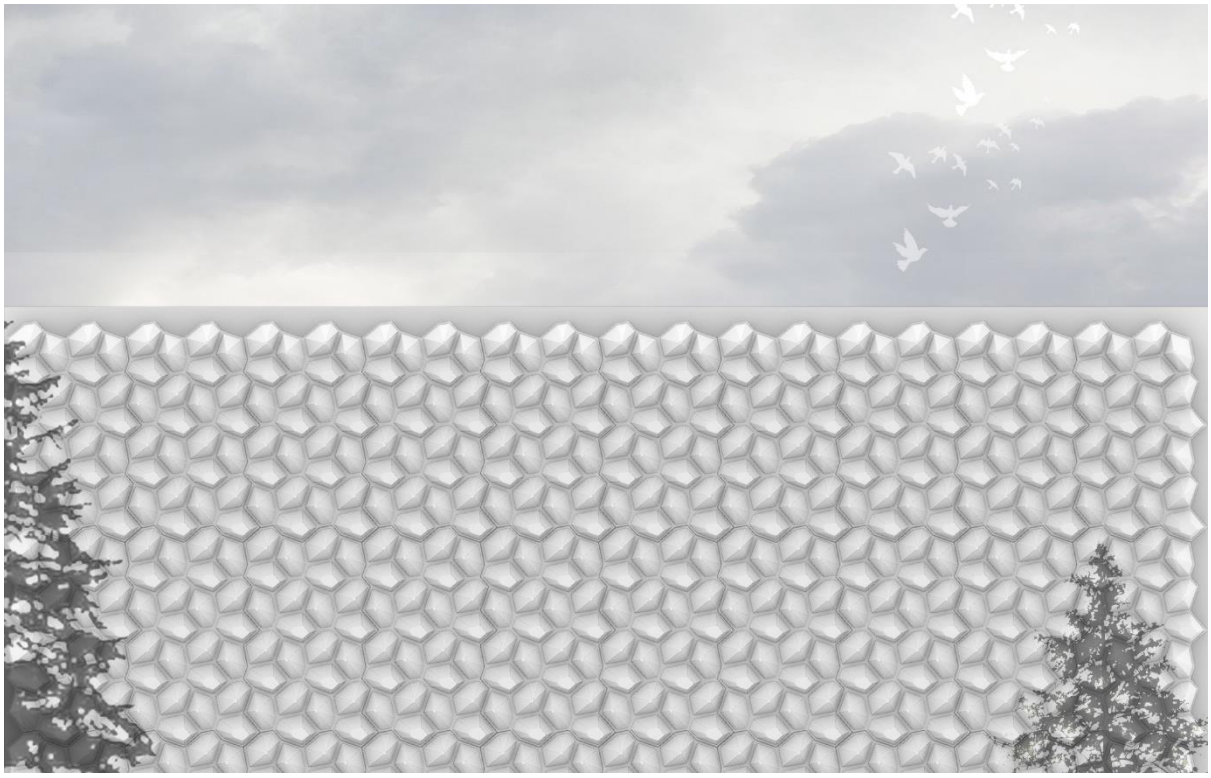

Figure 80 Front view of the facade panels installed on facade

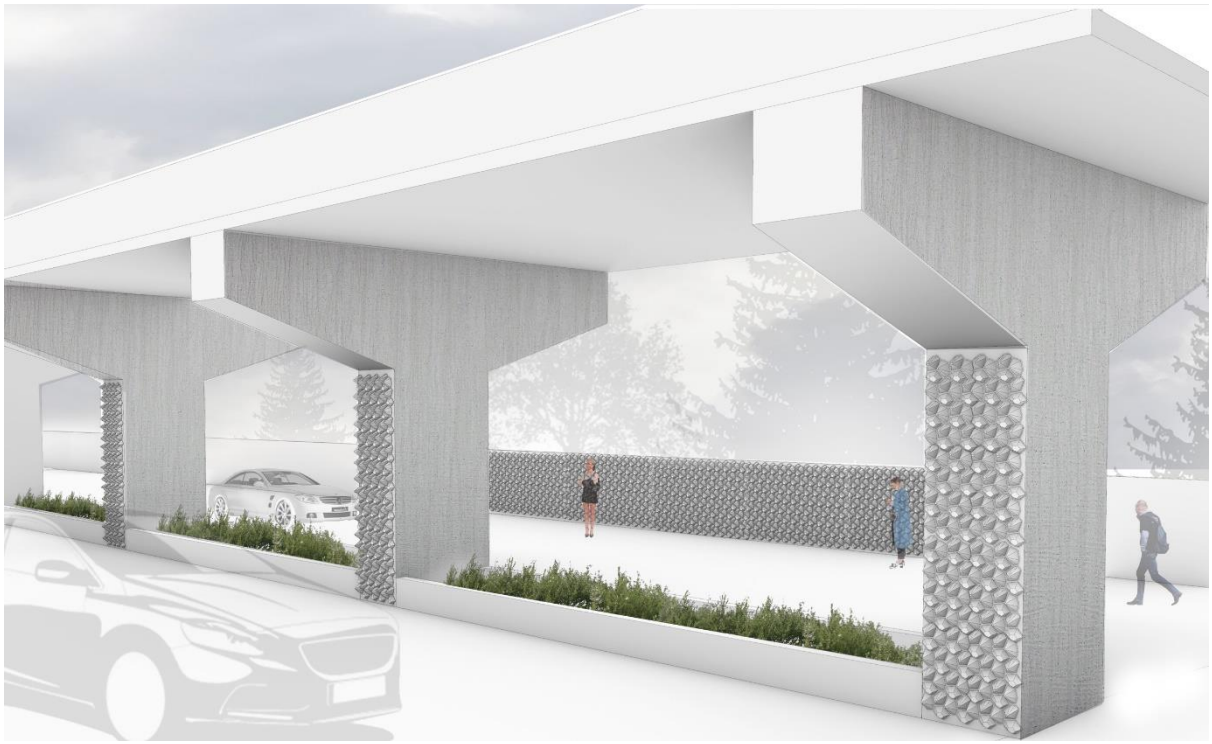

Figure 81 Application of facade panels as acoustic barriers and cladding for elevated roadways

07 AIR PURIFICATION EFFECT

Chapter Overview

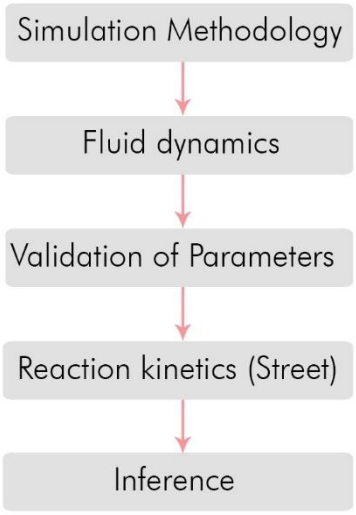

This chapter is about analyzing the air quality before and after applying photocatalytic panels on façade. Before applying the parameters onto the street model, a series of steps is taken to validate the analysis methodology.

The first part of this chapter explains the boundary conditions used in the analysis, software chosen and simulation methodology. While the second part is a brief on the input for fluid dynamics & mass balance equations chosen for setting up the simulation. The third part of this chapter includes application of parameters and constants for solving photocatalytic kinetic equations in a plug flow reactor whose simulation output is compared to the lab experiment result from literature review.

The last part of this section explains inputs used in simulating a section of the reference street canyon with an emission flux from the traffic and other parameters. Two scenarios; before and after application of TiO_2 coating is analyzed for climatic conditions of London for summer and winter. The effect achieved by the flat panel is compared to the designed panel. Also, minimum and maximum effect of purification is inferred.

The results obtained in each of the situation before and after photocatalysis are compared to conclude on the performance of these panels and their resultant NO (Nitric Oxide) abatement effect in an urban context at pedestrian level.

7.0. Evaluation of photocatalytic façade on air purification:

Literature studies of photocatalytic materials indicated less pollution abatement due to short residence time of the pollutants from highways and insufficient lighting in the context into which they had been implemented. **This had led to the assumption that geometry could have a strong impact on the pollution abatement performance of a photocatalytic façade panel.** Hence, the geometry of the façade panels was designed to have increased surface area, high UV irradiation and reduced wind speed over them. And the designed façade panel has been evaluated and proven to have high incident irradiation and reduced wind speed over them. However, it is also required to understand the difference in the performance of these panels when applied in an urban context.

To simplify the context and variables involved in modelling, few assumptions are made as boundary conditions for performing the analysis:

- Langmuir-Hinshelwood model is used to model the kinetics of the photocatalysis reaction. A brief on this model selected for the kinetics of photocatalysis and their extension into urban scenario are explained in section 2.4.
- Large number of pollutants like natural organic matter (NOM), Volatile organic compounds (VOC'S) such as benzene, aldehydes and toluene and inorganic compounds like NO_x, SO_x and NH_3 can be oxidized by TiO_2. However, to understand the pollution abatement effect of TiO_2 coated facade, **only NO has been considered as the input pollutant.** Also, intermediate appearance and disappearance of nitrogen dioxide (NO_2) and Ozone (O_3) gases are not considered.
- Dilution of pollutant as a function of distance from the source has not been considered.
- All the parameters chosen and calculated for solving the kinetic equations are for 70% RH (Humidity levels in London during most parts of the year).
- Though a transient study model would be the most appropriate to understand extent of pollution abatement for a real urban scenario, a steady state model is used as the goal is to understand the panels performance in a similar situation.
- Variation in the lighting levels at different heights of the façade are not included in the model.

7.1. Simulation Methodology:

COMSOL Multiphysics 5.3a is used to simulate the urban context mounted with photocatalytic façade panels. Various modules in this program can be used to combine physical and chemical phenomenon. An integral model can be created by combining the different modules that have common variables. The software derives the solution numerically by finite element method under appropriate boundary conditions based on partial differential equations (PDE's) programmed in different modules that can be instantly combined.

Two modules are used in this project for the wind flow and mass transfer. The first module describes the wind velocity profile in the street model while the second module describes the concentration of NO throughout the street model. Before coupling the modules, wind flow profile is independently solved. The simulation requires development of the wind profile in the street with the presence of pollutants to determine the effect of wind on the concentration of NO and its reaction with TiO_2 coating. TiO_2 coated surface is modelled with the reaction kinetics that are elaborated in section 2.4.

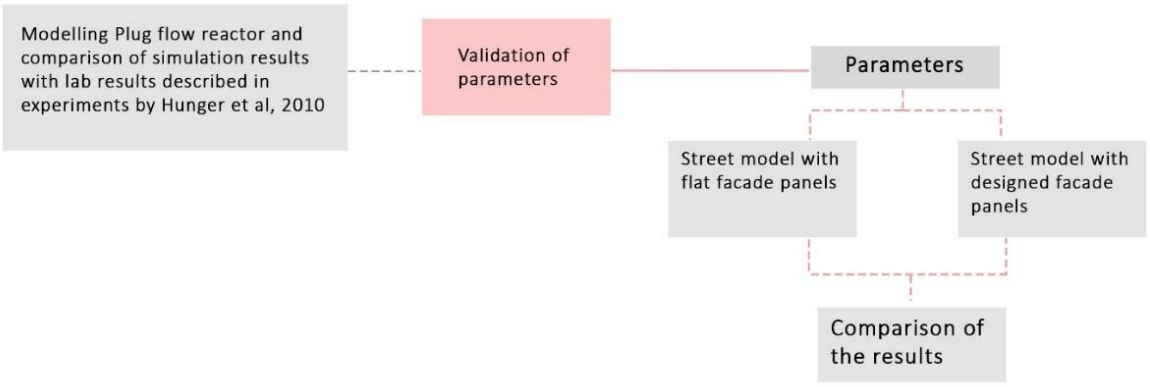

Figure 82 Process of Evaluation of the designed facade panel

In this project, the lab reactor and street canyon are modelled as a plug flow reactor for a steady state solution using stationary segregated solver with two modules namely:

- Fluid-flow model (Laminar/Turbulent for steady state wind velocity profile based on the Reynolds number calculated for the reactor and the street)
- Transport of diluted species (Modelling the pollutant concentration and transport of these pollutants in the wind)

The velocity profile from the fluid flow module is used in the transport of diluted species module to solve for NO concentrations. The process of evaluation of the photocatalytic façade panel is elaborated in the chart below:

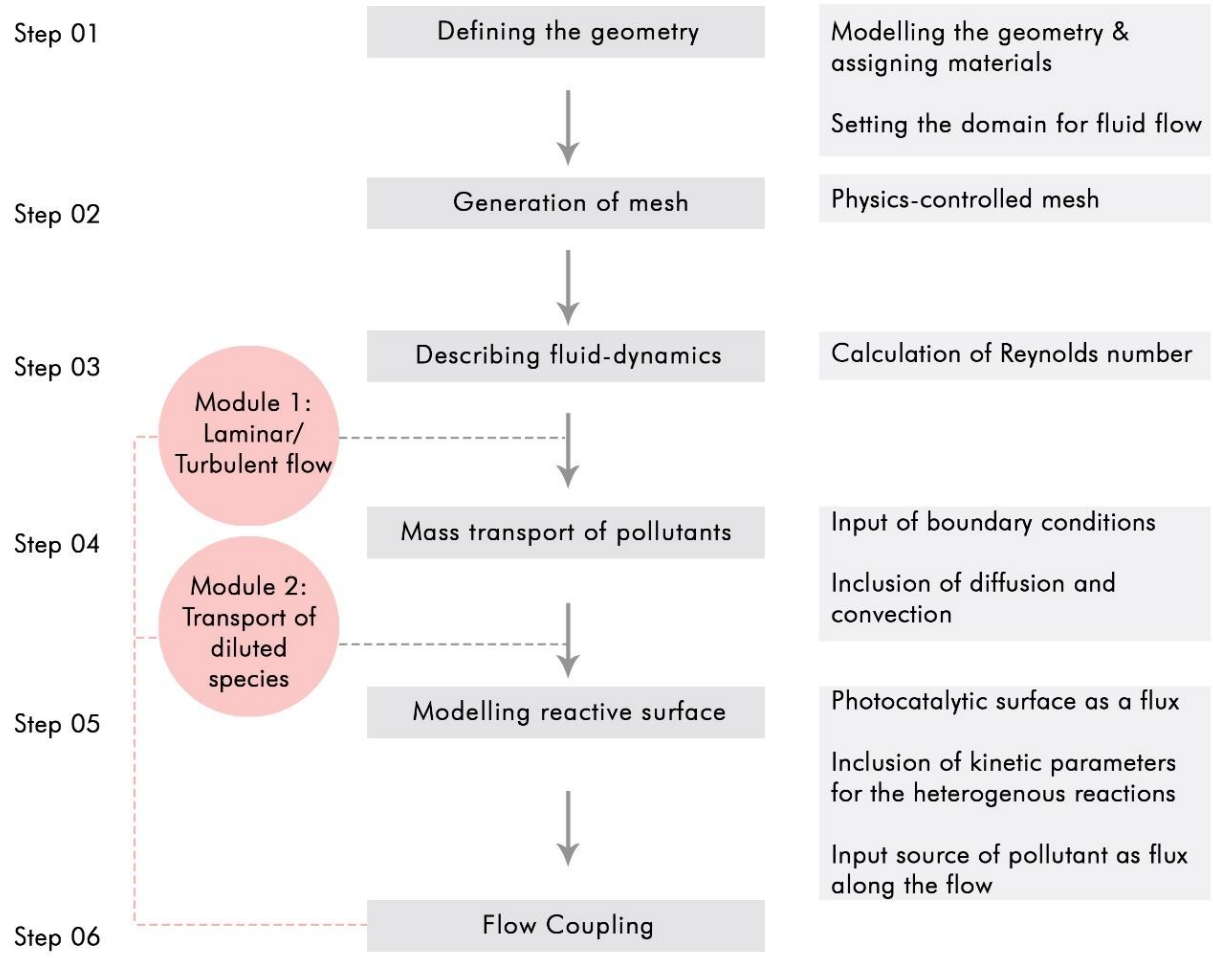

Figure 83 Steps involved in setting up the model in COMSOL Multiphysics

7.2. Fluid dynamics:

With appropriate initial values and boundary conditions, the model can be computed with differential equations that will be mentioned in sections below. It is necessary to understand the fluid dynamics for the reactor and street model. This section discusses the:

- determination of the type of flow using reynolds number,
- corresponding application of Navier-Stokes equation for laminar and turbulent flow and
- mass balance equations for reaction kinetics

7.2.1. Reynolds number:

Determining the turbulence of air flow through the reactor can be deduced from the following equation:

$$\mathbf{R_e} = \frac{\boldsymbol{\rho}\, \mathbf{u_0}\, \mathbf{L}}{\eta}$$

Where **ρ** is the density of the fluid [Kg/m3]; υ_0 is the mean velocity [m/s]; **L** is the width of the photoreactor; **η** is the viscosity of the fluid [Pa.s]

For values of R_e <2000, the flow is laminar and if R_e > 3000, the flow is determined to be turbulent.

S. No	Model Name	Reynolds number (R_e)	Flow modelling
1	Plug flow reactor model	38.32	Laminar flow
2	Street Model – Flat façade	19.95 E^{+05}	Turbulent flow
3	Street Model – Designed façade	19.95 E^{+05}	Turbulent flow

Table 21 Determination of type of in reactor and street models

7.2.2. Navier - Stokes Equation and mass balance:

For a laminar flow the equation is given as:

$$\boldsymbol{\rho(u.\nabla)u = \nabla\,[-pI + (\eta + \eta_T)(\nabla U + (\nabla u)^{T}\,] + F}$$

Where, **ρ** is the density of the fluid [Kg/m3];

υ is the velocity vector [m/s]

P is the pressure [Pa]

I is the unity vector

η is the viscosity of the fluid [Pa.s]

η_T is the turbulent viscosity of the fluid [Pa.s]

$(\nabla u)^T$ is the turbulent viscosity term based on the fluctuations of υ around its mean value

F is the body force vector [N/m^3]

With $\eta_T = 0$ for laminar flow, equation () can be rewritten as:

$$\boldsymbol{\rho(u.\nabla)u = \nabla\,[-pI + \eta(\nabla U + (\nabla u)^{T}\,] + F}$$

Continuity equation for mass balance of air under the assumption air is incompressible:

$$\boldsymbol{\nabla u = 0}$$

The following described equations are solved for the turbulent flow in the street model.

Turbulent kinetic energy (k):

$$\boldsymbol{\rho\, u\, \nabla k = \left[\left(\eta + \frac{\eta_T}{\sigma_k}\right)\right] + \eta_T P(u) - \rho\varepsilon}$$

Turbulent dissipation rate (ε):

$$\rho u\ \boldsymbol{\nabla \varepsilon} = \left[\left(\eta + \frac{\eta_T}{\boldsymbol{\sigma_\varepsilon}}\right)\boldsymbol{\nabla \varepsilon}\right] + \frac{\boldsymbol{C_{\varepsilon 1}\varepsilon \eta_T P(u)}}{\boldsymbol{k}} - \frac{\boldsymbol{C_{\varepsilon 2}\rho \varepsilon^2}}{\boldsymbol{k}}$$

Where;

Variable	Description	Unit
k	Turbulence energy	m^2/s^2
η_T	Turbulent viscosity: $\eta_T = \rho C_\mu \frac{k_2}{\varepsilon}$ Where $C_\mu = 0.09$	Pa.s
σ	Constant	1.0
P(u)	$\nabla u: (\nabla u + (\nabla u)^T)$	
ε	Dissipation rate of turbulent energy	m^2/s^3
σ_ε	Constant	1.3
$C_{\varepsilon 1}$	Constant	1.44
$C_{\varepsilon 2}$	Constant	1.92

Table 22 Description of variables in equations for turbulent flow

The general mass balance equation for NO is:

$$\boldsymbol{\nabla}\ (-\mathbf{D}\ \boldsymbol{\nabla}\mathbf{C_{NO}}) = \mathbf{R_{NO}} - \mathbf{u}\ \boldsymbol{\nabla}\ \mathbf{C_{NO}}$$

Where D is the diffusion coefficient [m^2/s]; C_{NO} is the concentration of NO [mol/m^3]; R_{NO} is the homogeneous reaction rate for NO [$mol/m^3/s$]; u is the flow velocity of the air [m/s]

The left half of the reaction indicates diffusion of NO onto the active surface, while R is the disappearance rate of NO and the remaining expression on the right side indicates convection.

7.3. Validation of parameters in the reactor model:

The goal is to verify the kinetic equations and parameters required to evaluate photocatalytic degradation NO using a simple case of pavement as a plug flow reactor. To verify the method of modelling, the experimental setup of the pavement coated with TiO_2 mortar by Hunger et al, 2010 is modelled in COMSOL based on the standards ISO 22197-1 (2007) and outlet concentration of NO is measured.

7.3.1. Geometrical setup and Boundary Conditions:

The geometrical setup is a constant and controlled experiment chamber with pavement coated with TiO_2 placed in a reactor of dimensions 0.197 x 0.087 x 0.003 m. A schematic diagram of the reactor is shown in Figure 84 where light intensity is kept at a constant 10 W/m^2. The polluted gas touches the active surface and there would be an immediate diffusion due to which it is modelled as a plug flow reactor.

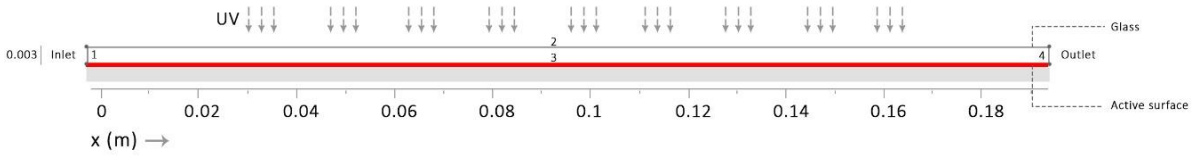

Figure 84 Pavement model in COMSOL for NO abatement evaluation

From Table 21, the calculated Reynolds number for the reactor is 38.32 clearly representing a laminar flow in the reactor. The equations representing the boundary conditions for fluid flow and mass balance are summarized in Table 23.

S. No	Type	Boundary Conditions for Navier Stokes	Boundary Conditions for Mass balance
1	Inlet	Normal inflow velocity ($u = u_0\, n$)	$n\, N_{NO} = n\, C_{NO}$
2	Wall	Wall condition: No slip ($u = 0$)	$-n\, N_{NO} = 0$
3	Active surface	Wall condition: No slip $u = 0$)	$-n\, N_{NO} = r_{NO}$
4	Outlet	$\eta(\nabla u + (\nabla u)^T)n = 0$, $P = P_0$	$-n\, D\, \nabla C_{NO} = 0$
	Variable description	**n** = unit vector perpendicular to the surface u_0 = mean velocity at the inlet [m/s]	**n** = unit vector perpendicular to the surface **N** = Flux over the surface

Table 23 Boundary conditions applied in Navier Stokes and Mass balance equation

7.3.2. Model Parameters:

The weather parameters like UV irradiation and RH mentioned in Table 24 are kept as constant while the input range of pollutants is varied in the model.

Parameters	Value	Unit
C_{NO} = 1 ppm (Inlet Conc. same as pollutant concentration at urban areas)	4.17E-05	mol/m^3
u_0 (Inlet Velocity for a flow rate of 3 L/min)	0.1917	m/s
E (UV irradiance)	10	W/m2
D (Diffusion Coefficient)	1.50 E^{-05}	m^2/s
ρ (Density of air @ T=293.17K)	1.20	Kg/m^3
η (Viscosity of air @ T=293.17K)	1.81E^{-05}	Kg/m/s
α (Correction factor in UV irradiance extension model)	9.1	m^2/W
k (Reaction rate constant for NO at 10 W/m^2)	3.33 E^{-08}	mol/m^2/s

K_d (Adsorption equilibrium constant for NO at RH=50%)	76.7 E^{+04}	m^3/mol
RH (Relative Humidity: Kept constant throughout the analysis)	50 %	-

Table 24 Input parameters applied for validation of the setup (Hunger et al., 2010)

The chosen concentration of the NO gas is same as the concentrations used in the experiments by Hunger et al., 2010 as mentioned in the table below:

ppm	mg/m3	mol/m3
0.1	0.125	4.17E-06
0.3	0.376	1.25E-05
0.5	0.627	2.09E-05
1.0	1.254	4.18E-05

Table 25 Concentration of NO in the inflow air for the reactor model setup

For these input pollutant levels, the concentration of NO is measured at the outlet of the reactor at various heights as shown in Figure 87. The average of these results at the mentioned heights of the outlet is calculated as the concentration of resultant NO after crossing the active surface for each of the input concentration of the pollutants.

7.3.3. Visualization of the Results:

The laminar flow developed at the beginning of the plug flow reactor is depicted in the figure below. Velocity of the air is maximum at the center of the reactor while the velocity is minimum closer to the walls of the reactor.

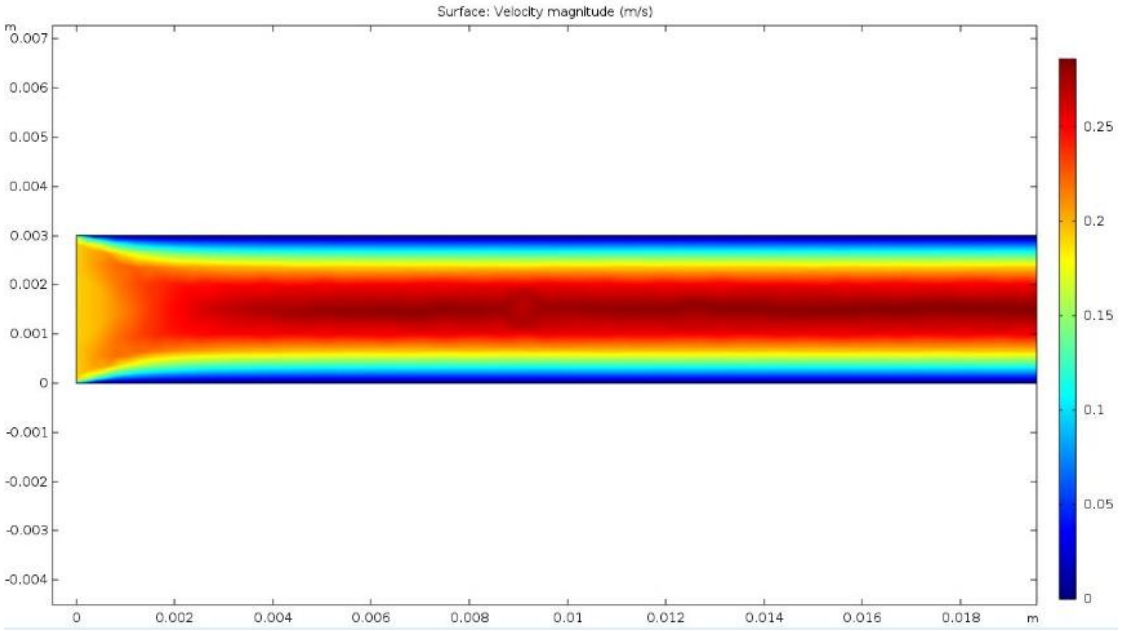

Figure 85 Velocity field in the reactor indicating the laminar flow

The concentration of pollutants is described in mol/m^3. As the pollutants flow over the active surface, the conc. of NO varies gradually along the x-axis and they are almost constant along y-axis at the outlet. With increase in flow rates higher than 0.19 m/s, conc. of NO along y-axis varied with highest degradation closer to the active surface gradually reducing toward the reactor wall. This indicates that during laminar flow, increase in velocity field leads to decrease in the extent of pollutant degradation in reactor volume. However, 4 points at different heights are measured to note the conc. of NO.

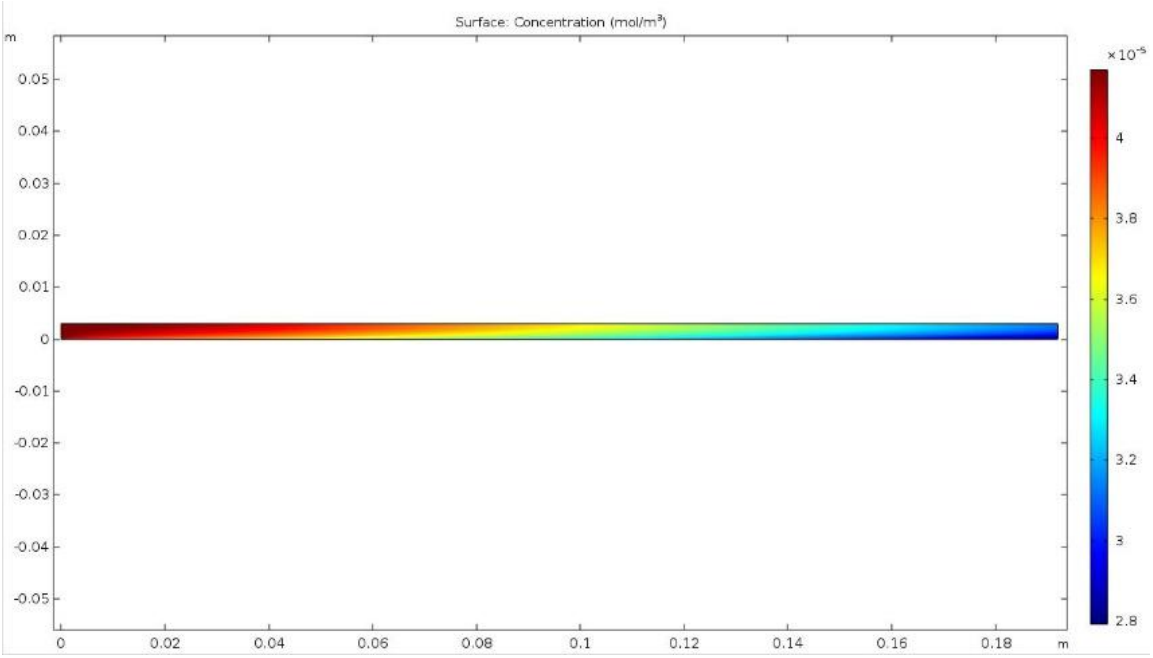

Figure 86 Concentration of NO flowing over the photocatalytic surface

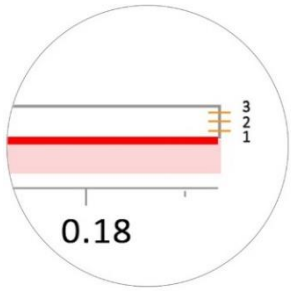

Figure 87 Points at which NO measurement is taken at the outlet

The reduction of NO can be calculated as:

$$\% \textbf{ Reduction of NO} = \left[\frac{\left[\mathbf{C_{NO(i)}} - \mathbf{C_{NO(o)}}\right)}{\mathbf{C_{NO(i)}}}\right] \mathbf{x\ 100}$$

Where $C_{NO(i)}$ is the concentration of NO at the inlet

$C_{NO(o)}$ is the concentration of NO at the outlet

7.3.4. Conclusion & Validation

The conc. of NO at three points in the outlet were measured are tabulated below:

PPM	Conc of NO at inlet (mol/m3)	Average_Out NO (simulation Model) (mol/m3)	Average_Out NO (Laboratory Model) (mol/m3)	% Conversion
0.1	4.17E-06	1.67E-06	1.5E-06	59.90%
0.3	1.25E-05	7.03E-06	6.89E-06	41.70%
0.5	2.09E-05	1.36E-05	1.35E-05	34.80%
1	4.17E-05	3.00E-05	3.08E-05	28.10%

Table 26 Comparison of the outlet NO concentration of the simulation model and the Laboratory experiment results from Hunger et al, 2010.

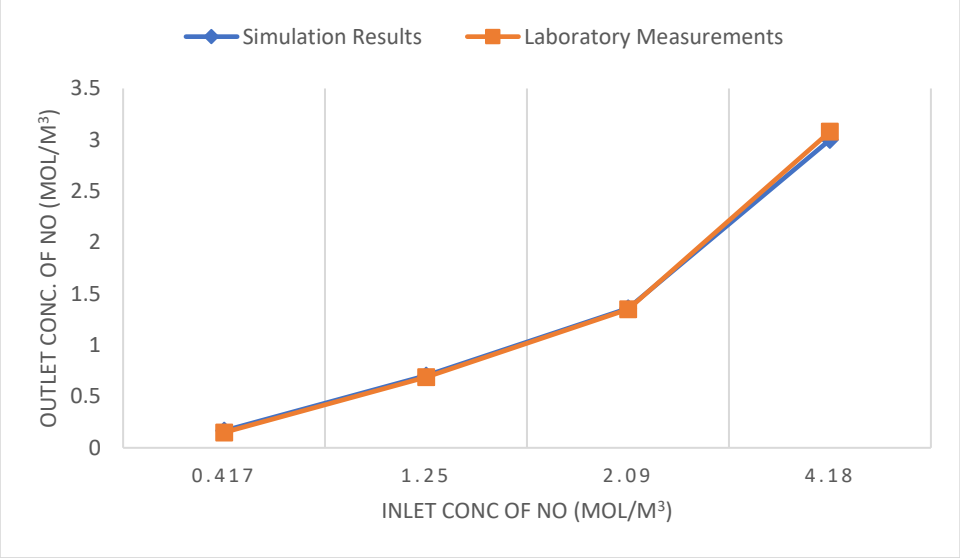

Figure 88 Comparison of the Concentration NO at the outlet of the simulated reactor and laboratory experiments.

From the table above and graph plotted below, the measurements of conc. of NO at the outlet in both the simulated model and laboratory measurements are similar. This proves that **the parameters applied and methodology of modelling for the plug flow reactor are appropriate in Comsol.** The model established would allow the prediction of performance of photocatalytic concrete products in various scenarios. Inclusion of influencing parameters like UV irradiance, relative humidity, volumetric flow and pollutant concentration helps in predicting the degradation in wide range of scenarios.

Laminar flow in the modelled plug flow reactor shows less potential for pollution abatement in a larger volume of space with increased wind velocities. A good mixing of the of flow can lead to better result of pollutant degradation. Hence, it is assumed that the turbulent flow model of the street can result in better mixing of pollutant in the volume of the street canyon.

7.4. Translation of reaction kinetics into Urban environment:

In the case studies of PICADA project and Umbreto tunnel discussed in the literature review, the NO_x degradation is measured at the surface of the façade and at 0.6 m from the coated surface respectively. The case studies do not indicate a verifiable decrease of pollutant concentration in the overall volume of the space before and after application of the photocatalytic coating. The samples are collected as measurements at one or a few points in the situation. Hence, a wholistic approach is necessary to understand the air-purifying effect of the material at various points in the space for both treated and reference situation.

To study the effects of the photocatalytic material, an environment showing some aspects of controllability for environmental influences is necessary. A closed street canyon seems to be favorable as the analysis situation. The UV irradiation levels on façade surface in the street canyon is measured as described in section () while the wind direction is kept as a constant perpendicular direction with varying wind velocity prevailing in London (2 m/s and 4 m/s).

7.4.1. Geometrical setup and boundary conditions

A cross-section of a street with aspect ratio 1 (Built height and road width 10 m each) is modelled with two types of façade; flat photocatalytic panels and designed photocatalytic panels. The analysis is done for the two-façade system with and without active surface which makes it a total of four cases.

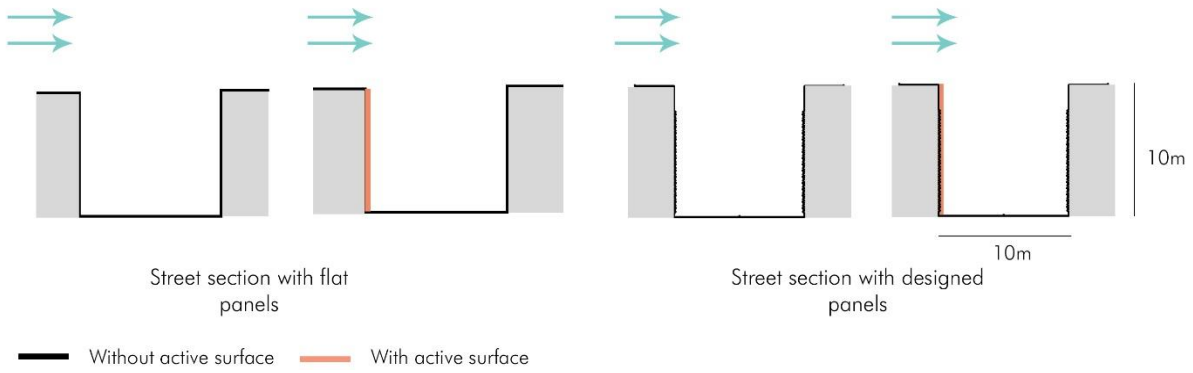

Figure 89 Representation of street scenarios indicating the treated surfaces

Scenarios	Street section with flat panels (1)		Street section with designed panels (2)	
Situation (RH 70%)	Without active surface	With active surface	Without active surface	With active surface
Wind speed	2 m/s		▪ 2 m/s ▪ 4 m/s	
UV Irradiance (W/m^2)		Summer: 16 Winter: 0.8		Summer: 34 Winter: 1.5

Table 27 Analysis scenarios for reference and TiO_2 treated street

Boundary conditions: An open boundary indicating sky is modelled at a height of 10 m from the roof of the street to allow for a stable flow of wind. This boundary condition allows the winds to pass through it and not act as a barrier. The inlet has constant velocity of wind flowing into the domain with the opposite side boundary as the outlet. The roof and walls of the building is modelled as a wall with no slip condition.

Exhaust: A 0.03 diameter circle is modelled as a reaction domain emitting NO in mol/m^3/s equal to the emission of the cars passing over the street per second (

Table 29) at a height of 0.1m from the ground level. To avoid the disturbance of flow field of the wind due to the exhaust domain, it is assigned the properties of air in the turbulence module.

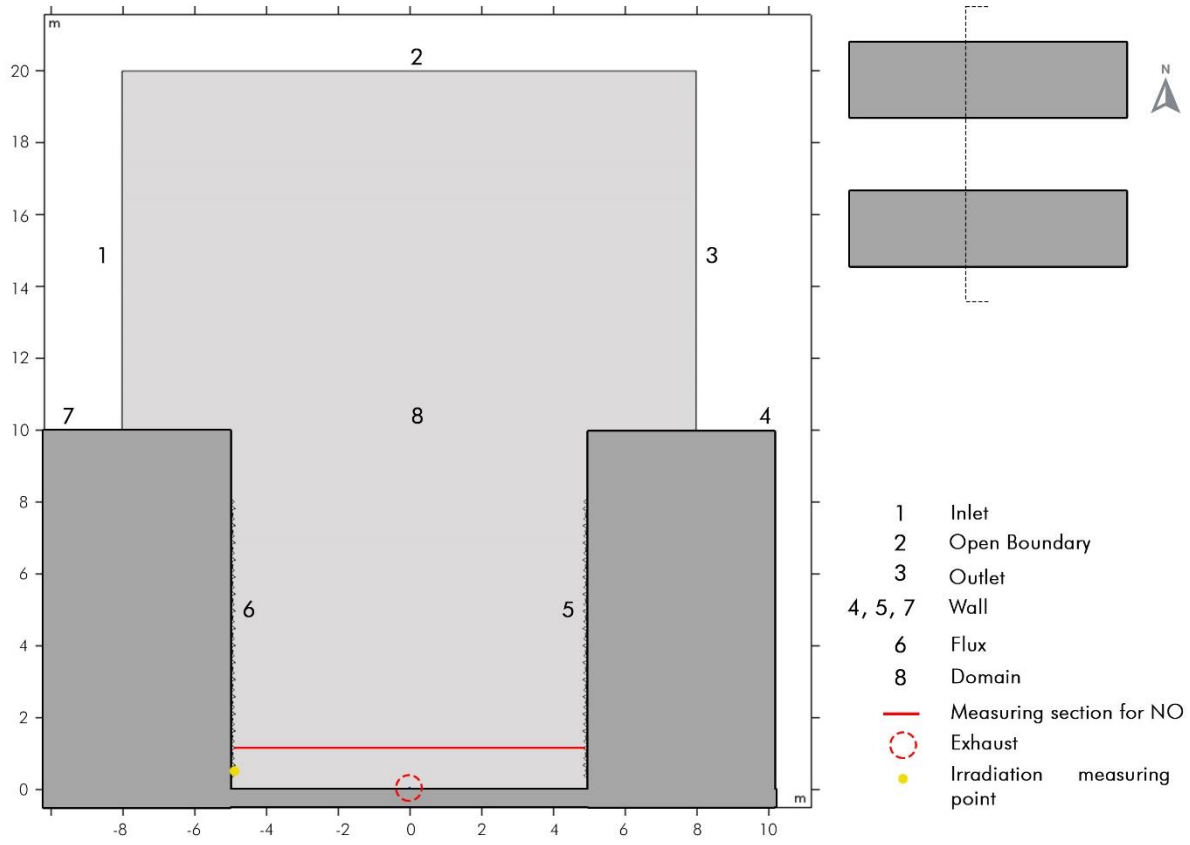

Figure 90 Section of the modelled street with the designed facade indicating the boundaries, flux and the measurement section (left); The surface highlighted in red are modeled as the flux (right)

Irradiance: UV irradiance is measured at 0.5 m from the bottom of the street for both summer and winter situation. The variation in the irradiation levels from the bottom to the top of the façade is not included in the model. The same irradiance values are used to calculate the reaction rate constant from bottom of the facade to the top.

Flux: Only one side of the façade is well lit by the sun. Hence, it is assumed that north façade contributes less towards pollution abatement. In this case, only south façade is modelled as the flux while the north façade is neglected due to low reaction rate constant

of NO (5.8E-09 mol/m^2/s) in both the street models. In the designed façade panel, faces oriented toward the bottom with low irradiation are neglected as indicated in Figure 90.

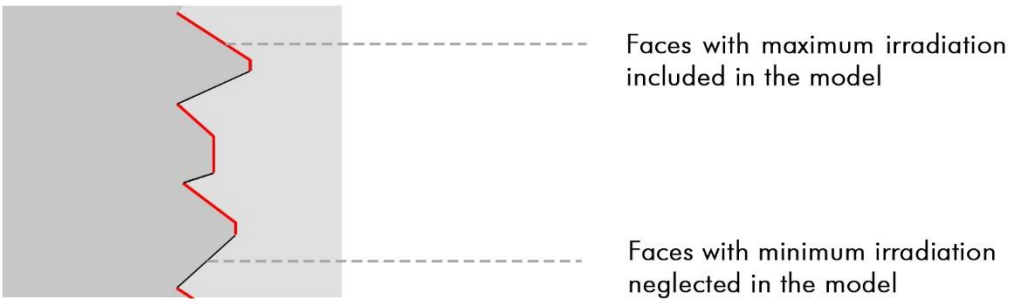

Figure 91 Faces of the facade panels included and excluded in the evaluation model are highlighted

Measuring section: Concentration of NO is analyzed at 1.5 m height (Pedestrian breathing height) in the longitudinal section. To understand the air purifying effect, the results of the concentration of NO at the measurement section is compared before and after application of photocatalytic surface for flat and designed panels for various scenarios.

Air purifying effect is measured by calculating pollution degradation percentage at each of the cell at 1.5 m height and taking an average of pollution degradation at all the cell at the same height. At each cell pollution degradation is measured by:

$$NO\ degradation\ (\%) = [(C_{(NO)ini} - C_{(NO)final})/C\_(NO)ini] * 100$$

Where; $C_{(NO)ini}$ is conc. of NO before photocatalysis at a cell

$C_{(NO)final}$ is conc. of NO after photocatalysis at cell

7.4.2. Model Parameters:

Boundary Conditions:

S. No	Type	Boundary Conditions for Mass balance
1	Inlet	$c_i = 0$
2	Wall	$-\mathrm{n}\,\mathrm{N_{NO}} = 0$
3	Active surface	$-\mathrm{n}\,\mathrm{N_{NO}} = \mathrm{r_{NO}}$
4	Outlet	$-\mathrm{n}\,\mathrm{D}\,\nabla \mathrm{C_{NO}} = 0$
5	Open Boundary	$c_i = 0$ (initial conc. of NO)
6	Exhaust	$\nabla\,(-\mathrm{D_i}\nabla C_{\mathrm{NO}}) + \mathrm{u}\nabla \mathrm{C_{NO}} = R_{C_{NO}}$
	Variable description	n = unit vector perpendicular to the surface N = Flux over the surface D = Diffusion coefficient

Table 28 Boundary Condition of the Street reactor model

Vehicular exhaust:

The vehicular exhaust is calculated based on the traffic intensity in the reference street model of Putney high street, London. The number of vehicles and density are described in Table 14.

To simplify the calculation of flux by each car:

It is assumed that all cars are Euro III, IV & V and he average emission of these cars would be 0.1 g/km. On an average day with a traffic flow of 17528 cars.

	Values	Units
Total emission/day	1752.8	g/km/day
Total emission per sec (Over 10 hours of traffic)	4.86*E-05	g/m/s
Area of exhaust (0.015 m dia)	0.00071	m^2
Molecular weight of NO	30.01	g
Emission flux	$\frac{(\text{Total emission})}{(\text{Area of exhaust}) * (\text{molecular weight})}$ $= 2.3\ E\text{-}3$	$mol/m^3/s$

Table 29 Emission from vehicles passing over the street per second

Parameters	Scenario 1(Flat façade)	Scenario 2 (Designed Façade)	Unit
$R_{C(NO)}$	*Emission flux* Table 29)	*Emission flux* Table 29)	mol/m^3
u_0 (A standard situation)	2	2	m/s
U_0 (High speed condition)		3	m/s
E (UV irradiance in Summer)	16	34	W/m^2
k (Summer)	3.78 E-08	4.88 E-08	$mol/m^2/s$
E (UV irradiance in Winter)	0.8	1.5	W/m^2
k (Winter)	5.63 E-09	8.48 E-09	$mol/m^2/s$
K_d (Absorption equllibrium constant at 70% RH)	6.72E+04	6.72E+04	m^3/mol

Table 30 Input data used in in kinetic equations

Rest of the parameters required for the model are used from Table 24.

7.4.3. Visualization of Results:

Wind velocity field:

Figure 92 depicts the velocity field inside the street canyon of aspect ratio 1 with flat panel and the designed panel.

A vortex is developed in the canyon irrespective of the inlet wind velocity. The arrows of the flow field do not change with any value of inlet velocity. The wind velocity field for scenario 1 and scenario 2 are different indicating the effect of façade panels geometry on the flow field. This in turn changes the pollution dispersion pattern for each of the situations. Hence, two independent reference situations are required without TiO_2 coating; one each for the flat and designed situations.

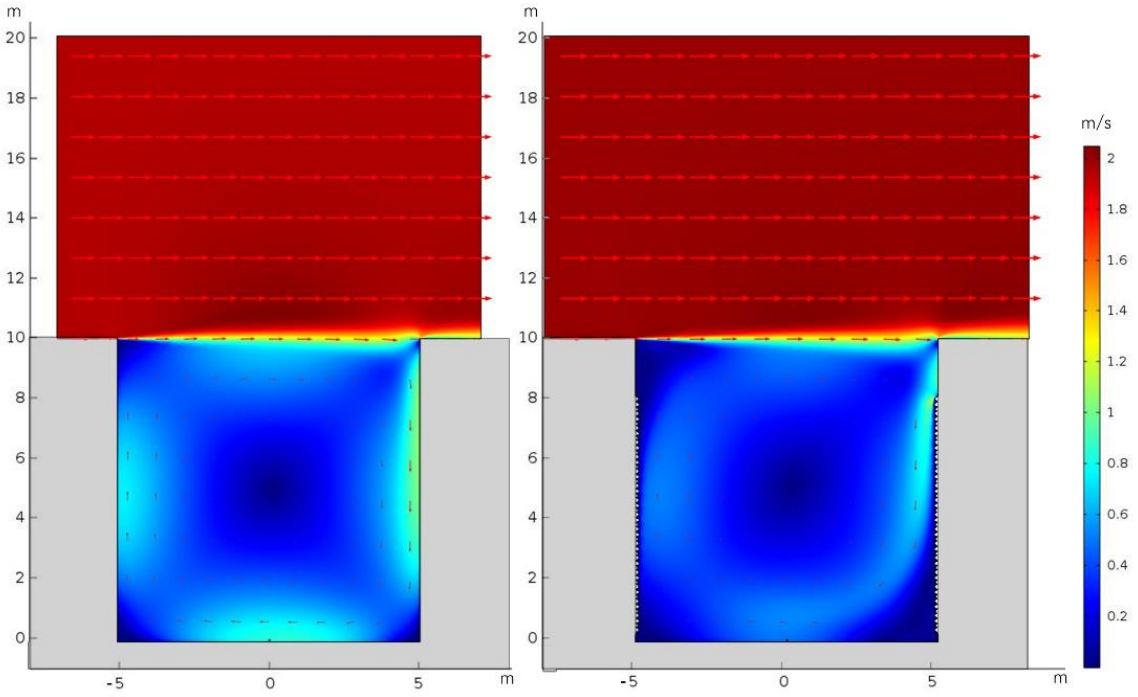

Figure 92 Wind Velocity field for the street with flat facade (Scenario 1: left); Designed facade (Scenario 2: right) at velocity = 2 m/s

Concentration of NO:

The pollutant dispersion pattern in a street canyon is depicted in the following section.

Scenario 1:

The wind at the bottom of the street transfers the exhaust from the center of the street towards the leeward active façade. A slight difference in change of concentration of NO is visually noticeable in Figure 93.

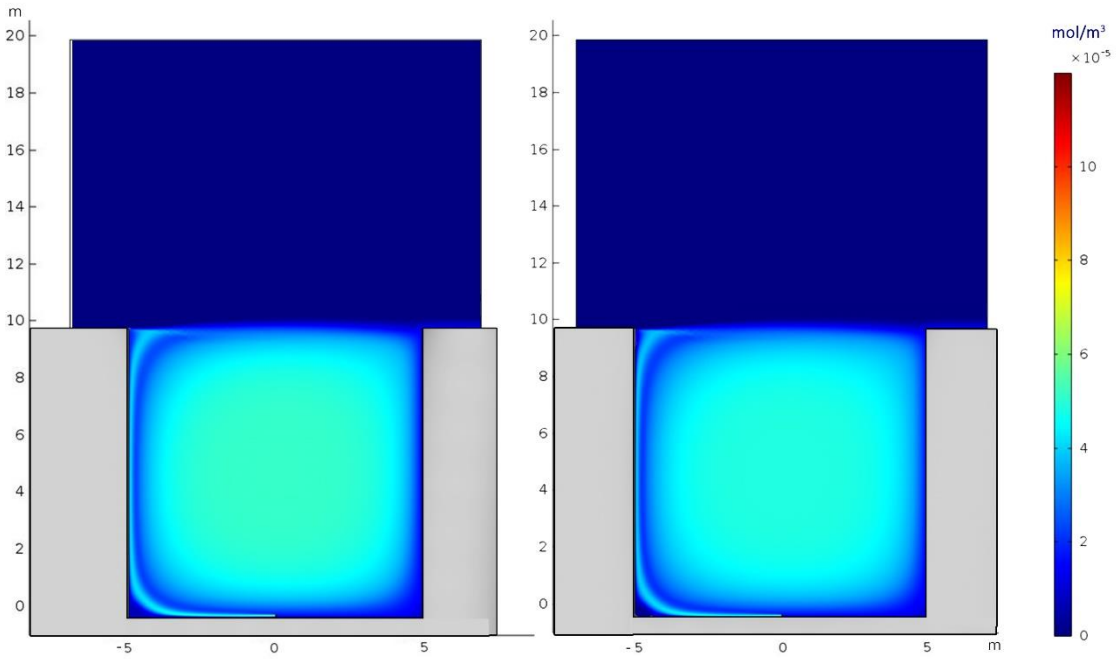

Figure 93 Flat panel: Pollutant (NO) concentration profile without (left) and with photoactive surface (right) for flat façade panels with inflow velocity of 2 m/s

Scenario 2:

The accumulation of NO is higher close to the façade panel compared to a flat façade panel due to the undulated profile of the panel. Closer to the surface of the photocatalytic surface, higher difference in concentration of NO is noticed.

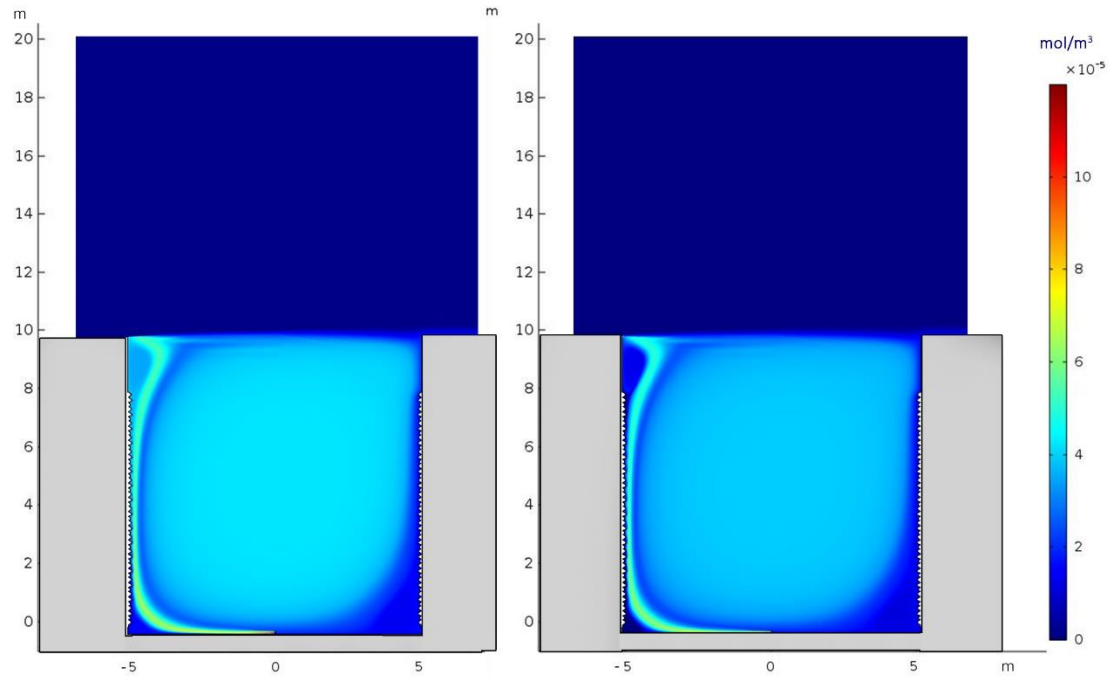

Figure 94 Designed Panel: Pollutant (NO) Concentration profile without(left) and with (right) photoactive surface (inflow velocity: 2 m/s)

7.4.4. Pollution abatement performance

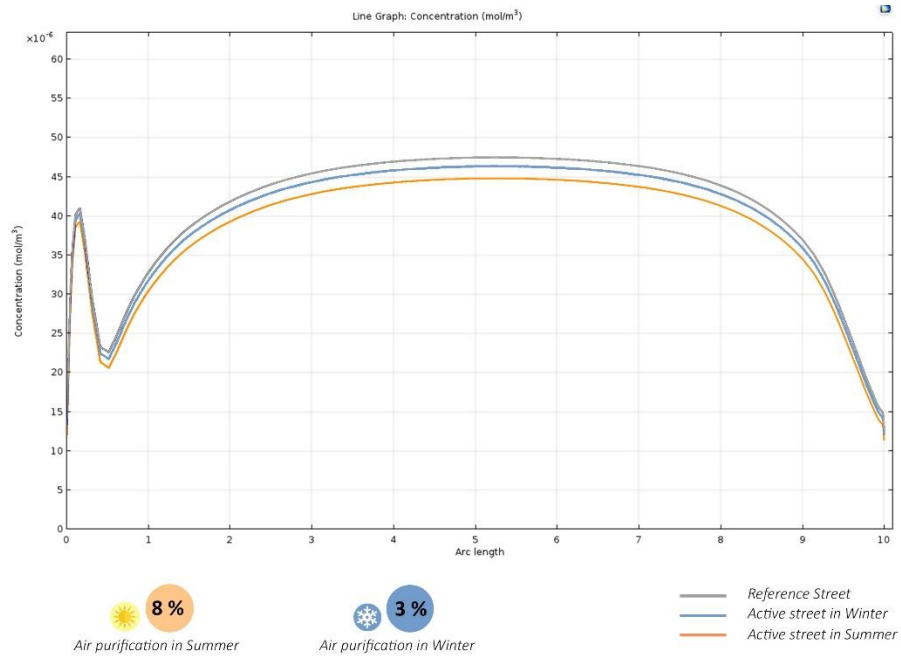

Figure 95 Pollution abatement by the flat facade with and without the photocatalytic active surface for summer and winter for inlet velocity of 2 m/s

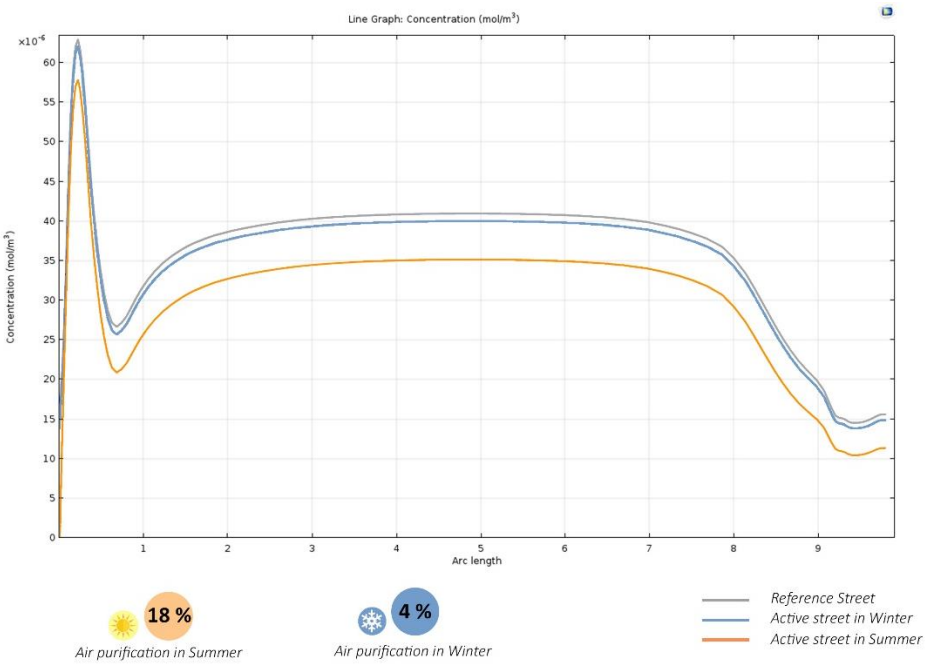

Figure 96 Pollution abatement by the designed facade with and without the photocatalytic active surface for summer and winter for inlet velocity of 2 m/s

The x-axis of the graph shows the width of the street while y-axis indicates the concentration of NO at a height of 1.5 from the ground. The air purification effect is the least for winter in both flat and designed façade which is about 4%. Highest purification effect is obtained in summer with an 18 % difference in pollutants.

A similar situation was analyzed for a wind velocity of 3 m/s (average velocity for most months in London).

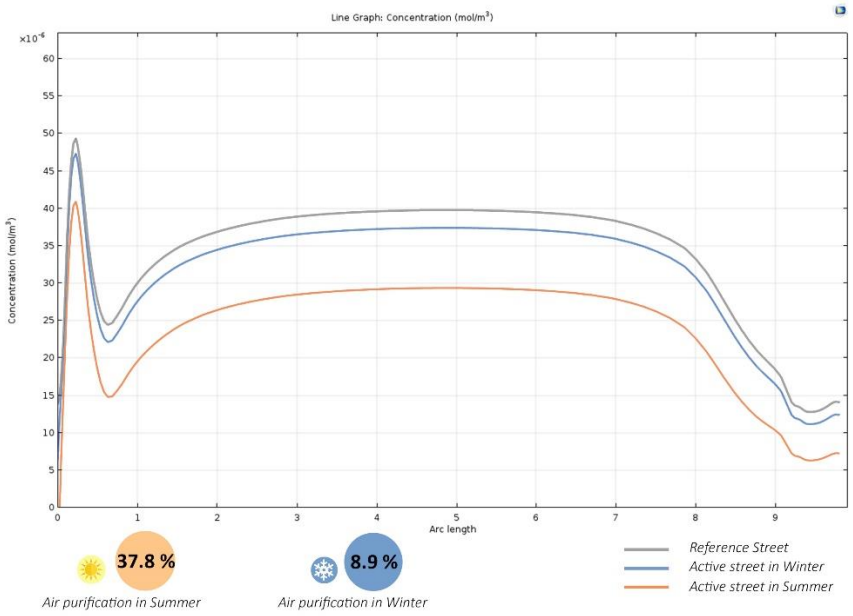

Figure 97 Pollution abatement by the designed facade with and without active surface for summer and winter for inlet velocity 3 m/s

The pollution abatement has doubled with increase in the inlet wind velocity. They can be attributed to the increased rate of mixing of air within the street canyon.

7.5. Conclusion

Comparing the results from scenario 1 and 2, shows that result in scenario 2 is better with higher air purification effect. The geometry of the panel slows down the movement of pollutants closer to the active surface that provides longer residence time. Also, higher residence time in combination with better irradiation increases its efficiency.

From this it can be concluded that the designed panel leads to a better performance compared to a flat photocatalytic panel. In winter (low UV irradiance), a range of 4 – 8.9 % of difference air quality is achievable for low and average wind speeds respectively. With increasing wind speeds, the air purification effect increases. In summer (high UV irradiance), a range of 18 – 37.8 % of air quality difference is attainable for low and average wind speed.

8.0. CONCLUSION

Air pollution is a common issue in all urban contexts, and they must be tackled from various perspectives. Studying pollution dispersion pattern in urban areas showed how leeward facades acted as pollutant receptors in densely built environments. With majority of the urban areas flanked by buildings, potential of these building envelopes to contribute to their surroundings is underutilized. While most of the applications like green facades and algal facades are highly maintenance intensive, alternative photocatalytic building materials were considered for further research.

- What are the parameters and constraints driving the design of the façade panels?

The Literature studies about the chemistry and material science behind the photocatalytic building materials helped in translating their performance indicators at an urban scale. The case studies provided supporting evidence of air purifying effect of these materials in contexts like that of Umbreto tunnel in Italy. However, other application of these materials on façade surfaces focused on purification effect closer to the façade and not in the bulk volume of air in the street canyon. It was also understood that high wind speeds were the most inhibiting factors for photocatalysis in outdoor applications.

Irradiance levels: No optimum orientation is required for the panels. They are required to have maximum amount of irradiation throughout the year due to which, the highest and lowest sun angle days were chosen to optimize the incident irradiation for the entire day. The optimized panels were compared with each other for the maximum available active surface with irradiation >10 W/m^2.

Manipulating wind speeds: The parameters were derived from conceptual design of roughness elements for certain modules and their application in high wind speed conditions. The alternating roughness elements of projection length 0.15 m for every height of 0.25 m was chosen to begin the design.

Finalization of geometry should be a balance between surface enlargement and incident irradiation. With higher surface enlargement factor, the incident UV irradiance decreases and geometries with less surface enlargement have high irradiance with lesser active area available for photocatalysis. Geometry with highest active surface area available during winter and summer solstice was chosen as the optimum outcome.

- How could this technology be integrated into façade systems for widespread applications?

It is necessary to accommodate the design into a conventional system for widespread application and easy fabrication and installation. Integration was based at different levels;

paneling, materialization, fabrication and fixing methods. Widespread application requires sustainable solutions to realize the benefit over the long term. 15 mm thick UHPC proved to be the most environmentally friendly material compared to light weight systems like TiO_2 coated polymer (ABS) panels. However, exceeding a 20 mm thickness of UHPC would not prove to have a positive environmental impact. In such a case, ABS plastic would be beneficial as they 7 times lighter and more environmentally friendly than 25 mm UHPC panels.

- What is the extent to which these materials can reduce the air pollutants in an urban scenario?

    - To what extent is the designed panel's performance better than a flat façade panel coated with TiO_2?
    - What would be the range of pollution abatement percentage that can be obtained in street canyons?

The extent of reduction was measured at a pedestrian breathing height along the longitudinal section of the street. For a flat photocatalytic façade, there was a 3.5% reduction during winter and 8% during summer at low wind speed.
For the designed façade, higher reduction of pollutants was noticed increased incident irradiance. At low wind speeds 4% and 18% of air purification was noticed. And at higher wind speeds air purification increased to 8.9% and 37.8%. The accumulation of pollutants was higher closer to the façade compared to a flat façade which shows the potential of the geometry slow down the movement of wind over it.

Maximum of 60% of the façade does not have enough irradiance in street canyons during winter. This leads to poor performance of these panels during winter. Irradiation levels are highly favorable in free standing structures than in densely built environments which can alleviate the pollution abatement.

9.0. RECOMMENDATIONS:

The project needs to be developed further on the following aspects:

1. Design:

- The aim was not designing an optimum solution but to come up with a concept responding to the performance inhibiting factors of the photocatalyst and evaluate them to understand the potential benefit of air purification. The design is a conceptual development for south orientation. Hence, this concept needs to be further optimized to suit the other orientations of the façade.

2. Materialization:

- More research in fabrication method is necessary and required iteration must be accommodated on the façade geometry to realize the concept.

- The shortlisted substrates for TiO_2 were UHPC and ABS plastic. These materials on their own have high embodied energy and carbon footprint. Hence, an additional life cycle assessment of the product would help in understanding if the photocatalytic panel can create a positive environmental effect from cradle to grave.

- Also, the environmental impact of these nanoparticles after they are washed into the soil must be assessed.

3. Simulation Models:

- Basic climatic factors like RH and irradiance were chosen with limited variables to keep the simulation simple and fast. Hence, analyzing the air purification effect in a transient model accommodating the varying humidity levels and irradiance would give a more accurate pollution abatement results of these materials.

4. Physical tests:

- Apart from simulation, fabricating these panels and testing them in real time environment would provide better understanding about their performance.

10. References

(2018, 5 16). Retrieved from UN DESA: https://www.un.org/development/desa/en/news/population/2018-revision-of-world-urbanization-prospects.html

A, A., E.S, M., A, L., & M.P., P. (2016). Photocatalytic self-cleaning coatings for building facade maintenance. Performance analysis through a case-study application. *Journal of Facade Design and Engineering, 4*, 115-129. doi:DOI 10.3233/FDE-160054

Águia, C., Ângelo, J., Madeira, L. M., & Mendes, A. (2011b). Photo-oxidation of NO using an exterior paint - Screening of various commercial titania in powder pressed and paint films'. *Journal of Environmental Management. Elsevier Ltd*, 1724-1732. doi:10.1016/j.jenvman.2011.02.01

Ângelo, J., Andrade, L., & Mendes, A. (2014). Highly active photocatalytic paint for NOx abatement under real-outdoor conditions. *Applied Catalysis A: General. Elsevier B.V, 484*, 17-25. doi:10.1016/j. apcata.2014.07.005

Angelo, J., Andrade, L., Madeira, L. M., & Mendes, A. (2013). An overview of phottocatalysis phenomena applied to NOx abatement. *Journal of Environmental Management, 129*, 522-539. doi:https://doi.org/10.1016/j.jenvman.2013.08.006

Ballari, M. M., Hunger, M., Hüsken, G., & Brouwers, H. J. (2010). NOx photocatalytic degradation employing concrete pavement containing titanium dioxide. *Applied Catalysis B: Environmental*, 245–254. doi:10.1016/j.apcatb.2010.01.002

Ballari, M. M., Yu, Q. L., & Brouwers, H. J. (2011). Experimental study of the NO and NO2 degradation by photocatalytically active concret. *Catalysis Today, 161(1)*, 175-180. doi:10.1016/j.cattod.2010.09.028

Barmpas, Moussiopoulos, N., & Vlahocostas, C. (2006). *Depollution prediction tool & Integrated economic assesment.* PICADA.

Beeldens, A., Cassar, L., Guerrini, G. L., & Pimpinelli, N. (2007). PHOTOCATALYSIS OF CEMENTITIOUS MATERIALS. *International RILEM Symposium on Photocatalysis, Environment and Construction Materials*, 131-145.

Bianchi, C. L., Pirola, C., Stucchi, M., Sacchi, B., Cerrato, G., Morandi, S., . . . Capucci, A. C. (2016). A New Frontier of Photocatalysis Employing Micro-Sized TiO2: Air/Water Pollution Abatement and Self-Cleaning/ Antibacterial Applications. *INTECH*, 635-666. doi:http://dx.doi.org/10.5772/62892

Cárdenas, C., Tobón, J. I., García, C., & Vila, J. (2012). Functionalized building materials: Photocatalytic abatement of NO by cement pastes blended with TiO nanoparticles. *Construction and Building Materials, 36*, 820-825. doi:https://doi.org/10.1016/j.conbuildmat.2012.06.017

Chen, D. H., Li, K., & Yuan, R. (2007). *Photocatalytic Coating on Road Pavements/Structures for NOx Abatement.* Durham, United States: Houston Advanced Research Center and Office of Air Quality Planning and Standards U.S. Environmental Protection Agency.

Depolluting facades. (2013). Retrieved from http://www.prosolve370e.com/how-it-works-1/

Devahasdin, S., Fan, C., Li, K., & Chen, D. H. (2003). TiO2 photocatalytic oxidation of nitric oxide: transient behavior and reaction kinetics. *Journal of Photochemistry and Photobiology A: Chemistry*, 161-170. doi:https://doi.org/10.1016/S1010-6030(03)00005-4

EIC. (2015). *A clear choice for the UK: Technology options for tackling air pollution.* London: The Environmental Industries Commision.

F. L. Toma, G. B. (2004). Photocatalytic removal of nitrogen oxides via titanium dioxide. *Environ Chem Lett, 2*, 117-121. doi:DOI 10.1007/s10311-004-0087-2

Folli, A., Jakobsen, U., Guerrini, G., & Macphee, D. (2009). Rhodamine B Discolouration on TiO2 in the Cement Environment: A Look at Fundamental Aspects of the Self-cleaning Effect in Concretes. *Journal of Advanced Oxidation Technologies, 12*, 126–133.

Fontana, P., Miccoli, L., Kocadag, R., Silva, N., Qvaeschning, D., Kreft, O., & Cederqvist, C. (2016). Composite UHPC façade elements with functional surfaces . *Ultra high performance concrete and high performance construction materials*.

G.J.M.Velder. (2013). *The Euro emission standards for cars and trucks in relation to NO2 limit value exceedances in the Netherlands.* Netherlands: Ministry of Health, Welfare and Sport - National Institute for Public Health and the Environment.

Gallus, M., Akylas, V., Barmpas, F., Beeldens, A., Boonen, E., Boréave, A., . . . Kleffmann, J. (2015). Photocatalytic de-pollution in the Leopold II tunnel in Brussels: NOx abatement results. *Building and Environment*, 125-133.

Guerrini, & Luca, G. (2012). Photocatalytic performances in a city tunnel in Rome: NO monitoring results. *Construction and Building Materials, 27*, 165-175. doi:10.1016/j.conbuildmat.2011.07.065

Guo, M. Z., & Poon, C. S. (2013). Photocatalytic NO removal of concrete surface layers intermixed with TiO2. *Building and Environment. Elsevier Ltd*, 102–109. doi:10.1016/j.buildenv.2013.08.017

Hashimoto, K., Irie, H., & Fujishima, A. (2005). TiO2 Photocatalysis: A Historical Overview and Future Prospects. *Japanese Journal of Applied physis*, 8269–8285.

Herrmann, J. (2010). Phottocatalysis fundamentals revisited to avoid several misconceptions. *Applied catalysis*, 461-468.

Herrmann, J.-M. P. (2007). Photocatalysis: From fundamentals to self-cleaning glass application. *Proceedings international RILEM symposium on photocatalysis, environment and construction materials*.

Hoffmann, M. R., Martin, S. T., Choi, W., & Bahnemann, D. W. (1995). Environmental Applications of Semiconductor Photocatalysis. *Chemical Reviews, 95 (1)*, 69-96. doi:10.1021/cr00033a004

Hunger, M., Husken, G., & Brouwers, H. (2010). Photocatalytic degradation of pollutants: From modelling to large scale application. *Cement and Concrete Research*, 313-320.

Hüsken, G., Hunger, M., & Brouwers, H. (2009). Experimental study of photocatalytic concrete products for air purification. *Building and Environment*, 2463-2474.

Hüsken, G., Hunger, M., & Brouwers, H. J. (2009). Experimental study of photocatalytic concrete products for air purification. *Building and Environment. Elsevier Ltd*, 2463–2474. doi:10.1016/j. buildenv.2009.04.010

Hwang, S., Lee, M. C., & Choi, W. (2003). Highly enhanced photocatalytic oxidation of CO on titania deposited with Pt nanoparticles: kinetics and mechanism. *Applied Catalysis B-Environmental, 46(1)*, 49-63. doi: doi: 10.1016/s0926-3373(03)00162-0

Ibhadon, A. O., & Fitzpatrick, P. (2013). Heterogeneous Photocatalysis: Recent Advances and Applications. *Catalysts*, Volume 3, 189-218.

J. Hot, J. T. (2017). Investigation on Parameters Affecting the Effectiveness of Photocatalytic Functional Coatings to Degrade NO: TiO2 Amount on Surface, Illumination, and Substrate Roughness. *International Journal of Photoenergy*. doi:https://doi.org/10.1155/2017/6241615

Jiang, J. O. (2008). Does nanoparticle activity depend upon size and crystal phase? *Nanotoxicology, 2(1)*, 33-42.

Lignarolo, L., Lelieveld, C., & Teuffel, P. (2011). Shape morphing wind-responsive facade systems realized with smart materials.

lumthaler, M. B., & Ellinger, W. A. (1997). Increase in solar UV radiation with altitude. *Journal of Photochemistry and Photobiology B: Biology*, 130-134.

Maggos, T., Bartzis, J., Leva, P., & Kotzias, D. (2007). Application of photocatalytic technology. *Applied physics A: Material Science and Engineering, 89*, 81–84. doi:DOI: 10.1007/s00339-007-4033-6

Maggos, T., Plassais, A., Bartzis, J. G., Vasilakos, C., Moussiopoulos, N., & Bonafous, L. (2007). *Photocatalytic degradation of NOx in a pilot street canyon configuration using TiO2-mortar panels.* doi:DOI 10.1007/s10661-007-9722-2

Martinez, T., Bertron, A., Ringot, E., & Escadeillas, G. (2011). Degradation of NO using photocatalytic coatings applied to different substrates. *Building and Environment, 46*, 1808 - 1816.

Marwa M. Hassan, T. R. (2010). Durability of Titanium Dioxide Photocatalytic Layer for Pavement surfaces .

Material data book. (2003). Retrieved from Cambridge university engineering department: http://www-mdp.eng.cam.ac.uk/web/library/enginfo/cueddatabooks/materials.pdf

Mayer, H. (1999). Air pollution in cities. *Atmospheric Environment*, 4029-4037.

Melo, J. V., Trichês, G., Gleize, P. J., & Villena, J. (2012). Development and evaluation of the efficiency of photocatalytic pavement blocks in the laboratory and after one year in the field. *Construction and Building Materials, 37*, 310-319.

Mills, A., & Elouali, S. (2015). The nitric oxide ISO photocatalytic reactor system: Measurement of NOx removal activity and capacity. *Journal of Photochemistry and Photobiology A: Chemistry, 305*, 29-36. doi:10.1016/j. jphotochem.2015.03.002

Muilwijk, C., Schrijvers, P., Wuerz, S., & Kenjeres, S. (2016). Simulations of photochemical smog formation in complex urban areas. *Atmospheric Environment*, 470-484.

Murata, Y., Kamitami, K., & Takeuchi, K. (2018). Air purifying blocks based on photocatalysis. *Catalysts*.

Nikolov, N., & Fox, J. T. (2015). Clean by Concrete: Use of Photocatalytic Concrete enables Buildings to be Passive Environmental Remediators. *Research Journal of Engineering Science*.

Poon, C. S., & Cheung. (2007). NO removal efficiency of photocatalytic paving blocks prepared with recycled materials. *Construction and Building Materials*, 1746–1753. doi:10.1016/j.conbuildmat.2006.05.018

R, O. T., & Brown, T. (1995). TIO2 PHOTOCATALYSIS FOR INDOOR AIR APPLICATIONS - EFFECTS OF HUMIDITY AND TRACE CONTAMINANT LEVELS ON THE OXIDATION RATES OF FORMALDEHYDE, TOLUENE, AND 1,3-BUTADIENE. *Environmental Science & Technology, 29(5)*, 1223-1231. doi: doi: 10.1021/es00005a013

R.B.Holland, & Kahn, L. (2016). Effect of different concrete materials on thecorrosion of the embedded reinforcing steel. *Corrosion of steel and concrete structures*.

S. Hanson, P. (2013). Fabrication Techniques for Concrete Containing TiO2 Photocatalytic Particles. *International Concrete Sustainability Conference*.

S. Hanson, P. T. (2013). Fabrication Techniques for Concrete Containing TiO2 Photocatalytic Particles . *International Concrete Sustainability Conference*.

Saravanan, R., Gracia, F., & Stephen, A. (2017). Basic Principles, Mechanism, and Challenges of Photocatalysis. *Nanocomposites for Visible Light-induced Photocatalysis*, 19-40.

Savage, A., & Turpin, K. (2011). *Emissions Sources Appointment: Putney high Street.* London: Transport Research Laboratory.

Serpone, N. (2018). Heterogeneous Photocatalysis and Prospects of TiO -Based Photocatalytic DeNOxing the Atmospheric Environment. *Catalysis, 8(11)*, 553. doi:https://doi.org/10.3390/catal8110553

Sugrañez, R., Álvarez, J. I., Cruz-Yusta, M., Mármol, I., Morales, J., V. J., & Sánchez, L. (2013). 'Enhanced photocatalytic degradation of NOx gases by regulating the microstructure of mortar cement modified with titanium dioxide. *Building and Environment. Elsevier Ltd, 65*, 55-63. doi:10.1016/j.buildenv.2013.07.014

Sung, D. (2016). A New Look at Building Facades as Infrastructure. *Engineering, 2*, 63-68.

T.-B. Ottosen, K. E. (2015). *Analysis of the impact of inhomogeneous emissions in the Operational Street Pollution Model (OSPM).* Copernicus Publications on behalf of the European Geosciences Union. doi:10.5194/gmd-8-3231-2015

Vardoulakis, S., Fisher, B. E., Pericleous, K., & Gonzalez-Flesca, N. (2003). MODELLING AIR QUALITY IN STREET CANYONS: A REVIEW. *Atmospheric environment, Elsevier, 37*, 155-182. doi:10.1016/S1352-2310(02)00857-9

Wang, G., Bosch, F., & Kuffer, M. (2008). MODELLING URBAN TRAFFIC AIR POLLUTION DISPERSION. *The International Archives of the Photogrammetry, Remote Sensing and Spatial Information Sciences, XXXVII*.

Wang, K.-H., & Hsieh, Y.-H. (2007). Heterogeneous photocatalytic degradation of trichloroethylene in vapor phase by titanium dioxide. *Environment International, 24*, 267-274. doi:https://doi.org/10.1016/S0160-4120(98)00005-1

World Health Organization. (2016, May 12). Retrieved from https://www.who.int/en/news-room/detail/12-05-2016-air-pollution-levels-rising-in-many-of-the-world-s-poorest-cities

World Heath Organization. (n.d.). Retrieved from https://www.who.int/air-pollution/news-and-events/how-air-pollution-is-destroying-our-health

Yang, L., Hakki, A., Wang, F., & Macphee, D. E. (2017). Photocatalyst efficiencies in concrete technology: The effect of photocatalyst placement. *Applied Catalysis B: Environmental, 222*, 200-208. doi:10.1016/j. apcatb.2017.10.013

Zhao, Y., Han, J., Shao, Y., & Feng, Y. (2009). Simultaneous SO(2) and NO removal from flue gas based on TiO(2) photocatalytic oxidation. *Environmental Technology, 30(14)*, 1555-1563. doi:doi: 10.1080/0959333090331378

11. APPENDIX A:

Initial conceptual outputs from Galapagos for various shapes of modules:

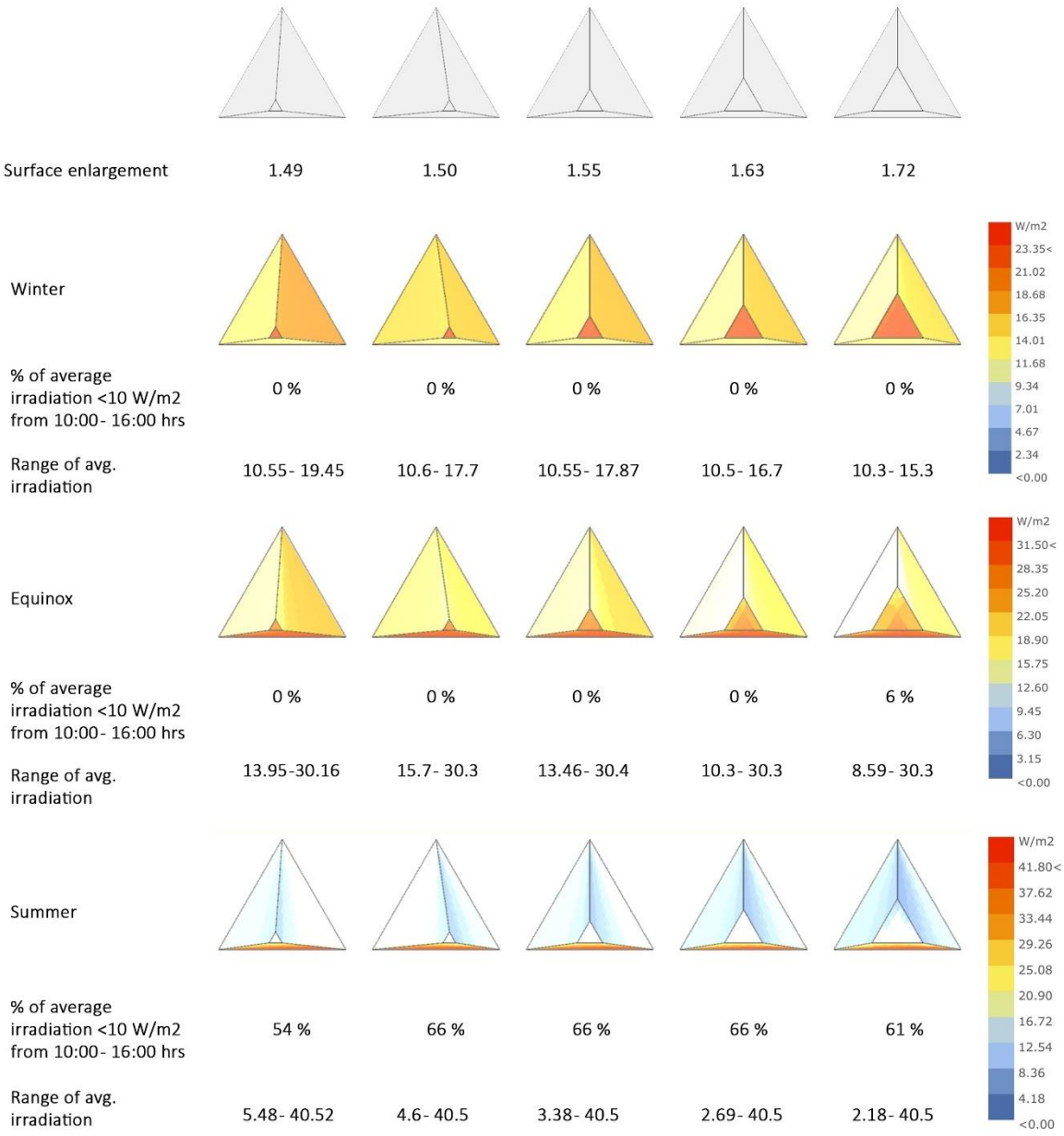

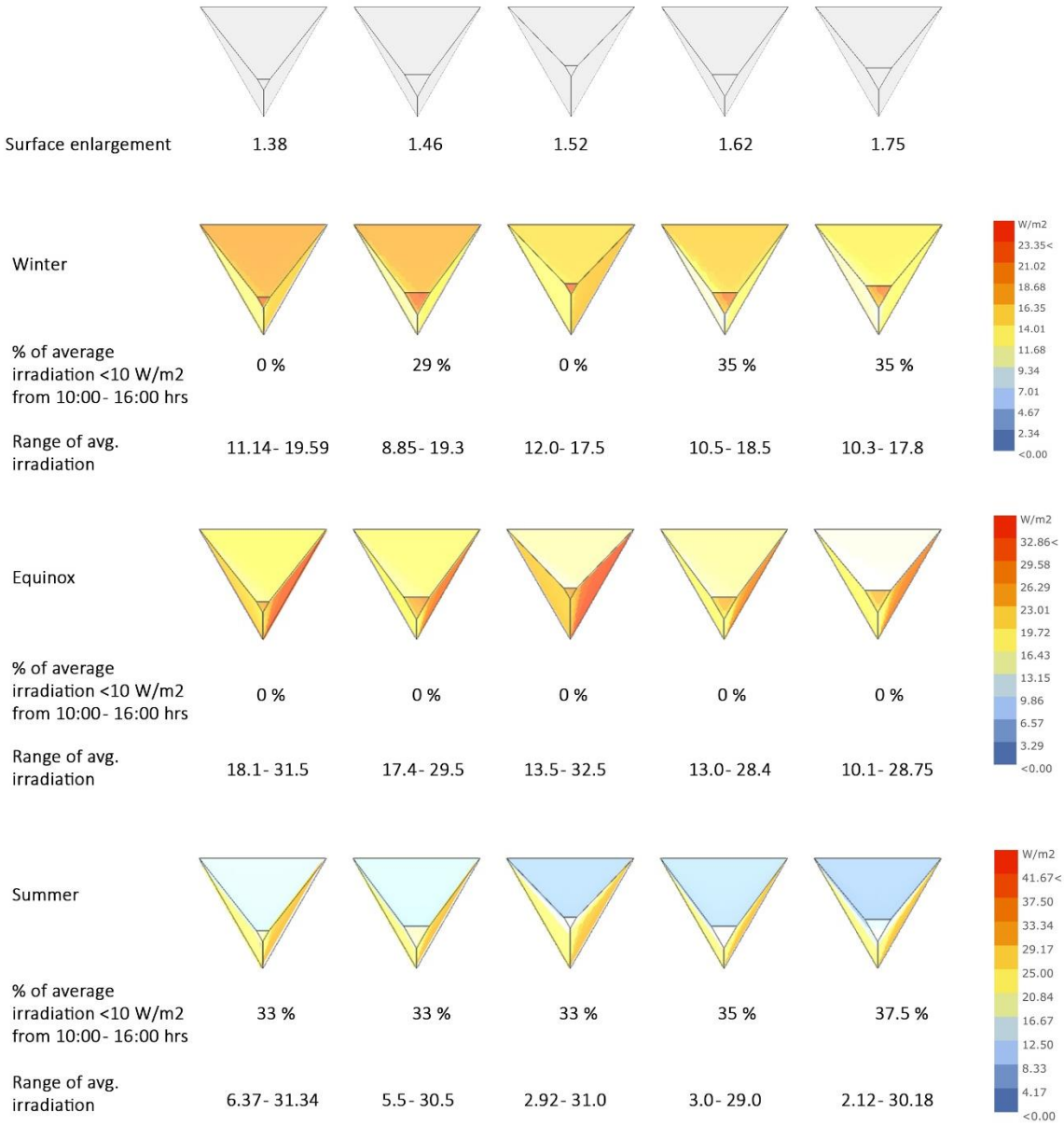
Surface enlargement
1.38
1.46
1.52
1.62
1.75
Winter
% of average irradiation <10 W/m2 from 10:00- 16:00 hrs
0 %
29 %
0 %
35 %
35 %
Range of avg. irradiation
11.14- 19.59
8.85- 19.3
12.0- 17.5
10.5- 18.5
10.3- 17.8
W/m2
23.35<
21.02
18.68
16.35
14.01
11.68
9.34
7.01
4.67
2.34
<0.00
Equinox
% of average irradiation <10 W/m2 from 10:00- 16:00 hrs
0 %
0 %
0 %
0 %
0 %
Range of avg. irradiation
18.1- 31.5
17.4- 29.5
13.5- 32.5
13.0- 28.4
10.1- 28.75
W/m2
32.86<
29.58
26.29
23.01
19.72
16.43
13.15
9.86
6.57
3.29
<0.00
Summer
% of average irradiation <10 W/m2 from 10:00- 16:00 hrs
33 %
33 %
33 %
35 %
37.5 %
Range of avg. irradiation
6.37- 31.34
5.5- 30.5
2.92- 31.0
3.0- 29.0
2.12- 30.18
W/m2
41.67<
37.50
33.34
29.17
25.00
20.84
16.67
12.50
8.33
4.17
<0.00

				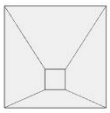	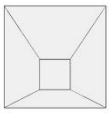
Surface enlargement	1.57	1.60	1.75	1.75	1.96
Winter	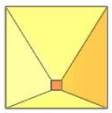				
% of average irradiation <10 W/m2 from 10:00- 16:00 hrs	0 %	10 %	25 %	0 %	25 %
Range of avg. irradiation	12.3-17.8	9.28-17.8	8.63-16.63	10.15-15.77	8.24-14.75
Equinox		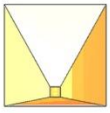	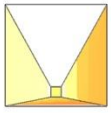		
% of average irradiation <10 W/m2 from 10:00- 16:00 hrs	7.8 %	0 %	14 %	25 %	25 %
Range of avg. irradiation	8.7- 33.3	10.2- 29.45	7.59- 28.7	4.55- 32.2	2.68- 32.2
Summer	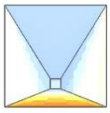		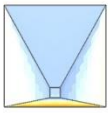	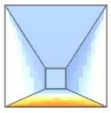	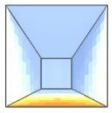
% of average irradiation <10 W/m2 from 10:00- 16:00 hrs	48 %	48 %	59 %	60.9 %	64 %
Range of avg. irradiation	1.7- 41.7	2.12- 40.01	1.56- 39.5	1.2- 41.2	0.93- 41.2

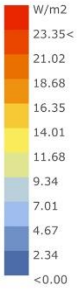

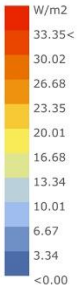

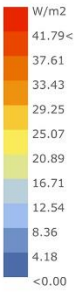

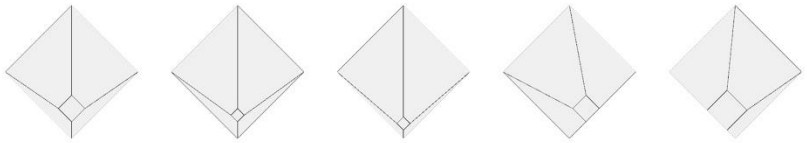

Surface enlargement	1.4	1.49	1.55	1.58	1.68
Winter	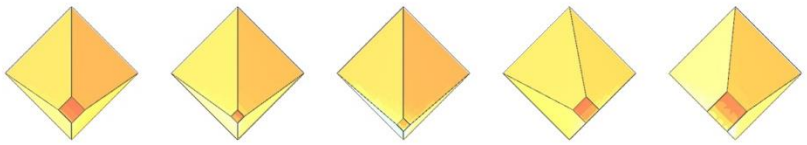				
% of average irradiation <10 W/m2 from 10:00- 16:00 hrs	0 %	26.5 %	26 %	25 %	26 %
Range of avg. irradiation	10.27- 19.6	8.55-19.13	5.19- 19.56	6.6- 17.5	4.5- 18.52
Equinox	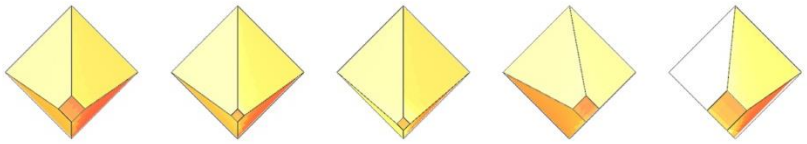				
% of average irradiation <10 W/m2 from 10:00- 16:00 hrs	0 %	0 %	0 %	0 %	0 %
Range of avg. irradiation	17.22- 32.38	15.7- 30.94	16.27- 27.55	15.9- 26.88	12.09- 30.9
Summer	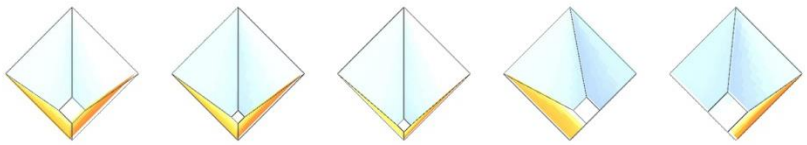				
% of average irradiation <10 W/m2 from 10:00- 16:00 hrs	50 %	50 %	50 %	50 %	50 %
Range of avg. irradiation	5.8- 36.2	3.8- 36.2	5.48 - 34.00	3.7- 31.6	3.1- 35.7

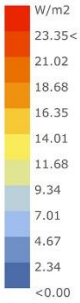

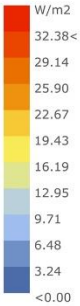

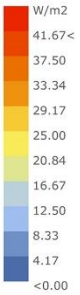

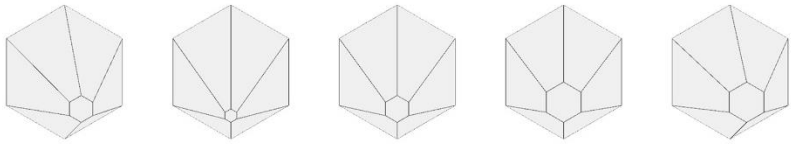

Surface enlargement	1.4	1.45	1.53	1.61	1.65

Winter					
% of average irradiation <10 W/m2 from 10:00 - 16:00 hrs	0 %	0 %	0 %	0 %	0 %
Range of avg. irradiation	10.3 - 20.5	10.15-20.3	10.14 - 20.8	10.14 - 20.5	10.10 - 21.2

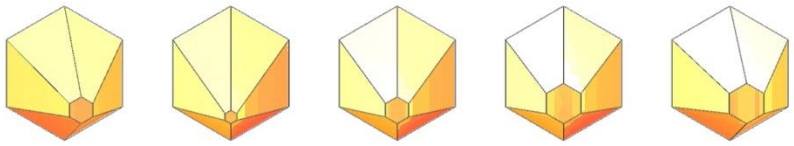

Equinox					
% of average irradiation <10 W/m2 from 10:00 - 16:00 hrs	0 %	0 %	0 %	0 %	0 %
Range of avg. irradiation	16.0 - 30.3	14.8 - 33.3	12.7 - 33.3	10.49 - 33.0	11.79 - 29.15

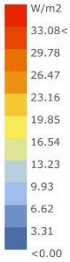

Summer					
% of average irradiation <10 W/m2 from 10:00 - 16:00 hrs	35 %	41 %	43 %	46 %	45 %
Range of avg. irradiation	3.9 - 38.0	3.55 - 39.89	2.98 - 39.89	2.0 - 39.8	2.13 - 37.7

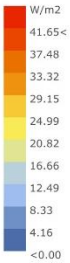

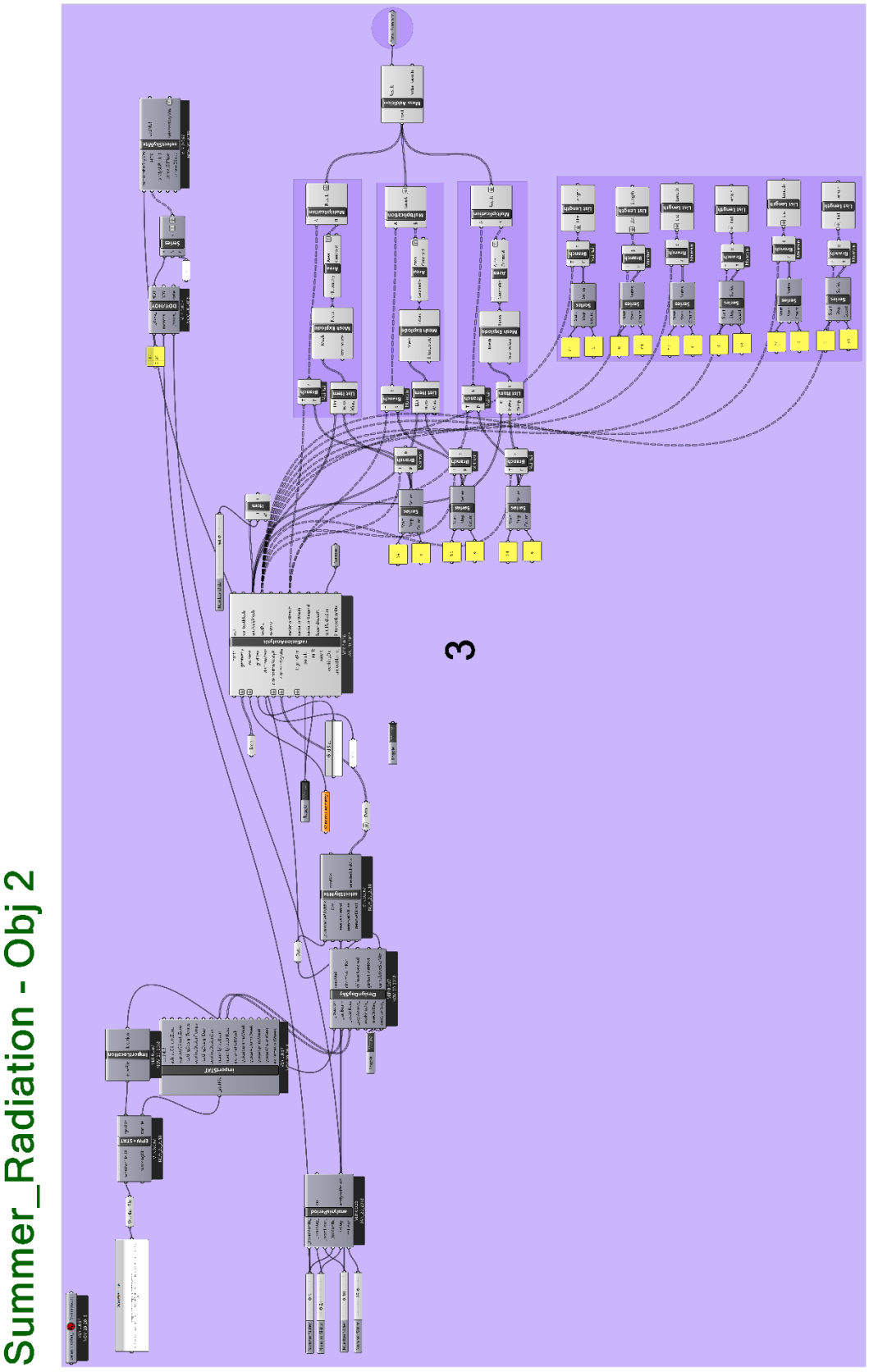
Summer_Radiation - Obj 2
3

Starting Geometry

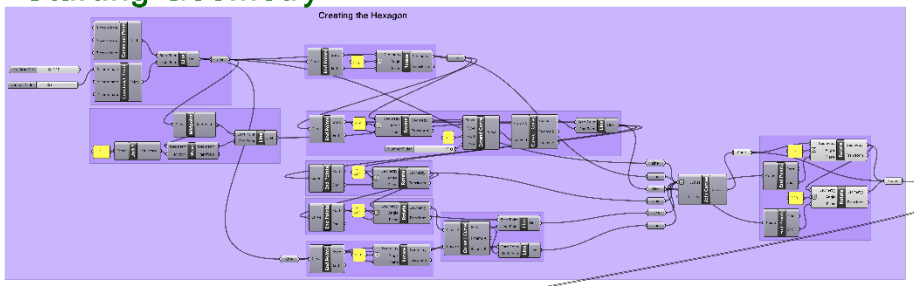

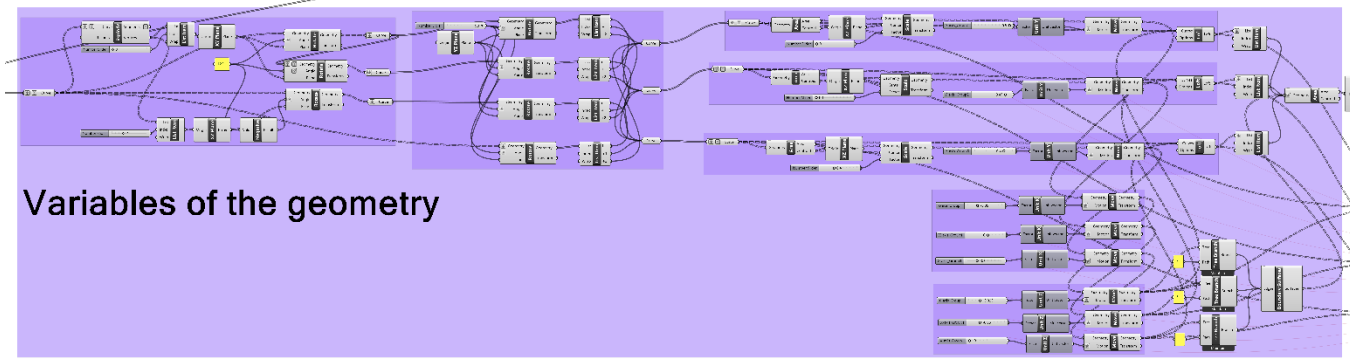

Variables of the geometry

Optimisation

Structural Analysis Conditions & Results

Model conditions:

Material : Acrylonitrile-butadiene-styrene (ABS Plastic)

Panel thickness: 0.7 mm

Wind load: 1.1 KN/m2

Result:

Maximum tensile stress in panel: 0.325 N/mm2

Allowable tensile stress: 0.5 N/mm2

Displacement: 3 mm

Maximum allowed displacement: 4 mm (L/250)

Resultant weight of the panel: 7.7 Kg

- Support points

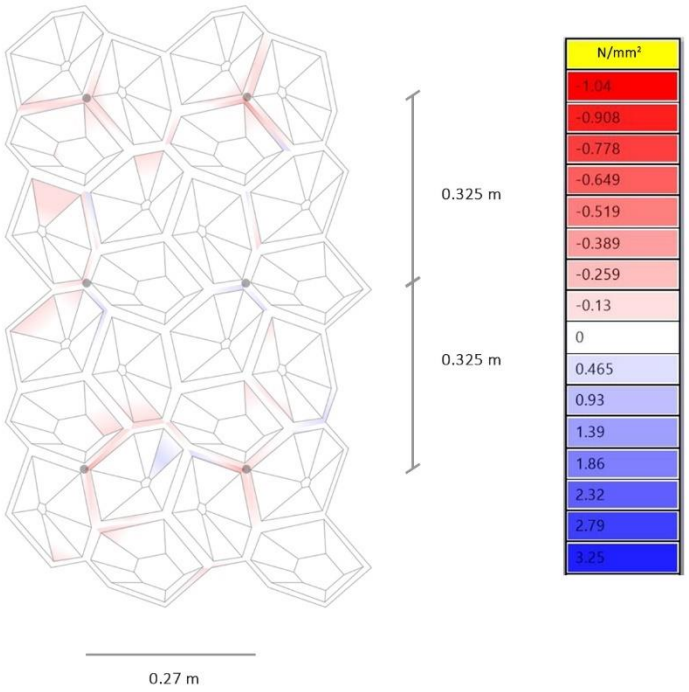

Model conditions:

Material : Ultra-high-performing concrete (UHPC)

Panel thickness: 15 mm

Wind load: 1.1 KN/m2

Result:

Maximum tensile stress in panel: 1.38 N/mm2

Allowable tensile stress: 9 N/mm2

Displacement: 0.03 mm

Maximum allowed displacement: 4 mm (L/250)

Resultant weight of the panel: 35.49 Kg

- Support points

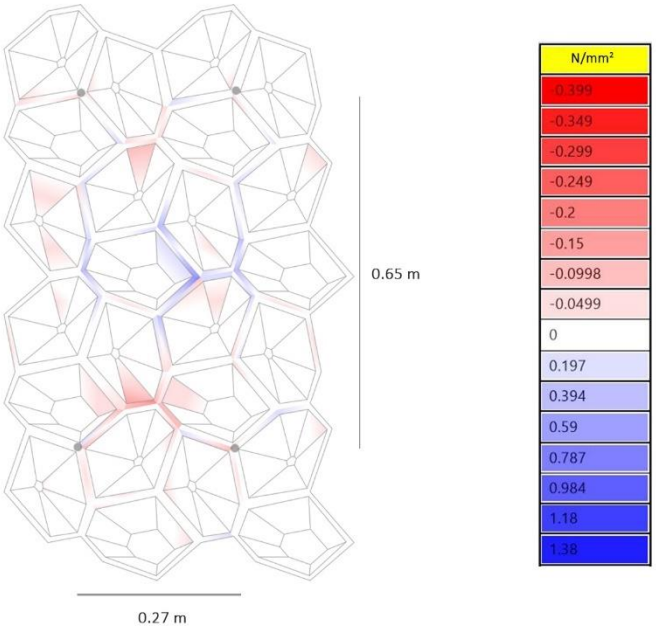

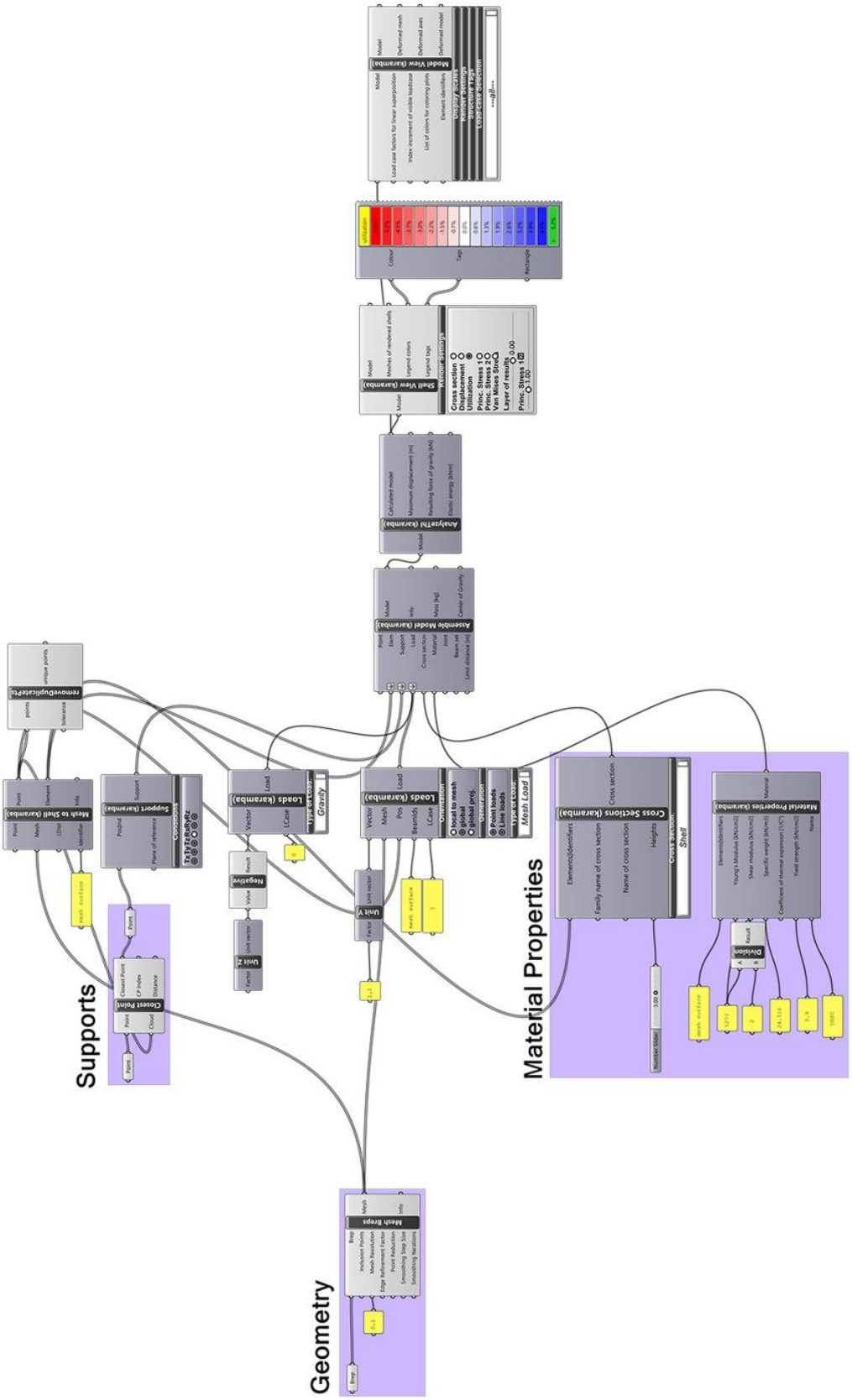
Supports
Geometry
Material Properties